Nagra
Nationale
Genossenschaft
für die Lagerung
radioaktiver Abfälle

Cédra
Société coopérative
nationale
pour l'entreposage
de déchets radioactifs

Cisra
Società cooperativa
nazionale
per l'immagazzinamento
di scorie radioattive

TECHNICAL REPORT 90-08

STRIPA PROJECT

WATER FLOW IN SINGLE ROCK JOINTS

EVA HAKAMI

MAY 1989

Division of Rock Mechanics
Luleå University of Technology Luleå, Sweden

Parkstrasse 23 5401 Baden / Schweiz Telephon 056 / 20 55 11

Nagra
Nationale
Genossenschaft
für die Lagerung
radioaktiver Abfälle

Cédra
Société coopérative
nationale
pour l'entreposage
de déchets radioactifs

Cisra
Società cooperativa
nazionale
per l'immagazzinamento
di scorie radioattive

TECHNICAL REPORT 90-08

STRIPA PROJECT

WATER FLOW IN SINGLE ROCK JOINTS

EVA HAKAMI

MAY 1989

Division of Rock Mechanics
Luleå University of Technology Luleå, Sweden

Parkstrasse 23 5401 Baden/Schweiz Telephon 056/20 55 11

Der vorliegende Bericht betrifft eine Studie, die für das Stripa-Projekt ausgeführt wurde. Die Autoren haben ihre eigenen Ansichten und Schlussfolgerungen dargestellt. Diese müssen nicht unbedingt mit denjenigen des Auftraggebers übereinstimmen.

Le présent rapport a été préparé pour le projet de Stripa. Les opinions et conclusions présentées sont celles des auteurs et ne correspondent pas nécessairement à ceux du client.

This report concerns a study which was conducted for the Stripa Project. The conclusions and viewpoints presented in the report are those of the authors and do not necessarily coincide with those of the client.

Das Stripa-Projekt ist ein Projekt der Nuklearagentur der OECD. Unter internationaler Beteiligung werden im Rahmen einer 3. Phase dieses Projektes von 1986-1991 Forschungsarbeiten in einem unterirdischen Felslabor in Schweden durchgeführt. Unter Anwendung des in den vorhergehenden Phasen 1 und 2 Gelernten sollen folgende Arbeiten realisiert werden:

- Anwendung verschiedener Felduntersuchungs- und Berechnungsmethoden, um den Wasserfluss und Nuklidtransport in einem unbekannten Felsvolumen des Stripagranites vorherzusagen und anschliessend zu überprüfen
- Evaluation verschiedenster Materialien und Methoden zum Abdichten wasserführender Klüfte im Stripagranit

Seitens der Schweiz beteiligt sich die Nagra an diesen Untersuchungen. Die technischen Berichte aus dem Stripa-Projekt erscheinen gleichzeitig in der NTB-Serie der Nagra.

The Stripa Project is organised as an autonomous project of the Nuclear Energy Agency of the OECD. Over the time period 1986-1991 (Phase 3 of the Project), an international cooperative programme of investigations is being carried out in an underground rock laboratory in Sweden. Building on experience gained in Phases 1 and 2, the following research will be carried out:

- Application of various site characterisation techniques and analysis methods with a view to predicting and validating groundwater flow and nuclide transport in an unexplored volume of Stripa granite
- Verification of the use of different materials and techniques for sealing water-bearing fractures in the Stripa granite

Switzerland is represented in the Stripa Project by Nagra and the Stripa Project technical reports appear in the Nagra NTB series.

Le projet de Stripa est un projet de l'Agence de l'OCDE pour l'Energie Nucléaire. C'est dans le cadre d'une troisième phase de ce projet allant de 1986 à 1991, que des travaux de recherches sont réalisés avec une participation internationale, dans un laboratoire souterrain de Suède. Il s'agit d'effectuer les travaux ci-dessous, en mettant en application ce que l'on a appris au cours des précédentes phases 1 et 2:

- Application de diverses méthodes de recherches sur le terrain et de calcul, pour prévoir puis contrôler l'écoulement de l'eau et le transport des nucléides dans un volume rocheux inconnu du granite de Stripa
- Evaluation des méthodes et des matériaux les plus divers, en vue de colmater des fractures aquifères du granite de Stripa

La Cédra participe à ces recherches pour la Suisse. Les rapports techniques rédigés à propos du projet de Stripa paraissent en même temps dans la série des Rapports Techniques de la Cédra (NTB).

PREFACE

The research work described in this Licentiate Thesis was sponsored by the Stripa Phase III programme on Site Characterization and Validation (SCV). Financial support was also provided by the Luleå University of Technology. The work was carried out by Eva Hakami, Division of Rock Mechanics, Luleå University of Technology. The work was commissioned by the Norwegian Geotechanical Institute, through NGI's role as one of the Principal Investigators in the Stripa SCV Project. Nick Barton acted as a research advisor.

The figure on the following page illustrates the different scales of rock mechanics investigation that are being followed in the SCV programme. Joints are characterized at three different scales in accordance with the availability of samples at different stages in the programme.

Index tests are performed on a large number of joint samples recovered from cores of 100 mm diameter. Larger scale coupled stress flow tests (CSFT) are performed on a limited number of joint samples recovered from 200 mm diameter cores. NGI, University of Newfoundland and Luleå University of Technology have performed tests at this intermediate scale. Tests of the same type (CSFT) are also being performed on a single joint of approximately 1.4 m in length, in a 1 x 1 m in-situ block test in the 3D drift. The ultimate goal is to be able to predict changes of joint aperture and joint conductivity in the disturbed zone created by a validation drift.

In this research study, Eva Hakami utilized joint samples from Stripa that were recovered in 200 mm cores. The joints were kindly provided by Chemflow from the 2D drift, and represent the N-S trending joint set that has been identified in the SCV programme. The replica technique requires that the joints are opened before replicas are cast. The samples are

therefore representative of disturbed joints. Additional joint samples from other localities are included in the study for comparison with the relatively smooth and nearly planar Stripa joints.

N. Barton

Oslo, May 1989

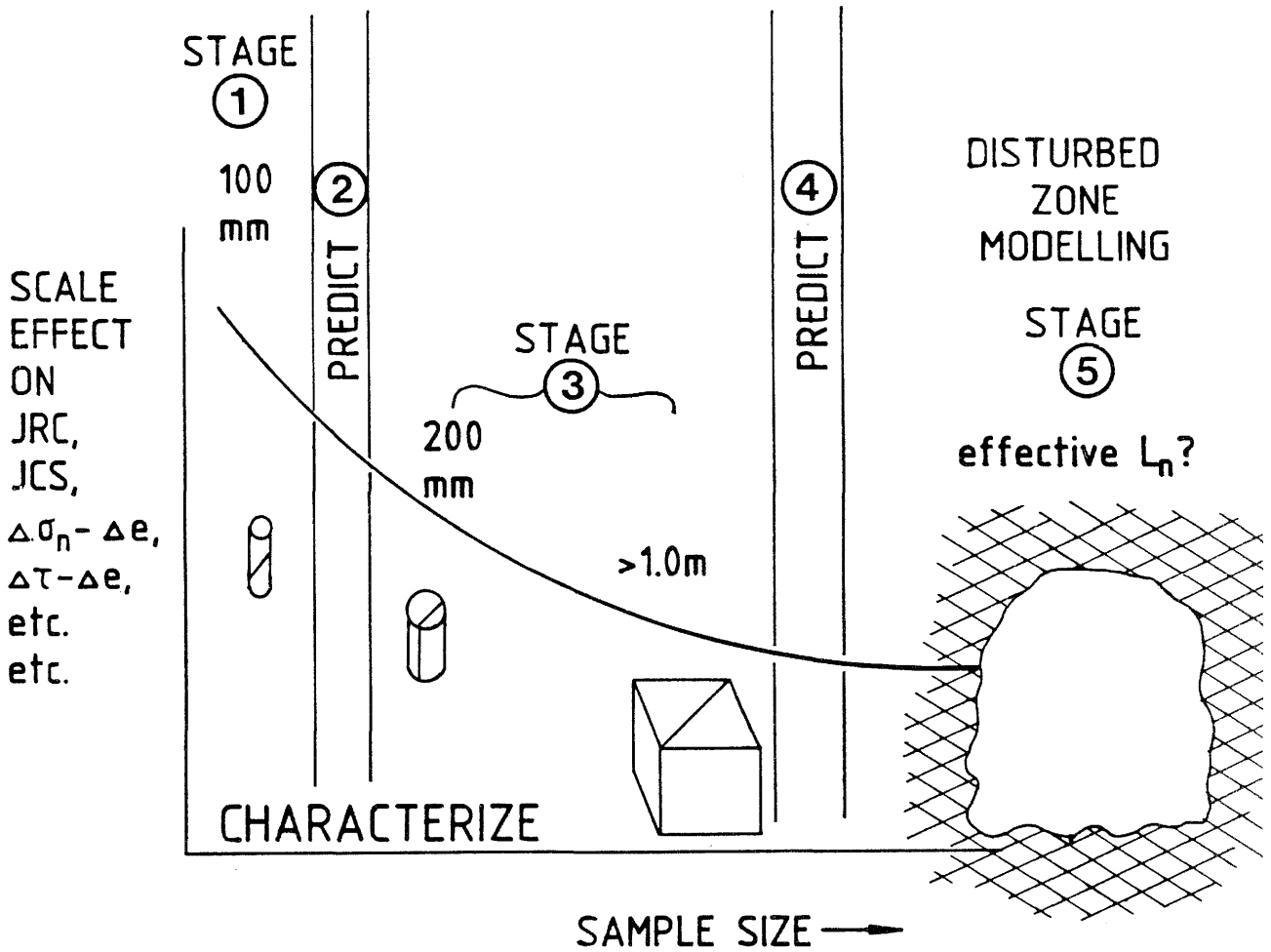

Joint characterization stages for the Stripa SCV programme. Sample size effects influence the data collected under each stage of joint characterization.

TABLE OF CONTENTS

SUMMARY

A prerequisite for successful modelling of groundwater flow in crystalline rocks is good estimates of the single joint conductivity. The hydromechanical properties of a single rock joint are governed by the geometry of the void space between the two joint surfaces. Closure of the joint due to compression will change this geometry and consequently change the permeability. The aperture distribution of rock joints has been studied by several different techniques including those of Gentier (1986), Gale (1987) and Pyrak-Nolte et al. (1987).

The variable aperture and the contact areas causes tortuosity of the flow. It is therefore difficult to calculate the permeability and velocities of the flow inside the joint. To study the coupling between void geometry and flow properties a technique to make transparent models of rock joints was developed.

Both sides of the rock joint is replicated using rubber casts from the surfaces and a strong clear epoxy. The replicas were subjected to cyclic normal loading before they were used in the experiments.

A method to measure the true aperture, E, inside the joint replicas was developed. Water drops, with a known volume, are placed at different points between the joint surfaces as they match together. The drops will cover certain areas of the surface depending on the actual apertures at each point. A record of the spots is taken by photographs. The joint replica is held compressed in a transparent fixture during the aperture measurements and the flow experiments.

The sides of the joint replicas were sealed off and a constant water pressure applied at the inflow. The total flow was measured for different pressures. The tortuosity of the water flow could be studied using colour injections. Diffe-

rent streamlines were made visible by separate injections. The velocity of the injected colour was also measured, thereby giving the flow velocity along different paths over the joint surface. Flow and velocity experiments on an ideal joint model consisting of two plexi-glass platens, showed good agreement between theoretical and measured values.

Five joint samples were used in the study. Three samples were selected from drillcores from Stripa mine. The size of the samples varied between 1 and 3 dm^2.

The apertures were measured with a density of about one point per cm^2. The result is presented in the form of frequency histograms, isoplots and terrain models. The result show that for all samples the aperture distribution is skewed towards larger apertures and that the spread is longer for the most open samples. All distributions fit well to log- normal functions. The average aperture varies between 0.1 - 0.5 mm for the five samples.

The equivalent hydraulic apertures, e, were determined from the flow experiments. The quotient $\bar{E}/e$ varies between 1.1 and 1.7 for samples with e varying between 0.13 and 0.43 mm. For a case with e smaller than 5 μm the quotient was shown to be higher than 16.

The velocity of the water flow varied strongly between different paths for the samples with a large spread in aperture. The sample which was well mated showed less variation in measured water flow velocity.

The tortuosity also varied in a corresponding way. The maximum ratio of the relative flow length was 1.34 for the sample with the most uneven and tortuous flow.

It was concluded from the experimental results that matedness is an important factor for the conductive properties of a joint. Matedness should therefore be considered in geohydrological surveys.

ABSTRACT

To study the hydromechanical properties of single rock joints a technique to make transparent replicas of natural joint surfaces has been developed. Five different joint samples were replicated and studied. The aperture distribution of the joints were obtained through a measurement method provided by the transparent replicas. The principle behind the method is that a water drop with a known volume, which is placed inside a joint, will cover a certain area of the surface depending on the average size of aperture at the actual point.

Flow tests were performed on the same joint replicas. The tortuousity of the flow and the velocity along singel stream lines were measured using colour injections into the water flow through the joints. The equivalent hydraulic apertures determined from the flow tests were shown to be smaller than the average mechanical apertures. The velocity of the flow varies strongly between different paths over the joint depending on the spatial distribution of the apertures. The degree of matedness between the joint surfaces is an important factor influencing the channeling character of the joints.

RESUME

Une technique pour la réalisation de répliques transparentes de surfaces de joints naturelles a été mise au point pour l'étude des propriétés hydromécaniques de simples joints rocheux. Cinq exemples différents de joints ont été reproduits et étudiés. La distribution des ouvertures dans les joints a été obtenue par une méthode de mesure fournie par les répliques transparentes. Le principe à la base de cette méthode est qu'une goutte d'eau de volume donné, placée à l'intérieur d'un joint, va recouvrir une certaine partie de la surface dépendant de la dimension moyenne des ouvertures au point en question.

Des essais de circulation ont été exécutés sur ces mêmes répliques de joints. La tortuosité de l'écoulement et la vitesse le long des différents chenaux de circulation ont été déterminées par des injections de colorants dans l'eau circulant à travers les joints. Les ouvertures hydrauliques équivalentes déterminées à l'aide des essais de circulation se sont révélées être inférieures aux ouvertures mécaniques moyennes. Les vitesses d'écoulement varient fortement entre les différents chenaux dans le joint, dépendant de la distribution spatiale des ouvertures. Le degré de correspondance entre les surfaces des joints est un facteur important qui influence la propension des joints à former des chenaux.

ZUSAMMENFASSUNG

Um die hydromechanischen Eigenschaften von Einzelklüften im Gestein zu untersuchen, wurde ein Verfahren entwickelt, um transparente Reproduktionen der natürlichen Kluftflächen zu erzeugen. Fünf verschiedene Kluftproben wurden reproduziert und studiert. Die Verteilung der Kluftöffnungsweiten wurde mittels einer auf den transparenten Reproduktionen basierenden Messmethode bestimmt. Das Prinzip dieser Methode ist, dass ein Wassertropfen mit einem bekannten Volumen innerhalb einer Kluft eine bestimmte Oberfläche decken wird, abhängig von der mittleren Grösse der Kluftöffnung am jeweiligen Messpunkt.

Mit den gleichen Kluftreproduktionen wurden Fliesstests durchgeführt. Die Tortuosität des Flusses und die Fliessgeschwindigkeit entlang einzelnen Strömungslinien wurden mittels Farbinjektionen in den Wasserfluss in den Klüften bestimmt. Es wurde gezeigt, dass die mit den Fliesstests gemessenen hydraulischen Oeffnungsweiten kleiner waren als die mittleren mechanischen Oeffnungsweiten. Die Fliessgeschwindigkeiten variieren stark zwischen den verschiedenen Fliesswegen in der Kluft, abhängig von der räumlichen Verteilung der Oeffnungsweiten. Der Grad der Paarung zwischen den Kluftflächen ist ein wichtiger Parameter, der die Kanalbildungscharakteristik der Klüfte beeinflusst.

1 INTRODUCTION

Radioactive waste from nuclear power plants and other hazardous waste is a growing problem in the industrial world. To find solutions to all the technical problems involved with safe final disposal is now the urgent task for researchers in different branches of science all over the world.

Many countries are considering to build their repositories in the bedrock and in this way make use of the ground as a further barrier against the spread of radioactive nuclides migrating from the waste. Effort is therefore put into a better understanding of groundwater flow and transport in rock masses.

Sweden has chosen to study the possibilities and conditions to construct a repository in crystalline rock. Chrystalline rocks generally occur as blocks of hard intact rock material intersected and bounded by fractures. This system or network of more or less connected fractures is the major conductor of water, since the permeability of the intact rock is very low. The flow through such a network will depend both on the properties of every single joint and on the geometry of the network itself.

Statistical treatment of field data can be used to develop stochastic models for the location, size and orientation of the joints in a network. These models are a tool in so called network modelling, where the real rock mass is simulated in simplified form using available data, in an attempt to predict the groundwater flow around an underground construction during different situations.

Good estimates of water flow through the single joints is however a prerequisite for a successful network modelling since they are the units out of which the network is built. The joint aperture and the water pressure are the controlling parameters of the flow through a single joint, but the fact that their values vary over the joint area is the main reason why the problem of flow-predictions is so complicated.

The geometry of the void space inside a joint plane is defined by the two joint surfaces as they are pressed against each other. Different rock types have different mineral compositions which influences the void geometry and how it changes due to compression. The roughness of the surfaces will naturally also be important to the character of the formed void space.

Due to changes of the stress situation in the rock mass the joints may undergo a series of shear movements and dilatation changes. The degree of fit between the two opposing surfaces, called matedness, is strongly governing the hydromechanical properties of the joint. The geological history may also cause filling material to form on the surfaces which normally has a tightening and softening effect.

To find these relations between joint surface topography, stiffness and permeability has been the aim for several researchers during the last decade, among others Iwai (1976), Gale (1982), Gentier (1986) and Brown (1987). Laboratory testing of natural and artificial joints has been performed along with the development of theories. This work has resulted in formulas for the total flow through a joint, see for example Tsang and Witherspoon (1981) and Barton et al. (1985).

However, predictions of average total flow is not sufficient in the safety analyses around a disposal of radioactive material, because they have to comprise travel times and retardation of radionuclides. Short travel times could allow still unacceptably radioactive particles to reach the accessible environment outside the controlled area of the repository. Therefore the speed and volume of the the fastest transport is very important. The flow pattern, or channelling, in the single rock joints has become a focus for attention, GEOVAL -87 and Tsang and Tsang (1987).

The aim of the present work has been to develop an experimental technique that gives a better understanding of the nature of flow inside a joint. Visual studies was judged as a good approach to the channeling problem. Using transparent models of rock joints the tortuos stream lines of the flow inside can be shown.

In the first part of the thesis the work on hydromechanical properties of single rock joints is reviewed, including a general discussion about limitations and conclusions. Next part describes the developed technique to make transparent replicas of natural joints and the experimental methods for aperture and flow measurements. The last part gives the results from experiments performed on five different joint samples followed by a discussion and conclusions.

2 HYDROMECHANICAL PROPERTIES OF SINGLE ROCK JOINTS

Bearing in mind that the hydraulic properties of a rock mass can only be calculated if the entire complex of influencing factors is known, this review is concentrating on the properties of single joints.

Researchers on flow in single joints have been involved in different aspects of the problem which are actually closely connected to each other. In the following review the previous work has been separated into three different themes.

Void geometry - which is the factor controlling the permeability.

Closure - is indirectly important since closure of joints changes the void geometry.

Calculation of flow - Theories and models based on different parameters.

2.1 Void geometry

The ability of a joint to transmit water depends primarily on the size of the void between the opposing rock walls, known as the joint aperture. Few workers have tried to directly measure the complex three dimensional geometry of this void space in the joint.

A direct attempt in measuring the aperture was performed by Gentier (1986). She measured the surface height along profiles, on the opposite sides of the joint. The profiles were put together to form the composite topography, i.e. the aperture profile at zero normal load (Fig. 2.1). Figure 2.2 shows the frequency histograms over the apertures derived in their experiments.

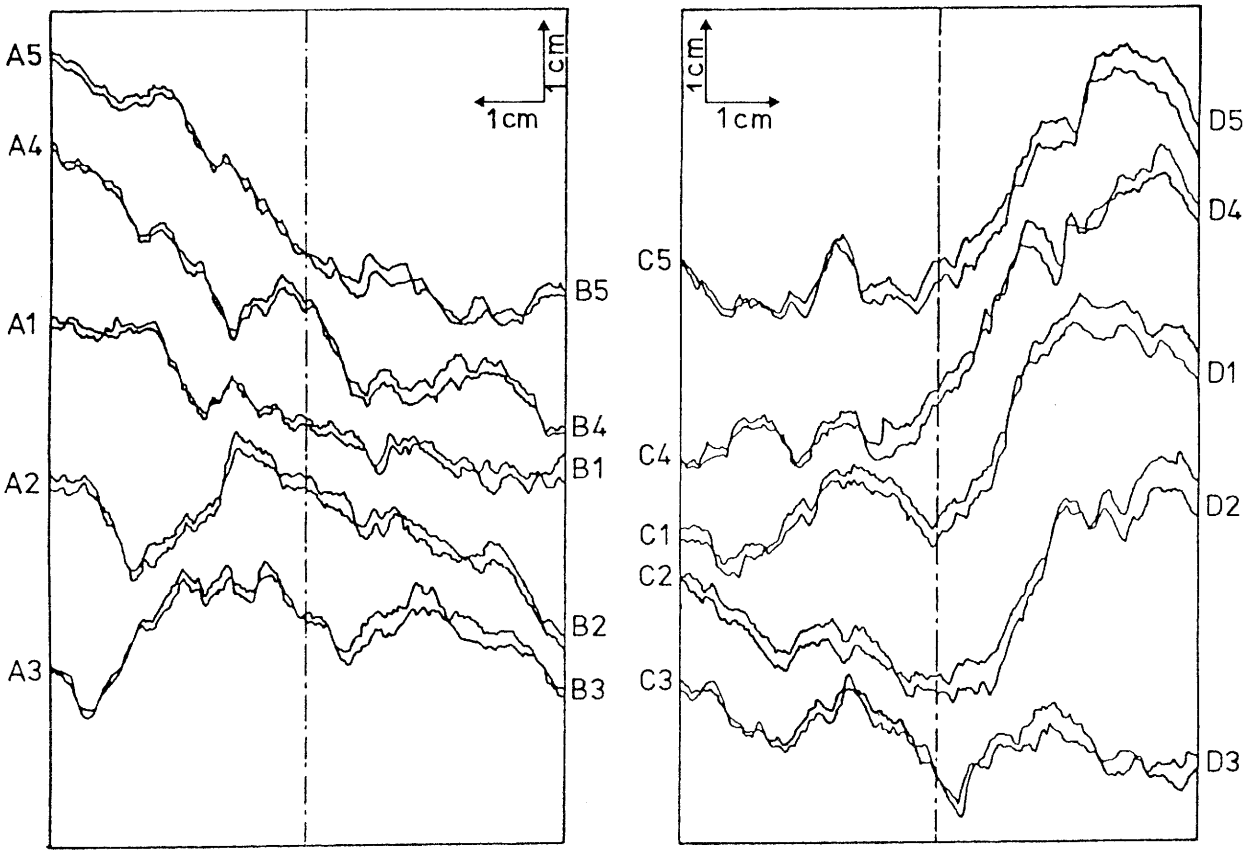

Figure 2.1 Profiles from upper and lower surface of a joint. The profiles AB are perpendicular to CD on the same joint surface. Gentier (1986).

Another technique to reveal the apertures inside a joint has been developed by Gale (1987). The experiments involves injection of an epoxy resin into the joint under normal load. After hardening the joint is cut into sections and the distances between the rock surfaces and the thickness of the resin is measured along the profiles, (Fig. 2.3). In Figure 2.4 the variation in aperture and resin thickness from all profiles is shown by frequency histograms. The joint specimen was obtained from the Stripa test site in Sweden.

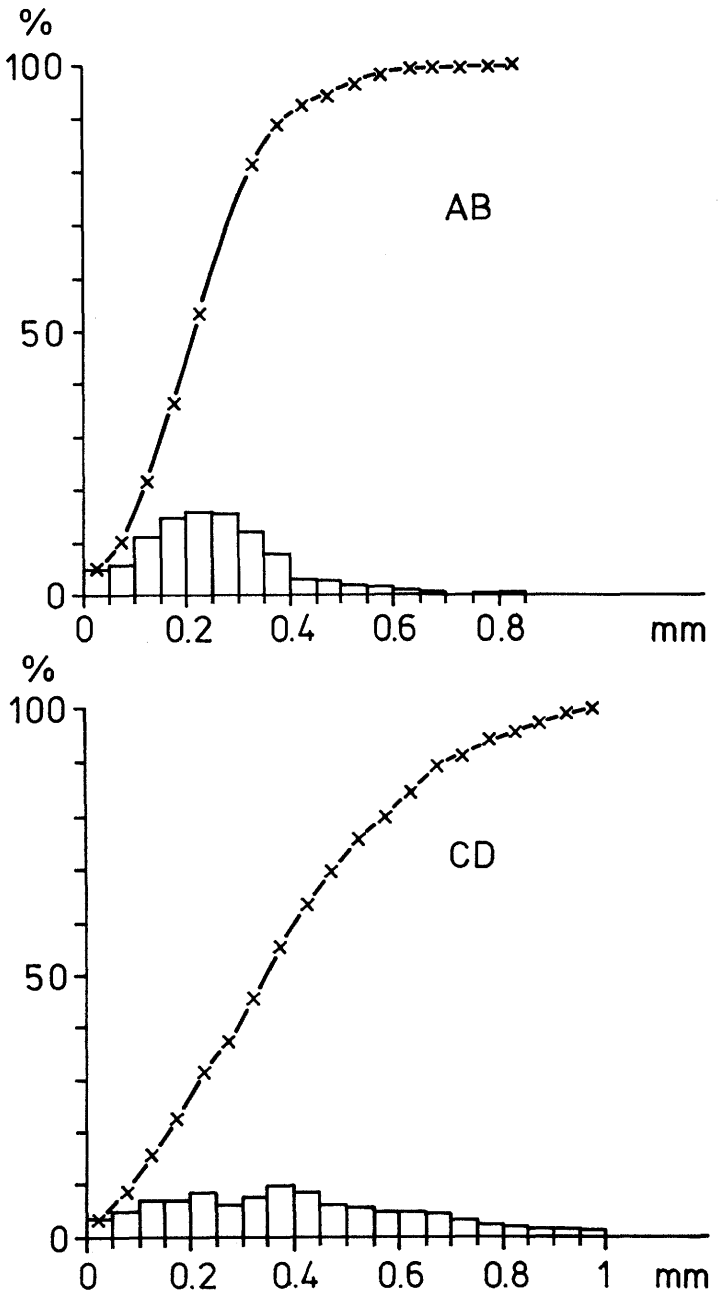

Figure 2.2 Histograms and cumulative histograms of the apertures along the profiles (Fig. 2.1) in the direction AB and CD respectively. Gentier (1986).

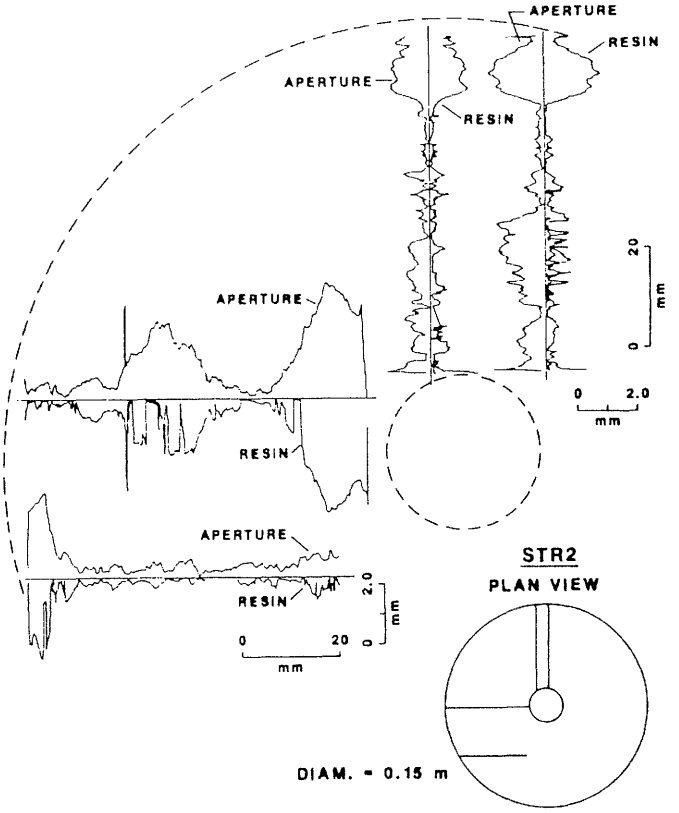

Figure 2.3 Distribution of pore space along four profiles in STR2. Gale (1987).

Barton et al. (1985) introduced in their work the term mechanical aperture E in contrast to the widely used hydraulic aperture e (Fig. 2.5). By this distinction they point out the difference between the real void geometry and the parallell-plate case which defines the so called hydraulic aperture. The average aperture of a specimen under very low normal load was defined as the initial mechanical aperture E_0. To directly measure the parameter E_0, Bandis (1980) inserted a tapered feeler gauge in visible gaps between the mated surfaces around the edges. The usual range of apertures for fresh and moderatly weathered joints was between 100 μm to 300 μm and between 300 μm to 650 μm for weathered joint specimens.

Barton and Bakhtar (1983) proposed an empirical equation for estimation of the E_0 values presented by Bandis (1980). This equation was based on the index parameters JRC and JCS, from the study by Barton and Choubey (1977).

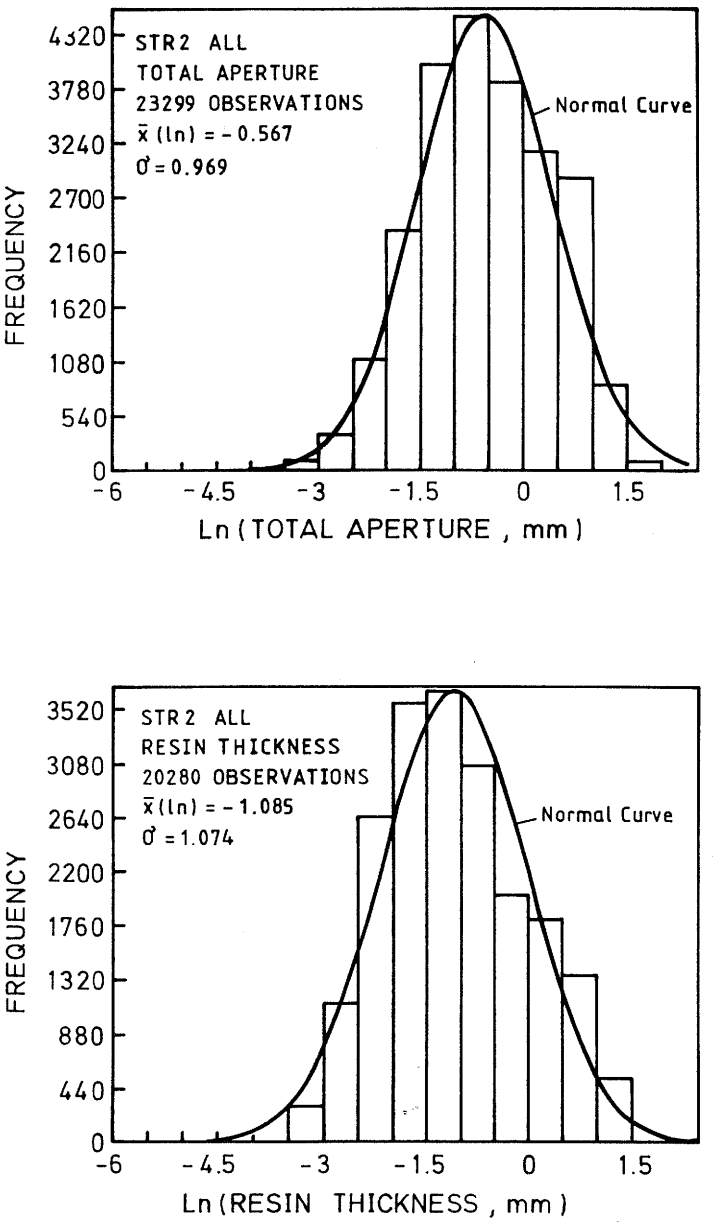

Figure 2.4 Frequency histograms of total aperture and resin thickness for all profiles in STR2. Gale (1987).

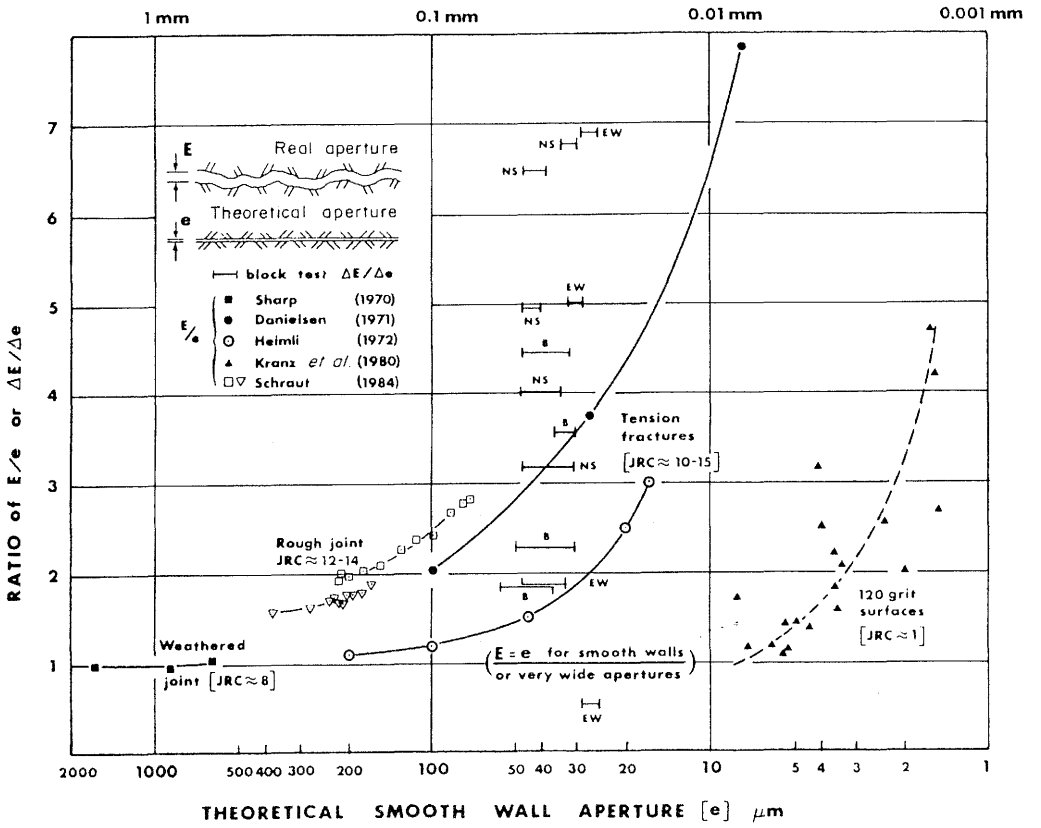

Figure 2.5 Comparison of real mechanical apertures (E) with theoretical smooth wall conducting apertures (e). Barton et al. (1985).

Some indirect informaton about the void space in a joint can also be gained by studying the distribution of contact points. Iwai (1976) has followed this idea and used thin plastic film between the joint surfaces that are pressed together. In Figure 2.6 his result shows the difference in nature between joints from different rock types and it shows the expected effect of increased normal load.

Another way of studying contact points was used by Pyrak-Nolte et al. (1987). They studied the deformation and flow properties of fractures in samples from Stripa granite (quartz monzonite) which were 52 mm in diameter. Wood's metal was pumped into the fractured sample while it was held in a triaxial test vessel at a temperature just above the melting point. The fluid pressure and the axial load was maintained

until the metal was solidified. When the to halves of the sample was separated the metal casts on the surfaces should correspond to the void geometry at the actual effective stress.

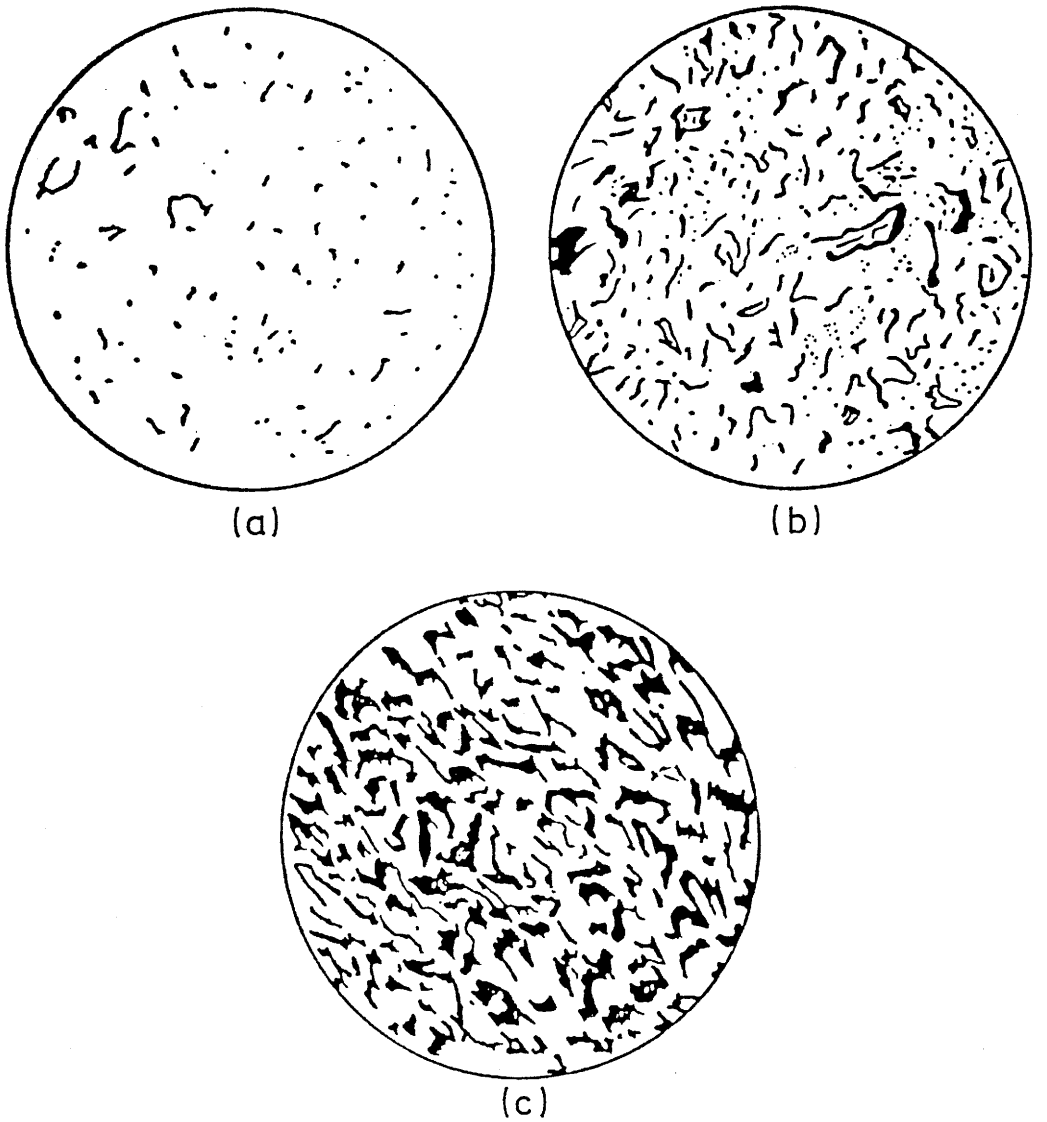

Figure 2.6 Sketch of contact areas obtained for granite with σ = 1.3 MN/m^2 (a), and σ = 20 MN/m^2 (b), and for marble with σ = 20 MN/m^2 (c). Iwai (1976).

Using SEM and photographic techniques the images from each surface was evaluated and superimposed to form the image of the joint area. Figure 2.7a-c shows images for sample E30 for 3, 33 and 85 MPa respectively. Figure 2.7d is a 25 times magnification of a part of Figure 2.7c. Black areas corresponds to metal and white areas corresponds to areas in contact.

The structure of the contact areas can be described as fractal geometries, Nolte et al. (1987). The fractal dimension of the images from the two studied samples, from Stripa granite, decreased from D = 2.00 to values near D = 1.96 as the stress increased up to 85 MPa.

Bandis (1980) studied the damaged contact areas after shear tests of joints. Using identical joint models, cut into samples of different size, he was able to study the effect of scale. The investigation revealed the following features:

1) increasing number of small contact areas on smaller samples

2) increasing size of individual contact areas on larger samples

3) the scale effect reduces for planar joints

A theoretical approach to the problem of void geometry is taken by Brown and Scholz (1985a,b) and (1986) and Brown (1987). They assume that each joint surface has asperities of all scales distributed randomly about the mean plane and that this can be described mathematically by a two-dimensional random function.

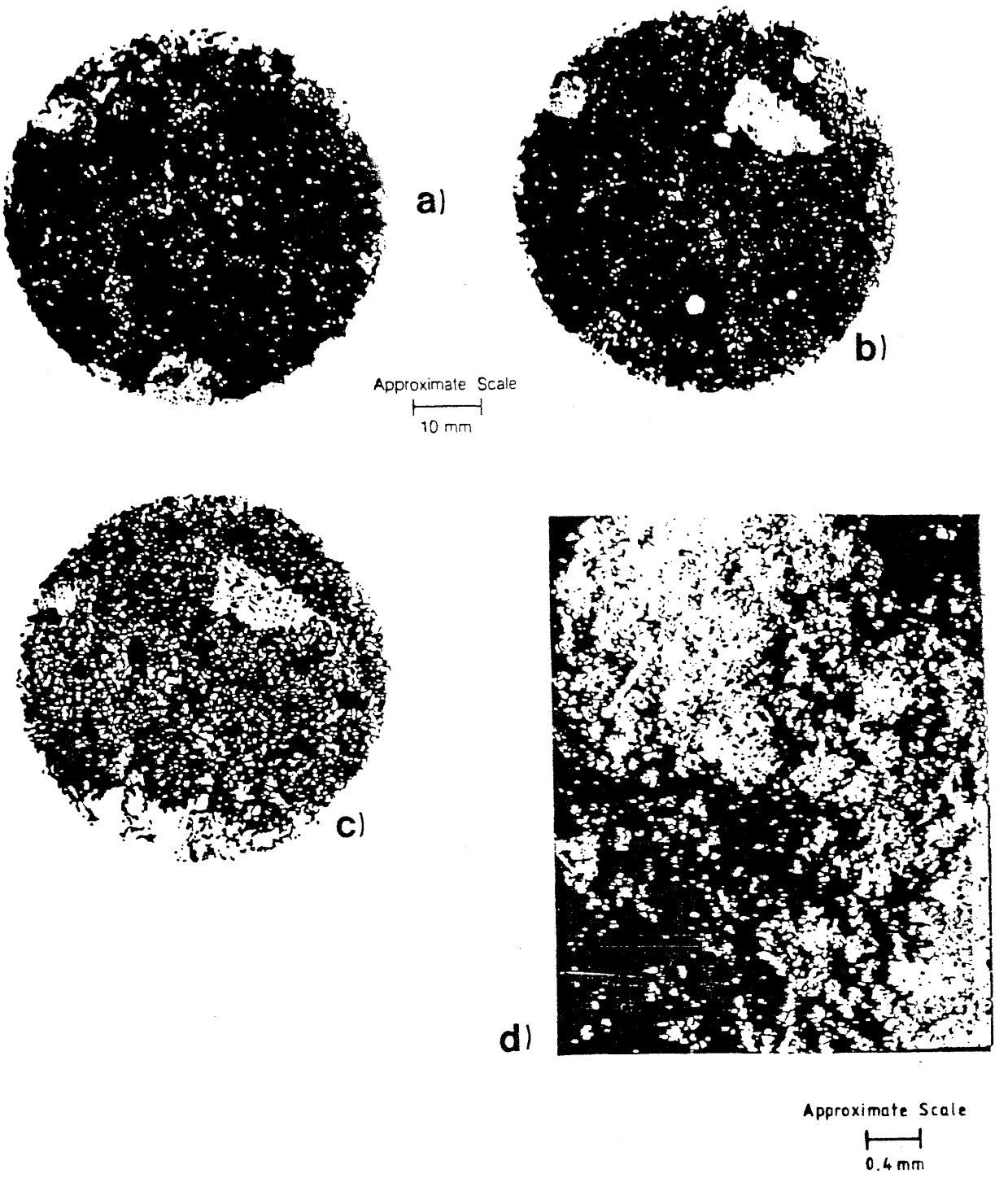

Figure 2.7 Contact area composite images for sample E30 for a) 3 MPa, b) 33 MPA and c) 85 MPa. The black portion is the flow path geometry; the white areas are the contact areas. The resolution of the patterns is about 3 % of the diameter. d) A computer enhanced composite image of SEM micro-graphs of E30 at 85 MPa under 25 times magnification.
Nolte et al. (1987).

The summed height of both surfaces, composing a joint, gives the so called composite topography (Fig. 2.8). The local maxima on the generated composite topography also becomes randomly distributed and was described by a probability density function that fitted best with profile measurements on joint surfaces, Brown and Scholz (1985a). Later a fractal model was connected to describe the auto correlation of the surface height distribution, Brown (1987). In both cases the slope of the power spectrum from linear profile measurements is an important parameter. Figure 2.9 shows two aperture distributions generated from surfaces, placed together to form a joint, at different separation.

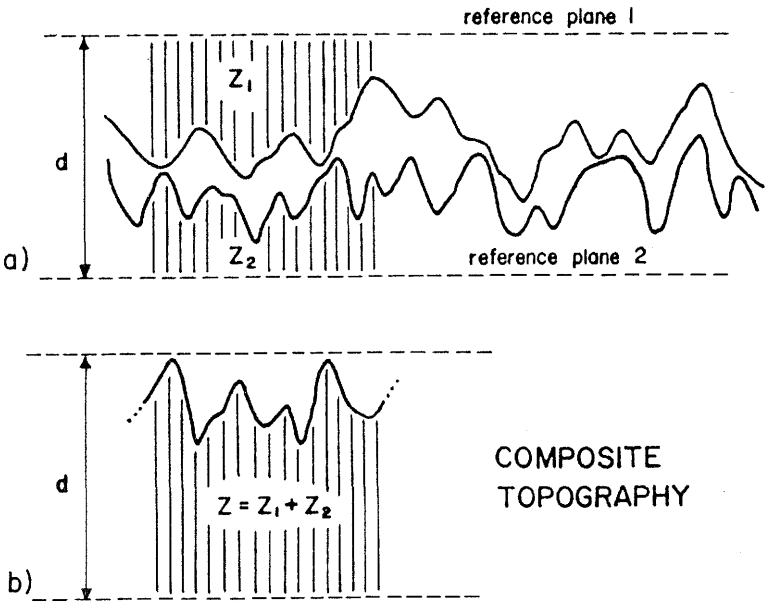

Figure 2.8 a) Schematic cross section through a joint. The surface heights are measured from parallel reference planes fixed in each surface.
b) The "composite topography" of a joint is defined by summing the heights of both surfaces at each point along the joint. The local maxima of the composite topography are the places where the surfaces are closest together.
Brown and Scholz (1985a).

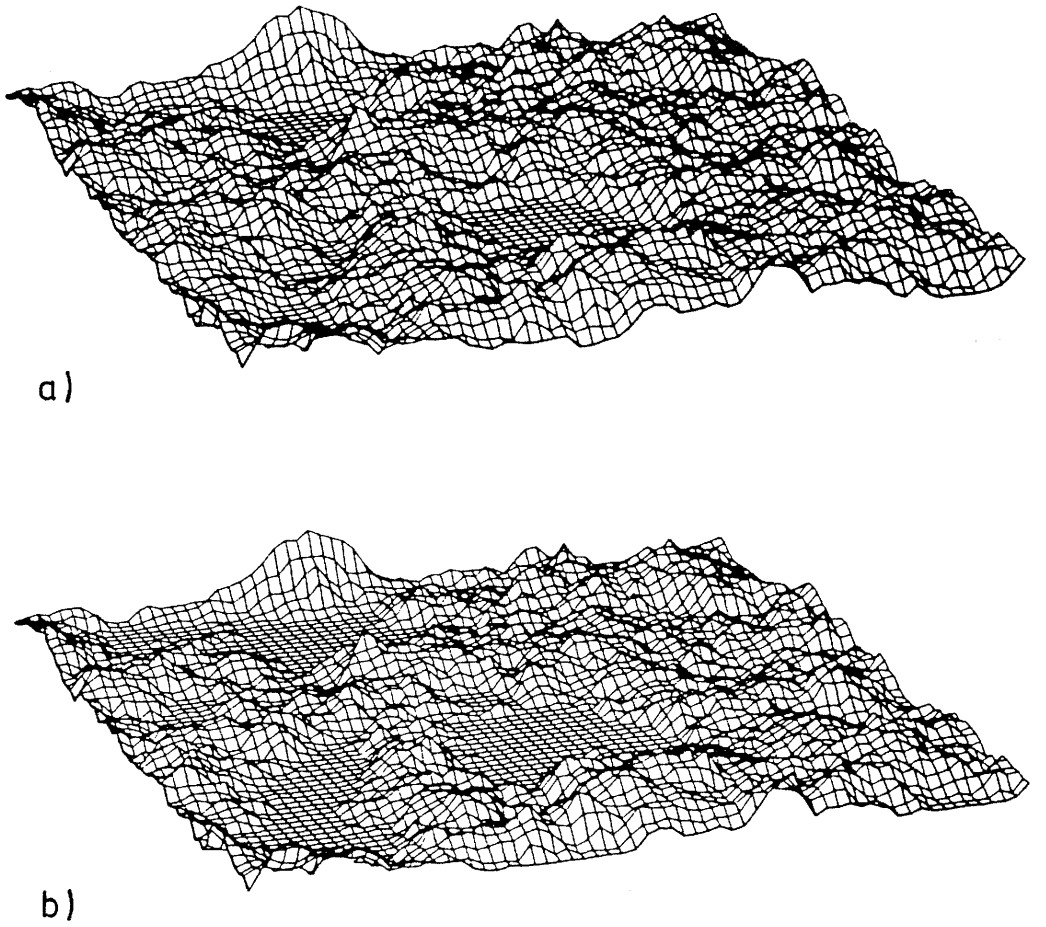

Figure 2.9 Aperture distributions d(x,y) formed by placing two surfaces (D = 2.5) together at separations of a) $d_m = 2\sigma$, and b) $d_m = 1\sigma$. Flat areas are regions of zero aperture or "contacts" defined by the overlap of the two surfaces. Brown (1987).

2.2 Closure

As will be discussed in section 2.3, the flow through a joint is very sensitive to changes in aperture. Therefore the influence of stress distribution cannot be neglected in a geohydrological study.

Any underground excavation will change the stress field in the surrounding rock mass. Some joints will close due to increased compressive stresses, while other joints will open due to a decrease in compressive stresses. Still other joints will be subjected to shear stresses causing shear movements and dilation, Barton (1986). In pace

with the general development of stress calculating techniques there has been a growing demand for stress-conductivity relationships for rock masses.

From the mechanical point of view the stress-closure relation is a matter of joint stiffness which is a commonly used parameter in rock mechanics. The common definition of joint stiffness is based on the testing procedure. The normal joint stiffness is measured with a loading machine that compresses the specimen, containing a joint, while the normal displacement of the specimen is measured. The obtained stress-dispacement curve is calibrated against a similar curve for an intact sample of the same rock. The slope of the resulting curve gives the stiffness of the joint at different normal loads.

Figure 2.10, from Bandis et al. (1983), shows examples of typical joint deformation behaviour due to cyclic normal loading. The permanent deformation after the first cycles and the increase in stiffness with cycles is often attributed to seating disturbances during sampling of the joint, e.g. Iwai (1976) and Bandis et al. (1983). In-situ joints probably follows a stress-closure relationship more similar to the third or forth cycle when these disturbances are removed, Barton et al. (1985).

The variable joint stiffness gives no direct information on the change of aperture distribution due to compression. It includes all possible factors of the joint such as weathered rock surfaces, joint filling and the degree of matedness. With the stiffness approach one can get round the problem of the real stress distribution over the joint area since it is based on average stress.

Tsang (1984) used an aperture distribution, n(b), derived from experiments by Gentier (1986), in her study of tortuosity effects on flow through joints at different degree of contact, (Fig. 2.11). When the fracture closed by Δb, as a result of applied stress, all the apertures smaller than Δb became zero, and a new aperture distribution was obtained. Mathematically this distribution is the same as the original n(b) truncated by Δb and translating the remaining plot to the origin.

In Figure 2.11 truncation corresponding to fractional areas of 15, 25 and 35 % are marked. Hypothetical analytical functions chosen for n(b) were also investigated in the study.

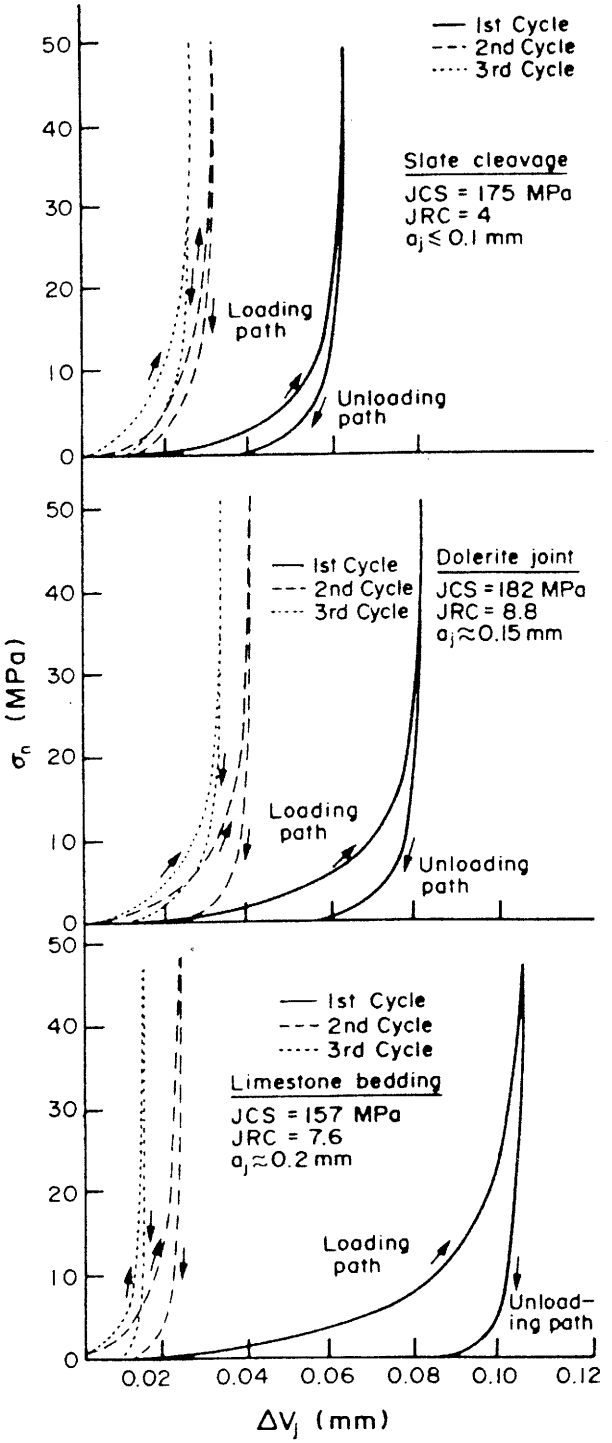

Figure 2.10 Normal stress (σ_n) vs closure (ΔV_j) curves for a range of fresh joints in different rock types, under repeated loading cycles. Bandis et al. (1983).

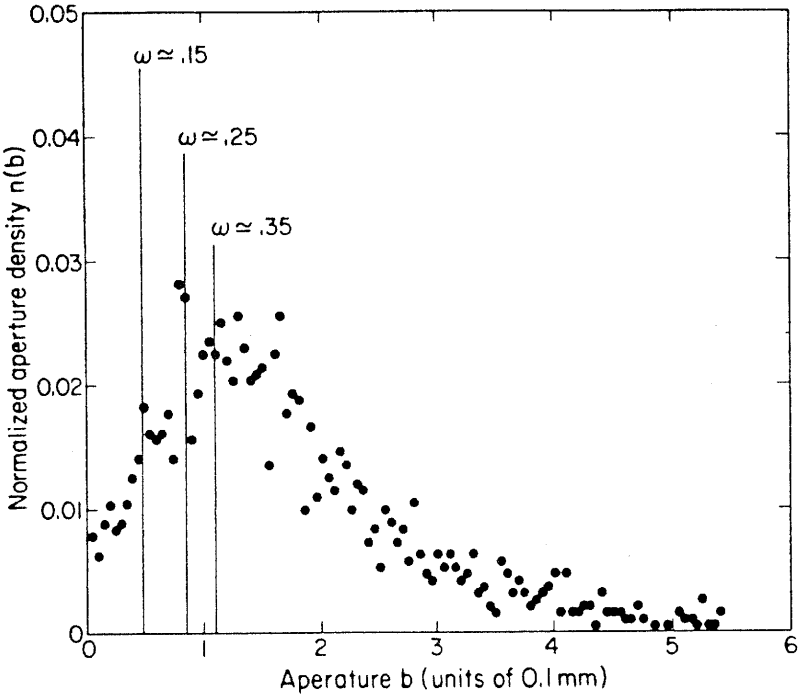

Figure 2.11 Aperture density distribution n(b) derived from 10 sets of surface roughness profiles of a granite fracture (measured by S. Gentier). Tsang (1984).

The work on joint stiffness by Brown and Scholz (1986) has many features in common with the work by Swan (1983). Both approaches are based upon theories presented by Greenwood and Williamson (1966) and Greenwood and Tripp (1971) who used the elastic analysis of Hertz to describe contact between two rough uncorrelated surfaces. The aperture model used by Brown and Sholz is described in section 2.1.

For the problem of closure Brown and Scholz also chose the truncation approach. The change in composite topography was obtained by subtracting the same closure distance from all the values, as if the contacting points were not connected to nor influenced by the neighbouring points, i.e. a truncation of the aperture distribution. Points with zero aperture or "overlapping" points are defined as contacts. The change in void geometry due to closure, or smaller separation between the two stiff surfaces, is shown in Figure 2.9.

The uneven distribution of contacts between the surfaces of a compressed joint will however give rise to stress concentrations and a varying amount of deformation. Hopkins et al. (1987) also showed that the interaction between contact points cannot be neglected. Figure 2.12 shows how the stiffness of the joint changes due to the configuration of contact points. Note that the percentage of contact area is the same in all cases, i.e. the average stress on the contacts is the same.

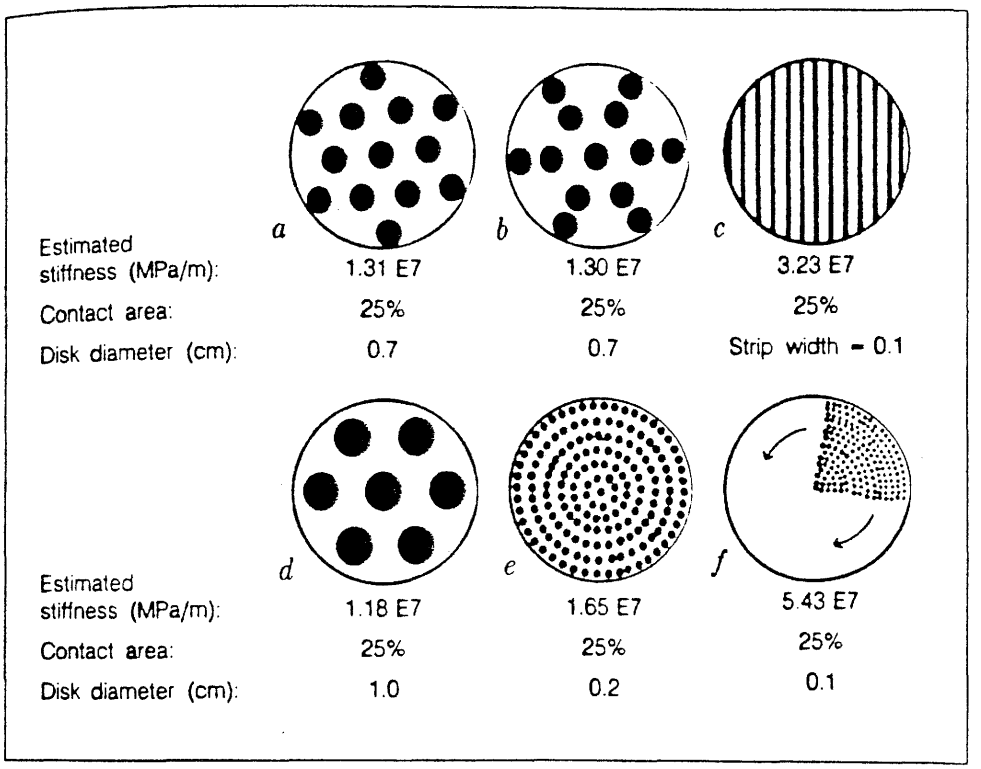

Figure 2.12 Specific stiffness calculated for spatial arrangements with equal contact areas of 25 % but varying disk sizes. Hopkins et al. (1987).

2.3 Calculation of flow

Even if we assume that the aperture distribution of a joint is fully known it is not a simple task to calculate the amount of water flowing through it. An analytical solution requires the significant simplification that the joint surfaces are smooth and may be regarded as parallel plates. For this case the Navier-Stokes equation can be solved

for laminar flow of a Newtonian fluid, see Figure 2.13. The boundary conditions applied is that the velocity

$$v_x = 0 \quad \text{at} \quad z = \pm e/2$$

The velocity of flow in the direction of flow v_x in the direction of gradient h is then expressed as

$$v_x = -\frac{1}{2}\frac{g}{\nu}\frac{\partial h}{\partial x}\left[z^2 - \frac{e^2}{4}\right] \tag{1}$$

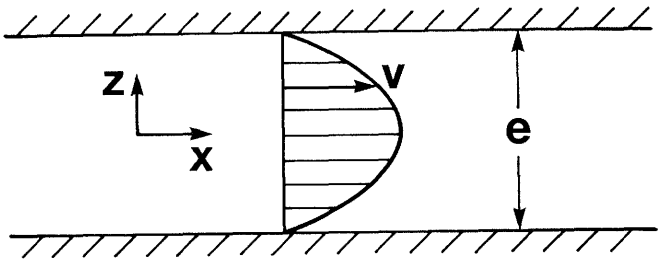

Figure 2.13 Flow between two parallel plates with ideally smooth surfaces.

The average velocity in the fracture is then

$$\bar{v} = \frac{1}{e}\int_{-e/2}^{e/2} v_x \, dx = -\frac{\gamma e^2}{12\,\nu} \cdot \frac{\delta h}{\delta x} \tag{2}$$

and the flow rate per unit width is

$$q = -\frac{g e^3}{12\,\nu} \cdot \frac{\delta h}{\delta x} \tag{3}$$

Equation (3) is called the "cubic law" since it says that the flow is proportional to the aperture cubed. Although this relation is based on a very idealized case it has been widely used because of its simplicity. Many workers have also tried to verify the cubic law with exper-

iments on rock joints, e.g. Iwai (1976), Raven and Gale (1985) and Witherspoon et al. (1980).

Witherspoon et al. (1980) conclude from their investigation that the cubic law is valid, since the flow per unit head was shown to be dependent on the aperture raised to the power of three. However, they have introduced a factor f in the relation to get a good fit with the experimental results. This factor was designed to take care of the effects of deviations from the parallel plate concept. Equation (3) can then be written

$$Q = \frac{C\, e^3}{f} \quad ; \quad C = \frac{g}{12v} \cdot \left(-\frac{\delta h}{\delta x}\right) \tag{4}$$

In the case when roughness or tortuosity retard the flow, $f > 1$. Values of f varied from 1.04 to 1.65 in their experiments.

The same conclusion was made by Elliot et al. (1985) also introducing a joint condition factor (JCF) into the pure cubic law. The JCF varied between 0.07 to 74 in their list of compiled values for the first test cycle (JCF = f in equation (4)).

Barton et al. (1985) use the roughness coefficient JRC (see section 2.2) in a modified cubic law. With the empirical relation shown in Figure 2.14 the hydraulic aperture, e, corresponding to measured values of mechanical aperture, E, is estimated. The ratio E/e becomes bigger for smaller apertures and rougher surfaces thereby correcting for the greater difference between real void geometry and the theoretical parallell plate. This relationship was used in numerical analyses to connect the mechanical effect of changes in stresses, ΔE, to the hydraulic effect, Δe, Barton and Makurat (1988).

The flow calculations based on the cubic law give only average values for the velocity of flow in the joint and this has shown to be insufficient in many hydrogeological analyses. For example a correct interpretation of the results from tracer experiments requires that the velocity and volume of each flow path is known. A physically explained coupling between mechanical and hydraulic properties can only be found

if the real distribution of aperture is understood and if models for flow calculations in complex conductors are developed.

However, the three-dimensional void geometry of a joint, as discussed in section 2.1, is not measurable in practice. Even if the full geometry of a joint was measurable there exists no analytical way to calculate the flow through it. Therefore all approaches to solution of this problem involves some simplifications and assumptions exemplified below.

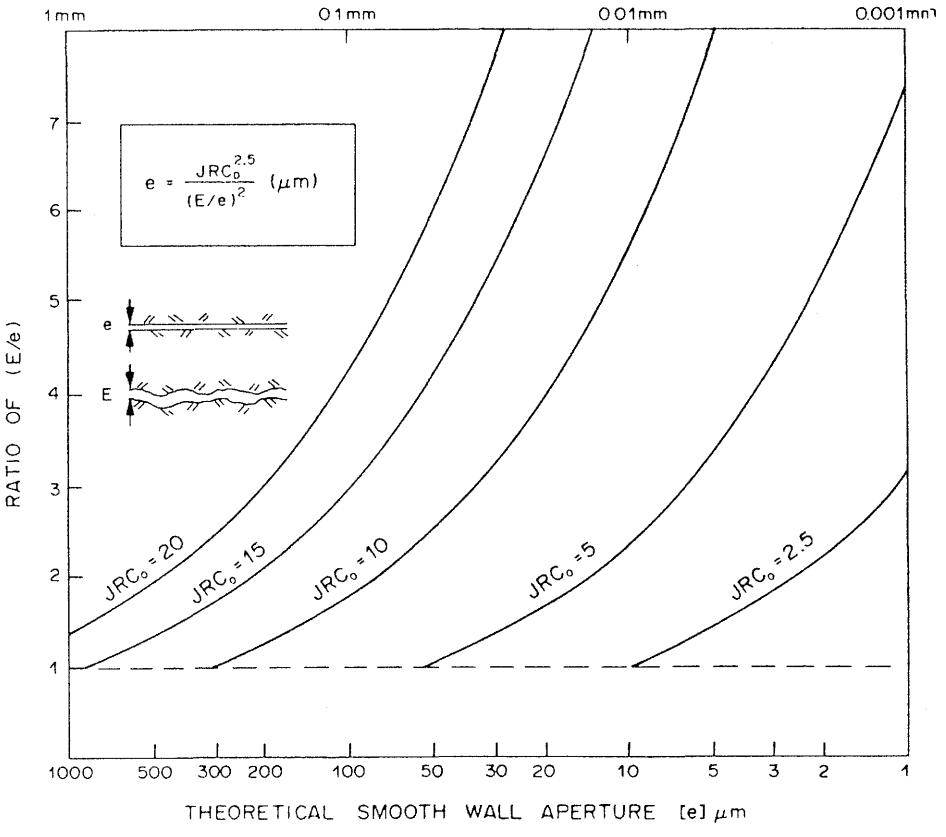

Figure 2.14 An empirical relation incorporating joint roughness (JRC) and aperture which broadly satisfies the trends exhibited by flow test data (see Fig. 2.5). Barton et al. (1985).

The three-dimensional geometry problem can be reduced to a two-dimensional one by neglecting the aperture variation in one direction. Iwai (1976) and Nolte et al. (1987) concentrated on contact areas and did not consider the aperture variation perpendicular to the joint plane. Neuzil and Tracy (1981) neglected the contact areas and assumed the aperture to be constant in the direction of flow, so that the joint consisted of many parallell plate conductors with different constant apertures. Tsang and Tsang (1987) assumed that the flow occurs in a number of channels that have statistically the same volume but a varying aperture in the direction of flow. The different conceptual joint models can be compared in Figure 2.15 and Figure 2.16.

Flow through a three-dimensional model of a joint has also been studied by Tsang et al. (1987). They divided a quadratic joint plane into many small parallell plate with a varying aperture, Figure 2.17. No flow conditions was imposed on upper and lower boundaries and a constant pressure head was kept between the left and right boundary. Using a matrix solver the system of mass balance equations yielded the pressure at each node, and the flow between adjacent nodes was calculated with the cubic law. The joints shown in Figure 2.17a and b have statistically generated apertures, following a log-normal distribution with a spatial correlation length of 0.1 and 0.4 respectively. The corresponding flow field for the same joints is shown in Figure 2.18a and b.

The same problem was also solved numerically by Brown (1987) for a joint aperture distribution, described in section 2.1 and shown in Figure 2.9. The flow field for this joint at two different degrees of contact is shown in Figure 2.19a and b. The length of the vectors represents the local flow rate. The total volume flow rate was calculated by adding the contributions from the vectors along any line across the fracture.

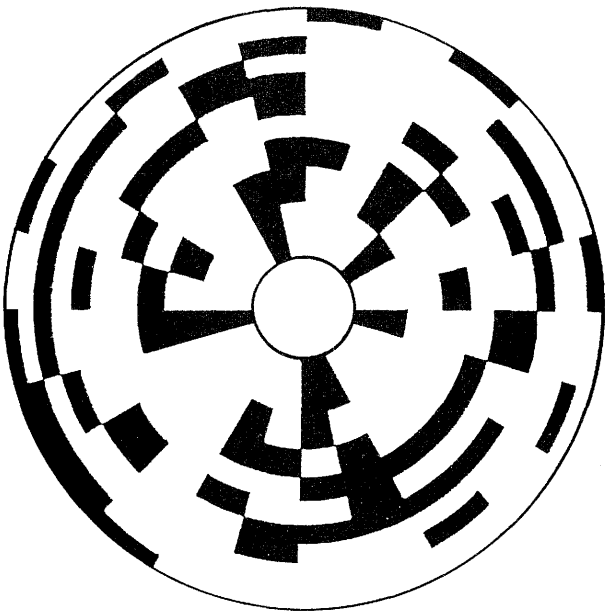

a)

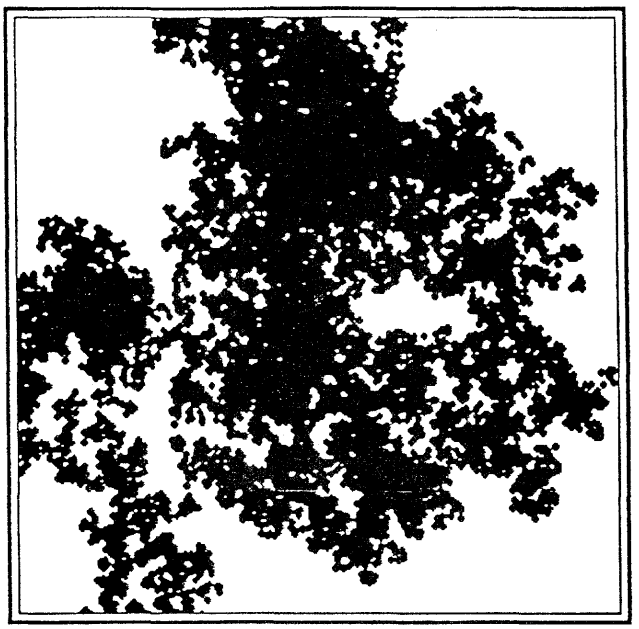

b)

XBL 8611-4763

Figure 2.15 a) An example of a distribution of contact area used in a numerical investigation of the effects of contact area on flow. The mesh simulates a radial flow and the contact area (black elements) is 30 %. Iwai (1976). b) Fractal stratified percolation plot with the fractal dimension D = 1.80. This type of model is used to simulate the contact area images from experiments shown in Figure 2.7. Nolte et al. (1987).

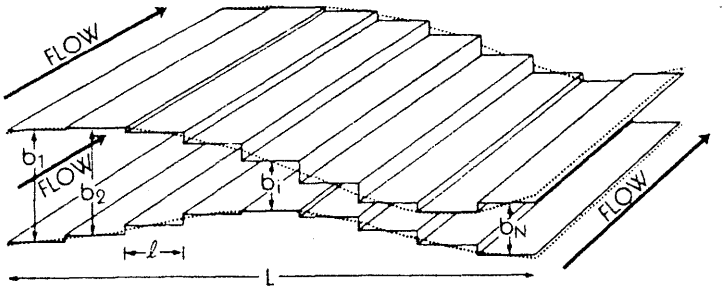

a)

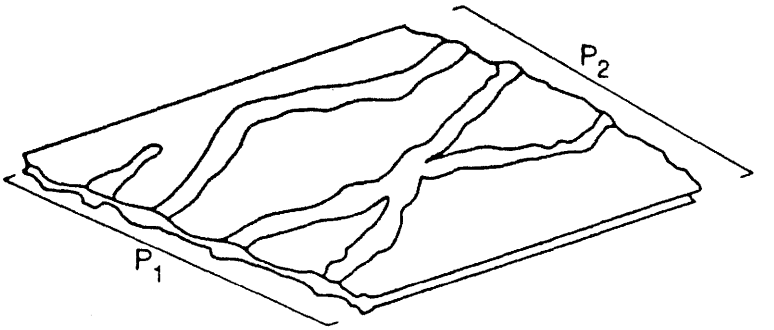

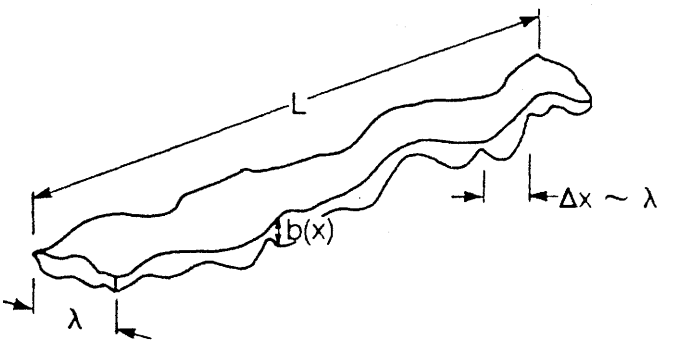

b)

Figure 2.16 a) Conceptual fracture model used to develop modified Poiseuille equation. Neuzil and Tracy (1981). b) Schematic diagram of the channel representation of fluid flow in a single fracture and a schematic sketch for one channel. Tsang and Tsang (1987).

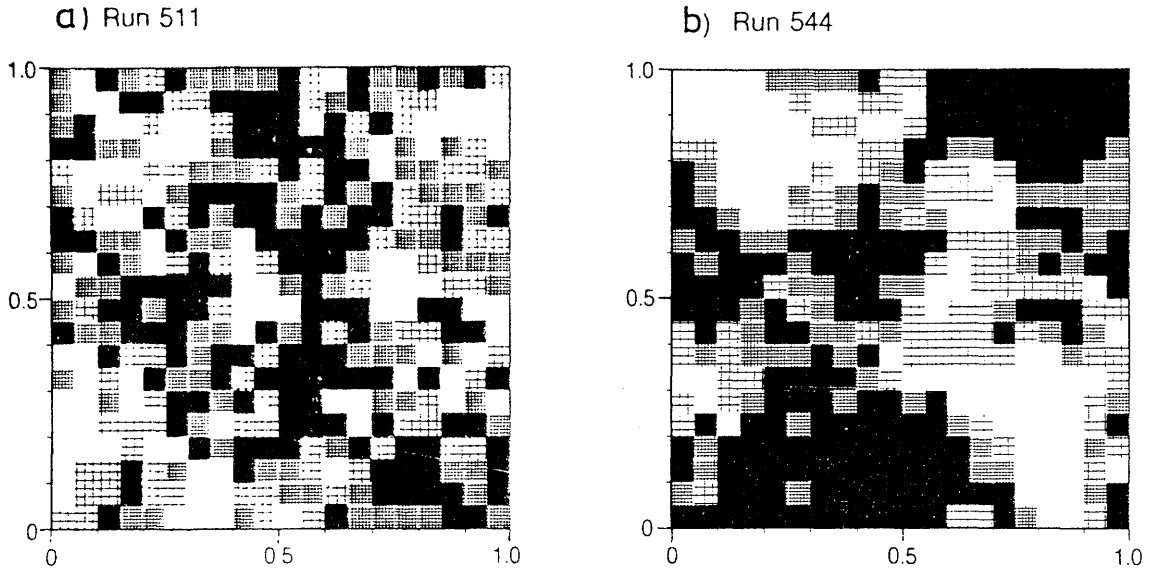

Figure 2.17 Statistically generated apertures with a spatial correlation length of a) 0.1 and b) 0.4 in the plane of a single fracture of linear dimension 1.0. Tsang et al. (1987).

Figure 2.18 Fluid flow rates for the fractures with aperture variations as shown in Figure 2.17. The thickness of the lines is proportional to the square roof of the flow rates. Tsang et al. (1987).

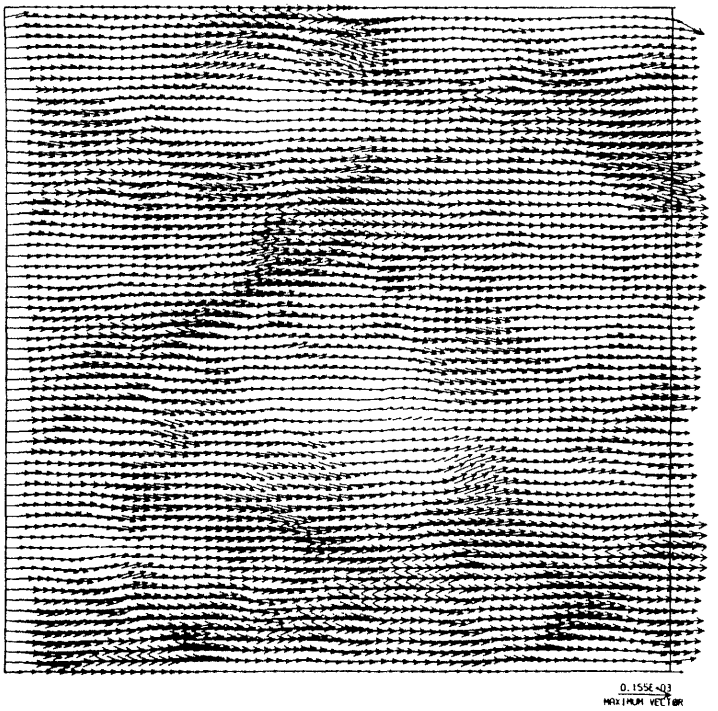

a)

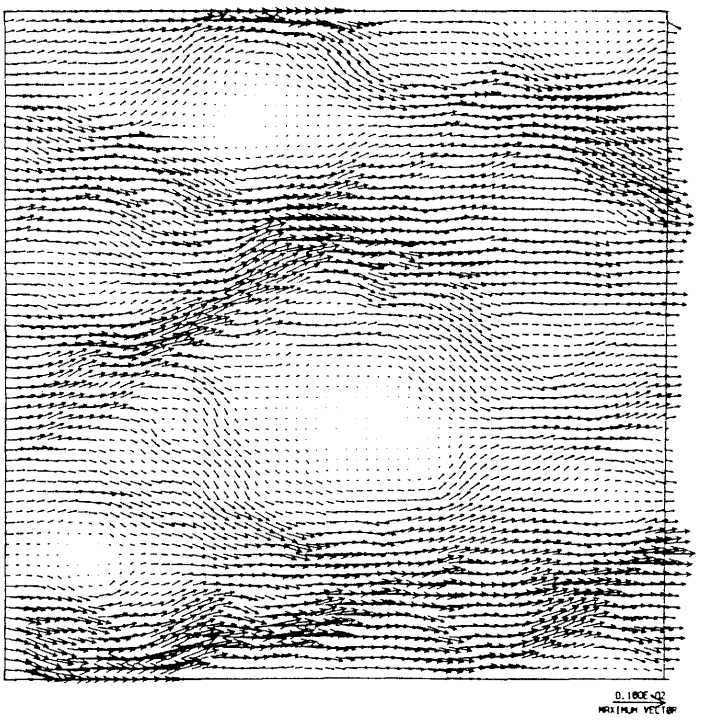

b)

Figure 2.19 a) Flow field resulting from the finite difference solution of Reynolds equation for a surface separation of $d_m = 10\sigma$. Surfaces are completely separated. b) Flow field for the same fracture as in figure a) but with a surface separation of $d_m = 4\sigma$. Surfaces are just touching with a fractional contact about area 0.4 %. Contacts are shown as blank patches. Brown (1987).

The major purpose of the simulations by Brown (1987) was to study the nature of the disagreement between the cubic law and flow through rough-walled joints. The simulations were done with statistically equivalent joint surfaces with the same standard deviation and the fractal dimension D = 2.5. The degree of closure, or separation between surfaces, was given by the parameter d_m/σ where d_m is the mean separation of the joint surfaces and σ is the standard deviation of the Gauss height distribution (see also section 2.2). An effective parallel plate aperture or "hydraulic" aperture d_h was obtained for each simulation using the total volume of flow obtained and the average gradient in the cubic law.

Different modifications of the aperture term to be used in the cubic law have been suggested by work of others. Therefore Brown compared the total flow rates from his simulations for a single joint with the flow rates predicted by different versions of the cubic law, Figure 2.20. A perfect prediction would plot as a horizontal line of level 1.0. The aritmetic mean aperture gave better results than either of the more complicated averages.

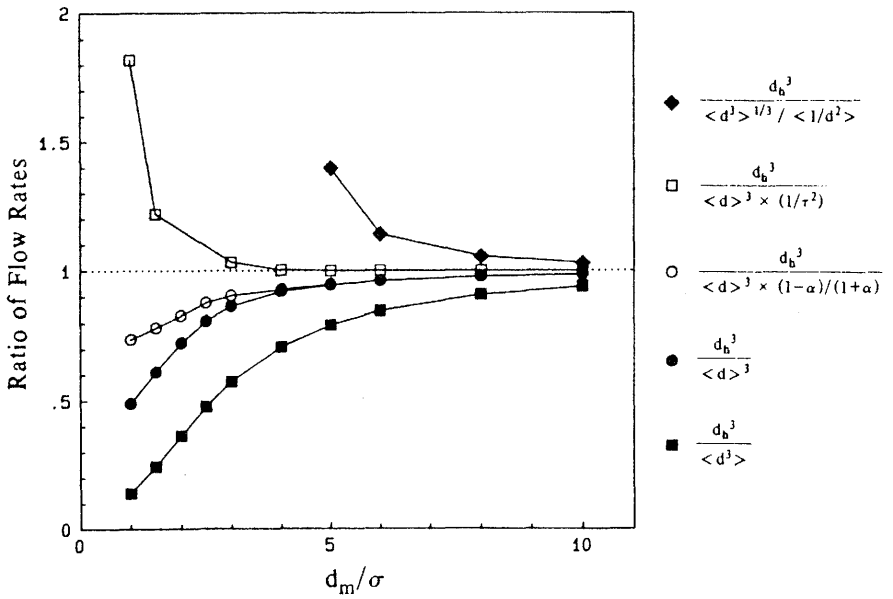

Figure 2.20 Comparison of the hydraulic aperture d_h from computer simulations to several corrections and modifications of the aperture term used in the cubic law. Brown (1987).

The conductive nature of a single joint may also be studied experimentally with tracer tests. This approach is especially attractive when the research is aiming at prediction models for groundwater transport. In a word tracer tests here means that tracer is injected at the inflow, at a known concentration C_0, and the tracer concentration C at the outflow is continuosly measured. The time-concentration relationship obtained is called the breakthrough curve of the experiment.

The transport in the joint will be influenced by molecular diffusion, chemical or physical interaction with the rock, and fluid velocity variations. To explain the experimental results a theoretical model for each mechanism must be adopted. For the model of fluid velocity variation, the question is again a matter of the most probable void geometry of a joint.

Moreno et al. (1985) carried out tracer tests on two natural joints (270 X 100 mm) from the Stripa mine. Their results were analyzed by two different models. In the first it was assumed that the velocity variation is due to hydrodynamic dispersion in a parallel walled joint. In the second model the joint consists of parallel unconnected channels, the channel widths having a log-normal distribution (cf. Neuzil and Tracy, Fig. 2.16a). The hydrodynamic dispersion in each channel was assumed to be negligible in this model.

Figure 2.21 shows an experimental breakthrough curve from a tracer run with Strontium together with curves fitted with the hydrodynamic model and the channeling model. Both models fit well although they describe different mechanisms. None of them could be disregarded based on these experiments. If the parameters obtained from the fitted curves are later used in a prediction of the breakthrough curve, for the same joint, in a different situation, the result will strongly depend on the selected model as illustrated in Figure 2.22. The channeling dispersion model predicted in this case a higher dispersion and a very much earlier arrival compared to the hydrodynamic dispersion model.

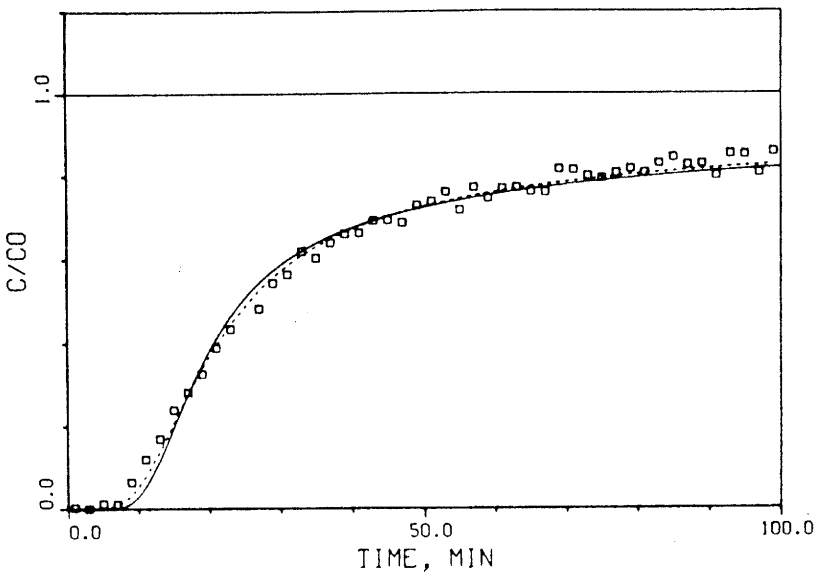

Figure 2.21 Curves fitted with the hydrodynamic despersion model (solid line) and channeling model (dashed line) for strontium (run A 16). Moreno et al. (1985).

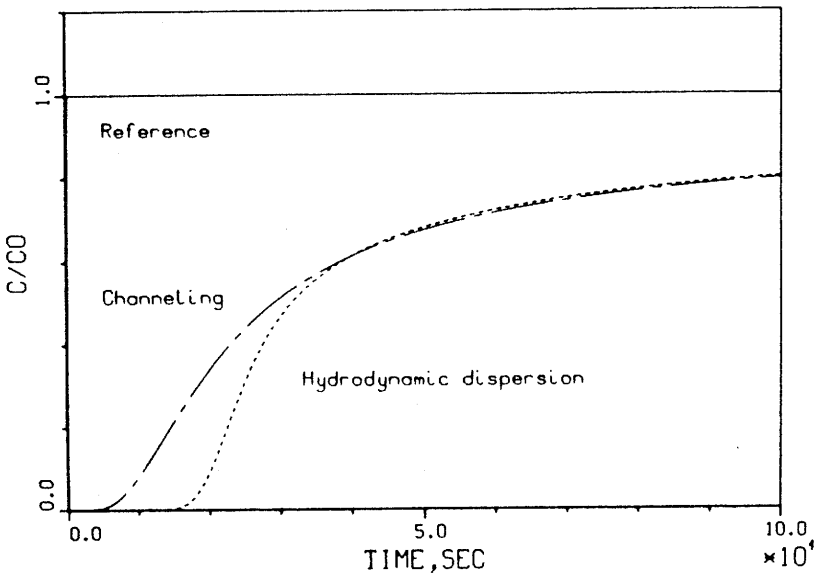

Figure 2.22 Predicted curves using the hydrodynamic dispersion model and the channeling dispersion model for sorbing tracer considering surface and volume sorption and diffusion into the matrix. The flow distance is longer and the water velocity lower than in the reference case. Moreno et al. (1985).

Tsang and Tsang (1987) further analysed the experimental results presented by Moreno et el. (1985). They noted that the breakthrough curves had a rather steep rise in the early times and some "stair-step" structure, Figure 2.23a. These features were explained by means of a channel representation of fluid flow.

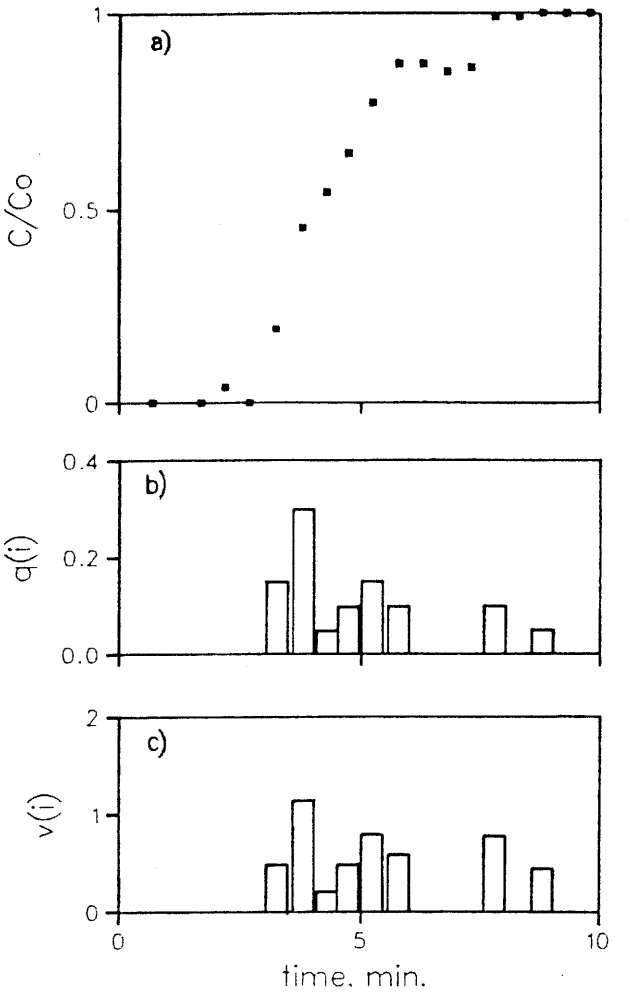

Figure 2.23 a) Experimental tracer concentration breakthrough curve (from Moreno et al. (1985). b) Derived flow rates of channels versus breakthrough time. c) Derived volume of channels versus breakthrough time. Tsang and Tsang (1987).

They propose that flow takes place only in a number of channels which have a variable aperture in the direction of flow and have a constant width (a schematic diagram of the concept was shown in Fig. 2.16). They further assume that the aperture density distribution can be approximated by a gamma function with a spatial correlation length λ and that all channels are statistically equivalent. This also implies that all the channels have essentially the same volume. One of the generated realizations of the channels, with a prescribed mean aperture $2b_0$ = 80 μm and correlation length λ = 0.15, is shown in Figure 2.24.

This flow model is interesting because it gives the possibility to abandon the idea of the single joint as a starting point in modelling the conductivity of a rock mass. The channels are one-dimensional elements which may lie in many different joint planes. The distribution of pressure and flow through such a system is shown to be mainly governed by the small apertures along the channels and consequently very sensitive to changes in the joint aperture.

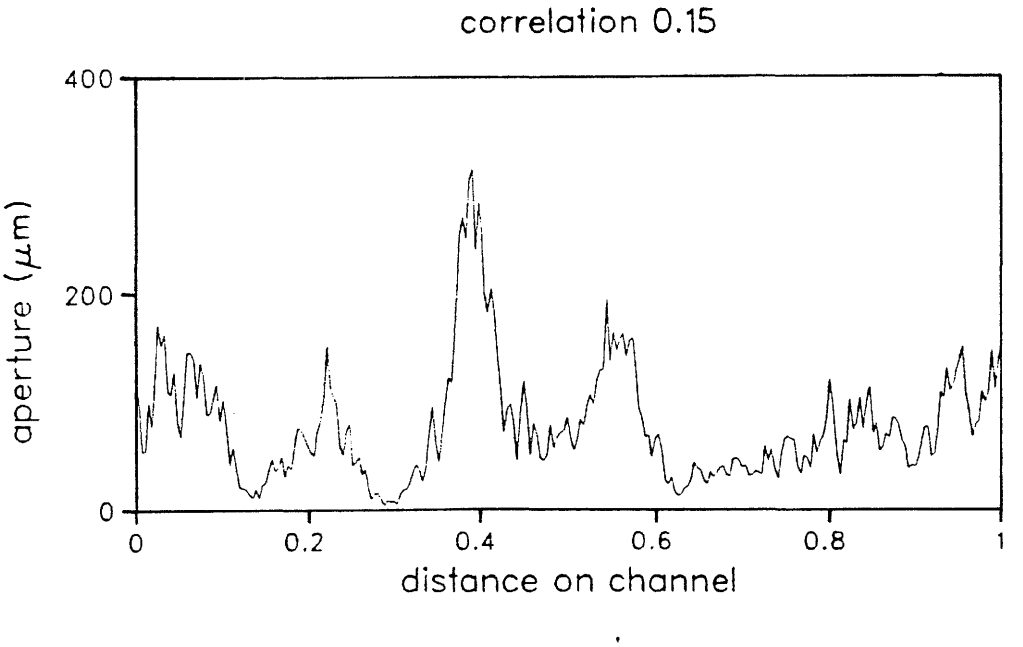

Figure 2.24 Statistically generated realization of the spatial variation of apertures with spatial correlation of 0.15 of channel length. Tsang and Tsang (1987).

On the basis of the described variable-aperture channel model, Tsang and Tsang backcalculated model parameters from the experimental data by Moreno et al. (1985), Figure 2.23a. The difference between consecutive data points was regarded as a measure of the flow q(i) carried in one channel, or a group of channels with the same arrival time, Figure 2.23b. The product of q(i) and the travel time gave the volume v(i) of the channels, Figure 2.23c.

These integrated values from the breaktrough curve were used to predict the curve for the joint after closure. They then assume that a single closure value δ can be subtracted from all aperture values so that the new volume of each channel simply becomes $(v(i) - \delta\lambda L)$. The problem of joint closure was discussed earlier in section 2.2.

2.4 Discussion

Many difficulties arises when the results from different work is to be compared. First of all few samples are tested and the types of joint samples are naturally varying.

Gale (1987) used two natural granite joints from different sites, both with a diameter of about 150 mm. Pyrak-Nolte et al. (1987) used three core samples of natural joints in granite, measuring 52 mm in diameter. They presented the result from woods metal injection in a picture representing an area of about 14 mm^2 (Fig. 2.7d). Abelin (1986) performed tracer tests with travel distances about 5 and 10 m.

In all the three examples above the authors are discussing the effects of channeling on their results. However, it is questionable if the term "channeling" in these different contexts can be quantitatively related to each other. The different scales could have different geometrical properties each causing channeling effects, for example channels along block edges in the bigger scale of a field test, Carlsson and Olsson (1977).

The term "single joint" that is often used, should ideally represent the whole joint element used in network modelling. However, only very small samples of joints are tested in the laboratory. The presumption that a joint has constant properties over its whole extension is optimistic. One must expect the joint to be different in some parts compared with other parts.

Another parameter which is difficult to define, and therefore complicates the comparison of results, is the aperture. The definition of aperture is not the same in different investigations. An explanation of this lies in the circumstance, discussed in section 2.2, that there has been no direct and easy means of measuring the aperture.

The different attempts to describe the complex geometry of a joint in more detail involve so strong simplifications that comparisons should be made with great caution. Extensive agreement between result from different work cannot be expected.

Regardless of the difficultes mentioned above in comparing the results, there seems to be some common conclusions:

- The contact area rises from a few percent up to 30 - 50 % at high normal loads.

- The aperture varies over the surface and can be described by statistical distributions.

- The flow will take on tortuos stream lines due to the complex void geometry.

- The concept of cubic law can be used for total flow estimations through joints if a correction factor is used.

- The flow will diverge to some extent from the cubic law especially when the joint is far from the parallell-plate case, i.e. at small apertures and big contact areas.

Numerical studies have given some quantitative results on subjects related to channeling. Yet on the experimental side there is a lack of quantitative results on these subjects such as:

- the correlation length of the aperture distribution
- the velocity variation of water flow inside a single joint
- the flow per rock joint surface
- the extent of tortuosity, i.e. the real travel length

All theoretical models for flow in rock joints need a further confirmation from experiments in laboratory and in-situ, to be justified. More knowledge about the hydraulic character of the rock joints will therefore be needed to judge which single joint model that is closest to reality.

3 EXPERIMENTAL TECHNIQUE

A flow visualization technique was first used by Maini (1971). He made a transparent replica of a natural joint surface and another replica was then made from the first so that two identical but mirror image surfaces were obtained. This pair of surfaces was used to study the influence of water gradient on the so called dead water area and on the flow paths inside the joint model.

However, Maini copied only one side of the real joint and the two surface replicas he used should have given a zero aperture if they had been ideal images. It is not clear what caused the joint aperture of about 0.1 mm. A conducting space between identical surfaces actually has almost the same features as the parallell plate-case regardless of the roughness of the surfaces. In fact the roughness is not directly an important factor from a hydraulic point of view since it is the geometry of the void between the surfaces that governs the flow.

The distribution of aperture will therefore strongly depend on the "matedness" of the surfaces. Matedness is not a well defined property of joints but the two extreme degrees of matedness represents the case of zero aperture and the case of two randomly rough surfaces in contact. None of these cases can be expected to exist in nature. Even the tightest joint has got some aperture which shows that the fracturing process results in two slightly mismatching surfaces. On the other hand a shear joint or a fault, which has undergone shear movements, still shows some correlation between the two surfaces on a larger scale.

The roughness of joint surfaces, however, will gain much importance when the hydraulic response to shear stresses is considered. This is because shear movement of joint surfaces will cause dilation and consequently a change in aperture.

In the present work attempts were made to further develop the approach of visualizing the flow. It was decided to make transparent copies of both sides of natural joints as they were matching in the drill-core

samples. This provides a realistic type of variation in the aperture caused by the difference in topography of the opposite rock surfaces and the coating.

Possible channeling features and tortuosity then becomes detectable with the aid of colour injections in a water flow through the transparent joint model. We also desired to have some knowledge about the actual void geometry of the joint replicas used in the flow experiments to gain some further insight to the coupling between mechanical and hydraulic properties.

A summary of the used techniques is given below and more detailed description of the procedures can be found in the following sections.

3.1 Summary of experimental technique

- The joint model consists of a replica from each side of a natural joint made of transparent epoxy. Figure 3.1a shows an example of a rock joint surface and the epoxy replica.

- The aperture of the joint model is measured by placing a small known volume of water between the two surfaces. The area covered by the drop gives the average aperture over this area. Figure 3.1b shows a terrain model of the void space inside the joint model calculated from aperture measurements. High points correspond to larger apertures. Figure 3.1c shows isocurves from the same calculation. The results from aperture measurements can also be presented in a histogram as in Figure 3.1d.

- Different constant water pressure is applied to one side of the joint, with the sides sealed off, and the flow is measured. When a colour dye is injected at different points at the inflow of the joint model the stream lines becomes visible. Figure 3.1e shows a compilation of stream lines from photographs of colour injections.

- The time for the colour front to move from one side to the other is a measure of the water flow velocity along the actual stream line. Figure 3.1f presents the results from velocity measurements along several flow paths.

a)

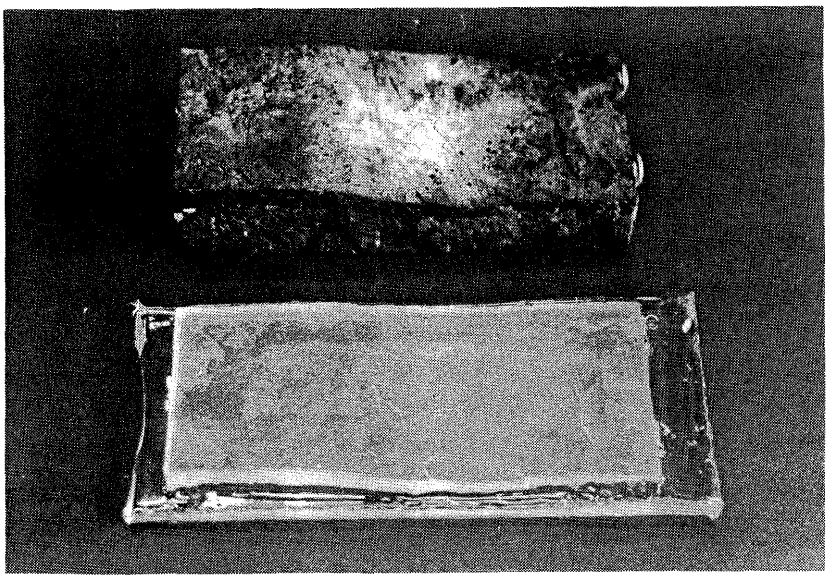

b)

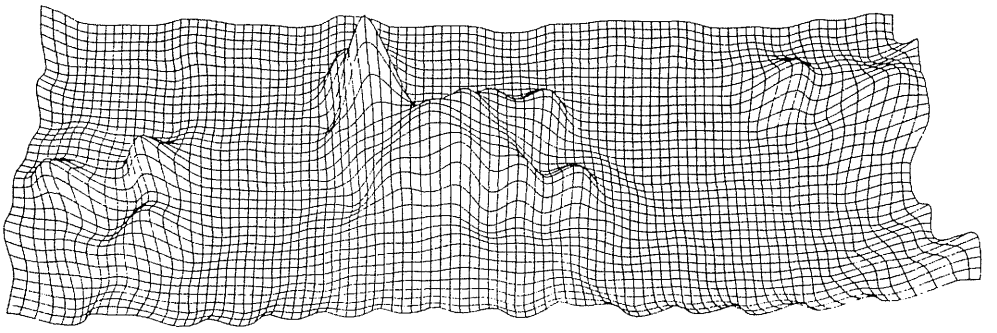

c)

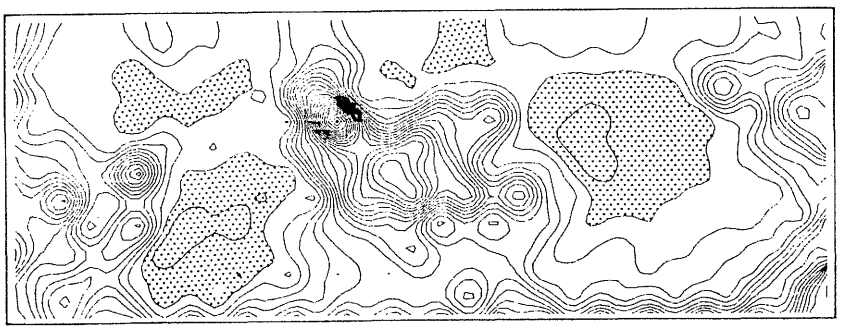

Figure 3.1 a) Rock joint and the replica in epoxy (sample B).
b) Terrain model of the void space (sample B).
c) Isoplot of the apertures (sample B).

d)

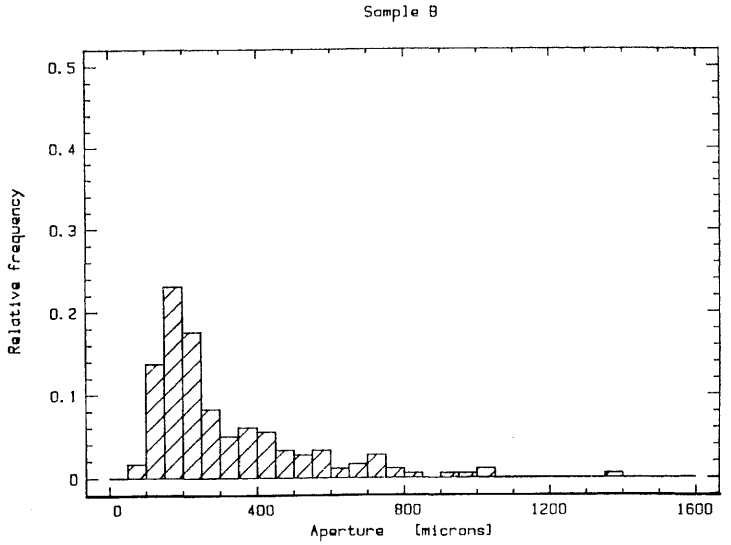

e)

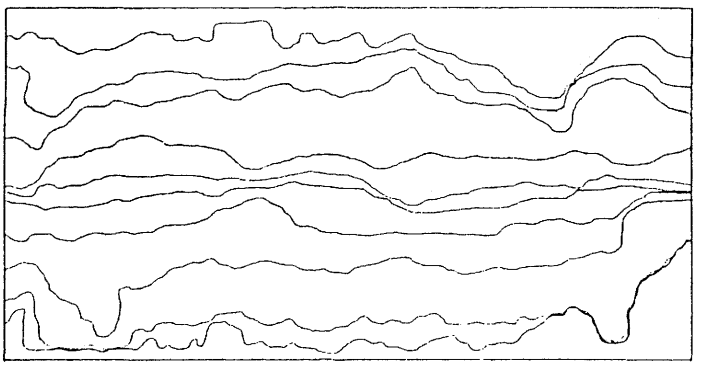

f)

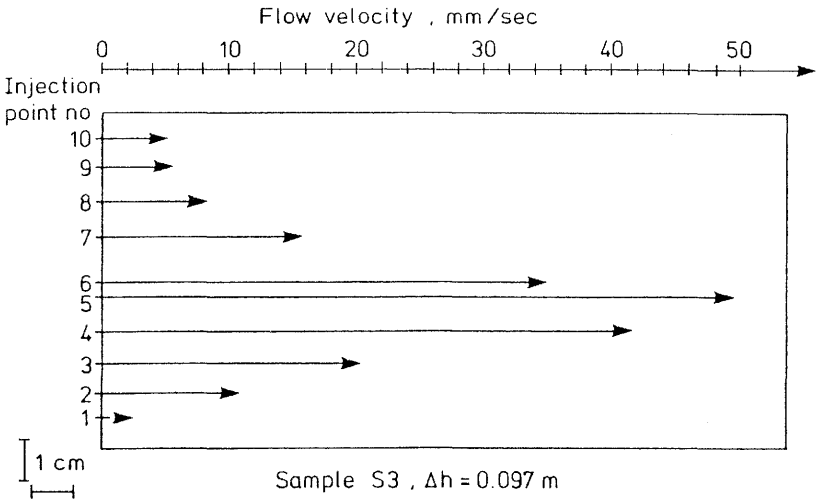

Figure 3.1 Contd.
d) Aperture frequency histogram (sample B).
e) Stream lines from colour injections (sample S3).
f) Result from flow velocity measurement (sample S3).

3.2 Transparent replicas of rock joints

A natural joint is selected from drill-core or from a rock exposure. After necessary cutting of the specimen the surfaces are cleaned and dried. Joints with very weathered or soft coatings might be difficult to copy correctly since the mere drilling and handling of the core will disturb the original condition of the joint significantly.

A two-component silicon rubber (Silastic 3112 RTV) is applied in a thin layer on the surfaces. To assure a good release between rubber and rock, in particular when there is no coating, a very thin film of teflon is sprayed on the surfaces prior to the application of rubber. The rubber should be properly de-aired by vacuum-pumping to avoid air bubbles to form on the surfaces. When this layer of rubber is cured the rock specimen is put upside down, standing on short "legs" glued to the boundaries or, in case of a big specimen, held by a fixture as in Figure 3.2. A second layer of rubber is moulded to fill up the space under the surface and around the specimen (Fig. 3.3). After curing, the silicon rubber can be pealed off from the rock specimen.

The two rubber casts are then used as moulds in the second phase. The pealed off rubber surface is a negative copy of the original. If small pieces from the rock joint sticks to the rubber surface they should be pealed off to give a correct replica.

A strong, transparent two-component epoxy (see chapter 3.3) is used for the replicas. It can be molded in layers if desired. The epoxy must also be de-aired, in particular in the first layer, to assure a proper surface and a good transparency.

Before using them in any experiments the edges of the replicas are cut off since the rock joint surfaces often are damaged at the edges due to drilling and cutting. Figures 3.4 and 3.5 shows an original joint from the Stripa Mine (S2) and the finished epoxy replica of this joint.

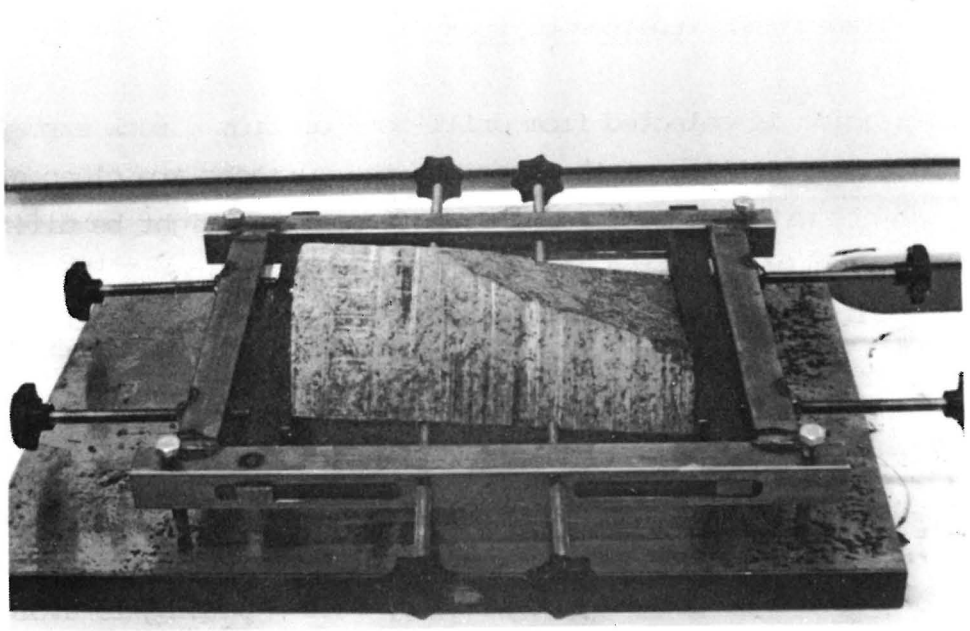

Figure 3.2 Rock joint sample (S4) held in a fixture with the surface downwards during the moulding of the second layer silicon rubber.

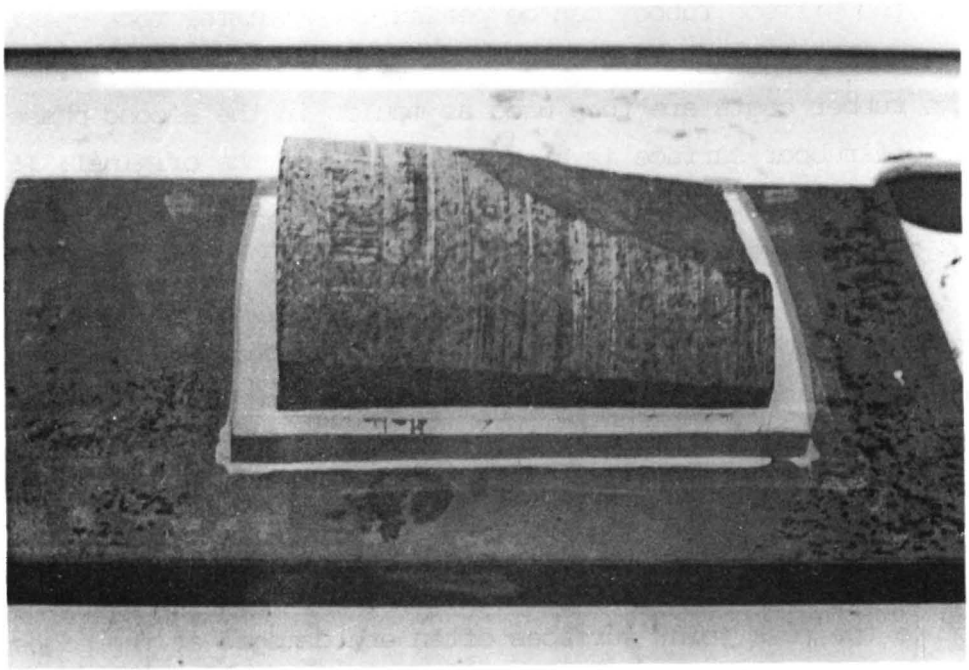

Figure 3.3 The silicon rubber is cured and can be pealed off from the joint surface. The rubber cast is used as a mould for the epoxy replica.

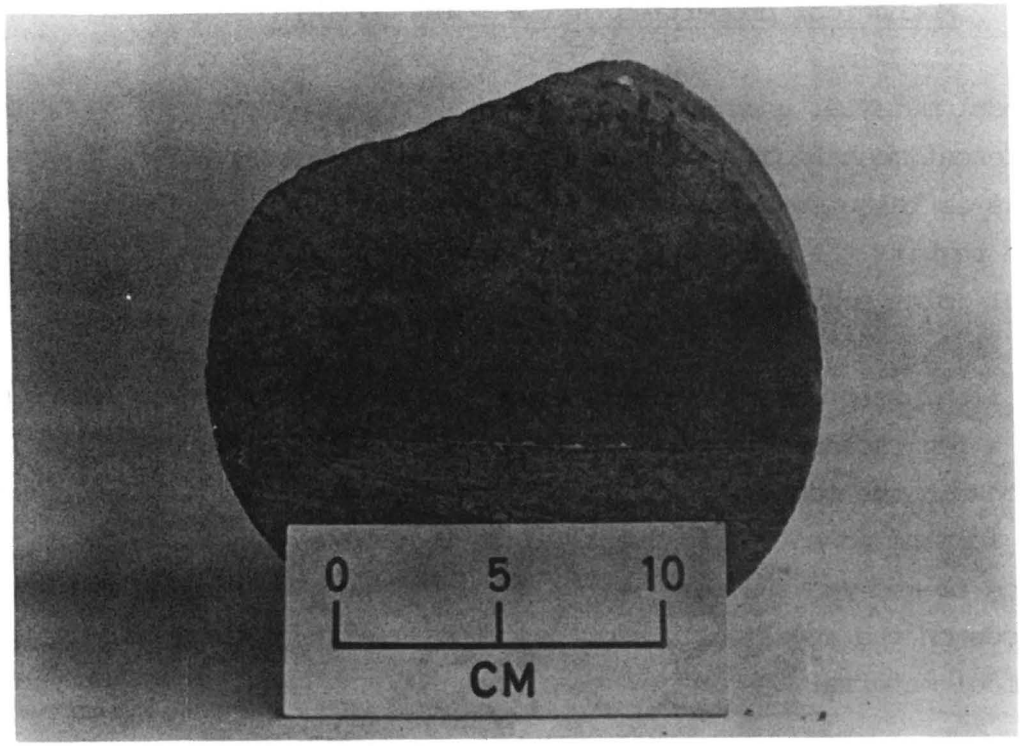

Figure 3.4 Rock joint sample S2.

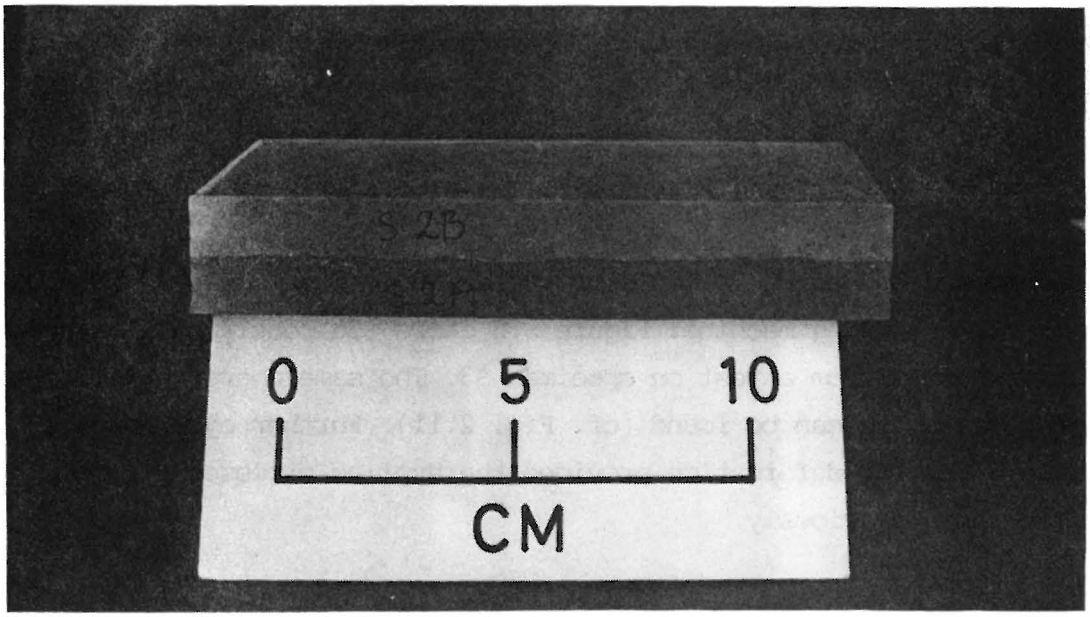

Figure 3.5 Epoxy replica of the joint S2.

3.3 Mechanical properties of the joint models

The model material used in the replicas is an epoxy and has of course a different mechanical behaviour compared with rock material. However, if this is taken into acount in the experiments and in the evaluation of the results the models will still give valuable information on natural joint behaviour.

It is found that natural joints behave elastically to normal loading after a few cycles (Fig. 2.11). It is then reasonable to assume that the rock in the contact areas is subjected to stresses in the elastic range for the rock type in question. We therefore expect the joint replica to undergo the same series of deformation as long as the stresses on the specimen is kept low with respect to the strength of the model material.

According to the specification the epoxy used, Araldite F with Härter HM (Ciba-Geigy), has a compressive strength of 40-50 MPa and an elastic modulus of 3.0-3.1 GPa. We performed two uniaxial tests on a cylinder in the epoxy (Φ 42 mm, L = 80 mm). The load-deformation curve showed a plastic behaviour after peak and elastic behaviour up to peak. The compressive strength, counted from the onset of plasticity, was calculated to 70 MPa and 74 MPa respectively. The secant elastic modulus at 50% of peak load was 3.6 GPa and 3.5 GPa and the initial elasic modulus was 2.5 GPa for both. This implies that the model material is about twenty times as compliant as a granite.

Loading and unloading cycles were performed on the models in a servo-controlled testing machine. Figure 3.6 shows the resulting load-deformation curves from a test on specimen S3. The same characteristics as for rock joints can be found (cf. Fig. 2.11). Further cycling will cause a similar deformation provided the applied stresses are not higher than previously.

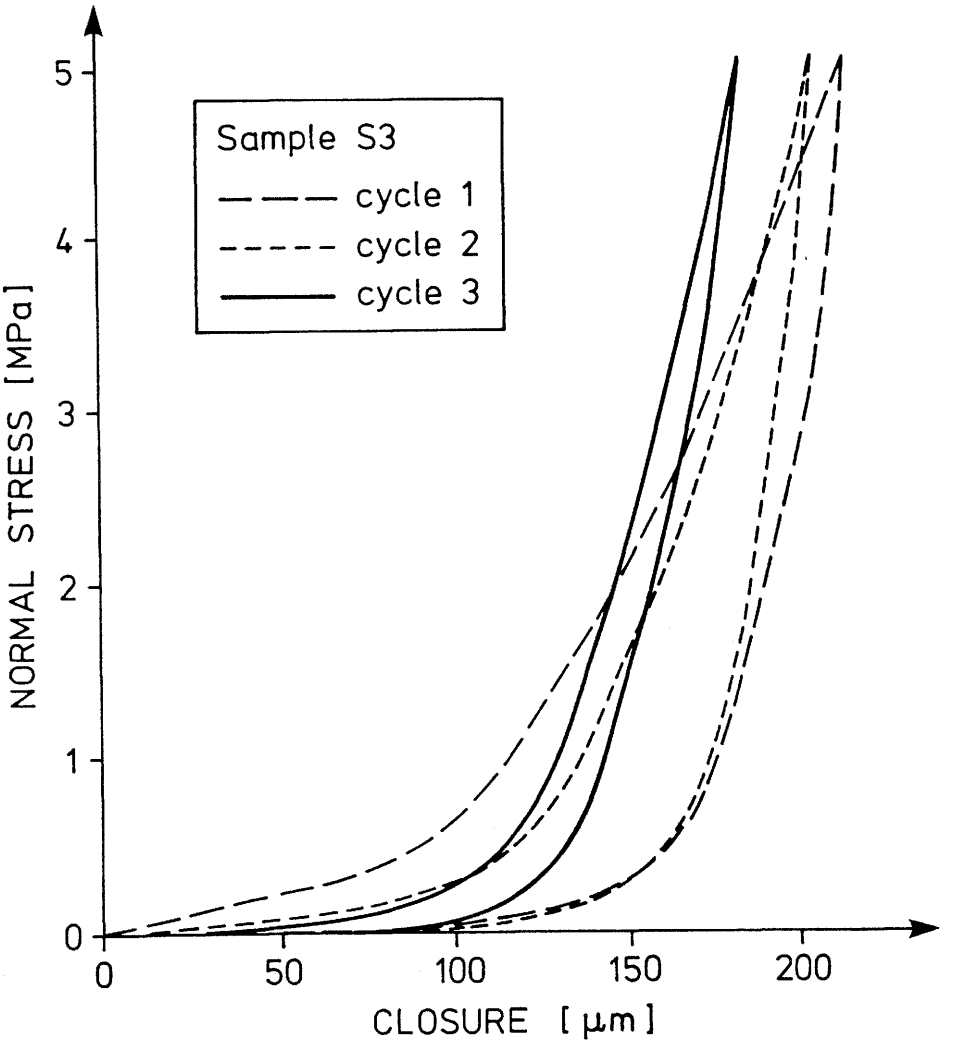

Figure 3.6 Load-deformation curve from cyclic loading of the epoxy joint replica (sample S3).

3.4 Measurement of joint aperture

3.4.1 Procedure

The joint replicas were made transparent mainly to give the possibility of visual studies of flow. However this property of the replicas also made it possible to develop a special technique for aperture measurements. This technique consists of the following steps.

- A small volume of water is measured with a constrictionspipette (Fig. 3.7). Volumes from 500 µl down to 5 µl can be measured with an accuracy of 0.5 µl. Drops with a volume of 10 µl were used in our measurements.

- A set of water drops are placed between the two joint surfaces. A grid pattern of dots is placed underneath the sample as an aid to get an even spread of the measuring points. The density of points in the grid is about one point per cm^2.

- The joint is pressed together in a loading arrangement with plexi glass platens, as shown in Figure 3.8.

- The shape of the water drops are recorded, most conveniently with a photograph. Figure 3.9 shows 10 drops each 10 µl, which are inside the specimen A.

- The area A_n of each drop is calculated. This can be done with a digitizing table and a computer program for area calculation.

- The average aperture E_n over the small area A_n covered by one drop is calculated as

$$V_{drop}/A_n = E_n$$

- The procedure is repeated for new sets of points on the joint surface until all points of the grid have been measured.

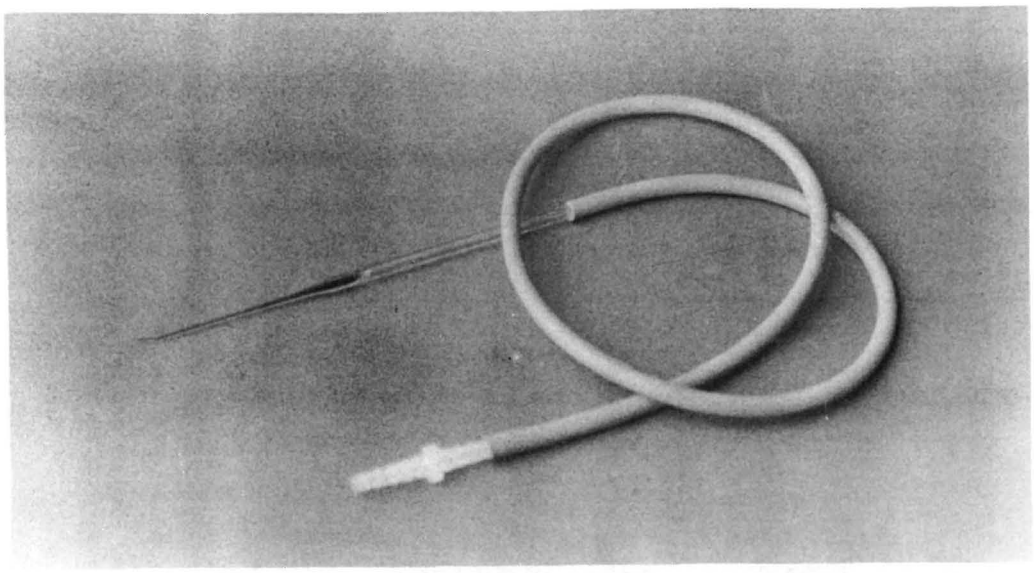

Figure 3.7 A constrictionspipette used for accurate measurement of small volumes of liquid (the water is coloured in the photo for clearness).

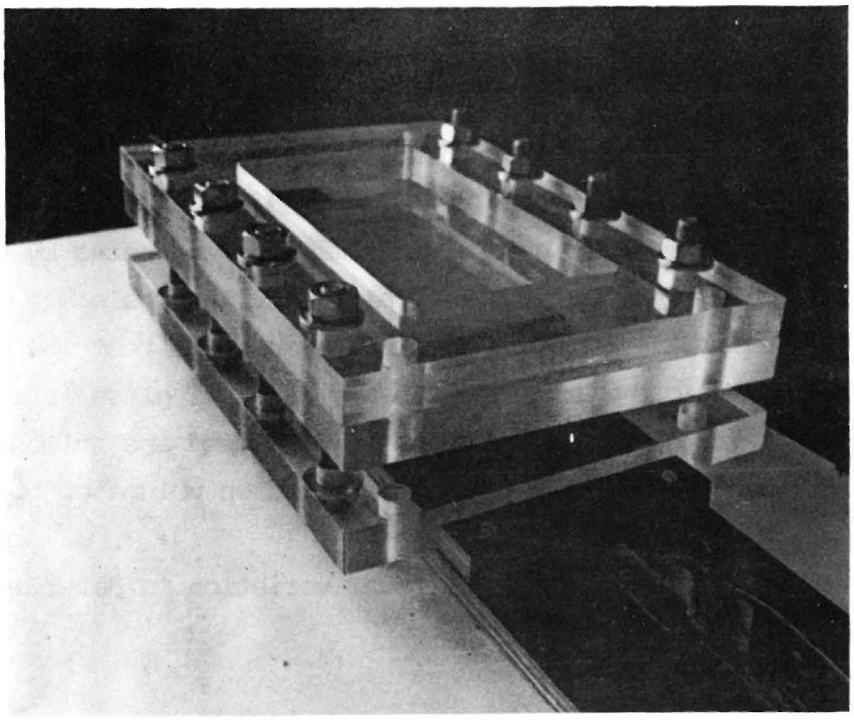

Figure 3.8 The three plexi glass platens used to compress the joint replicas (2 cm thickness). The bolts are tightened in the same order each time. The final tightening is controlled with a torque wrench.

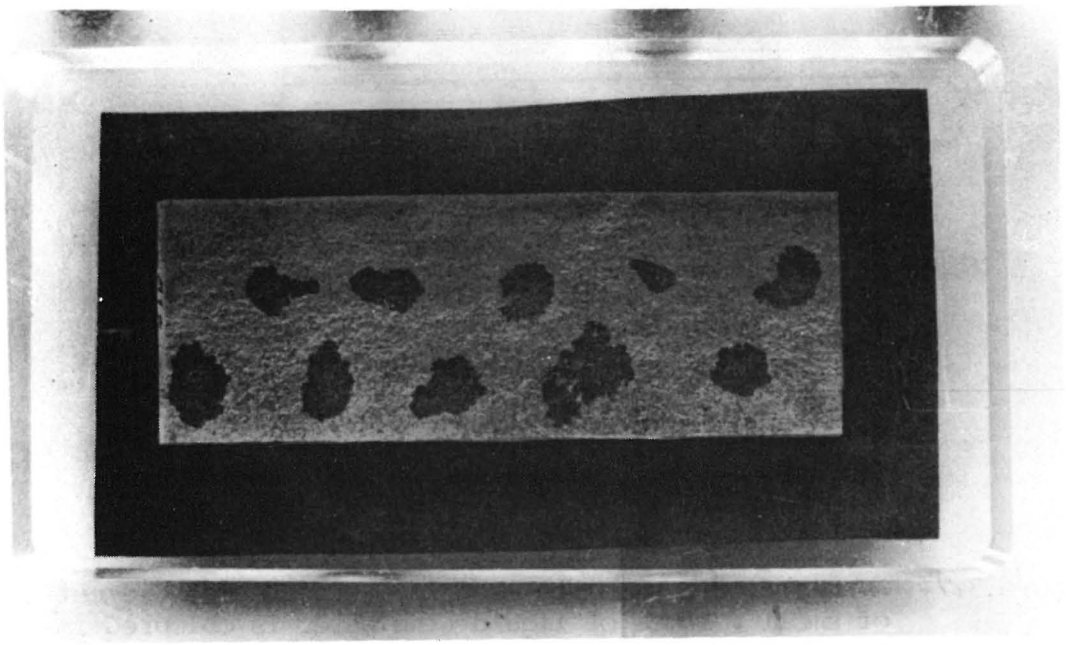

Figure 3.9 Ten drops of water (10 µl) inside sample A sitting in the loading arrangement shown in Figure 3.8. The wetting of the surfaces by the drops increases the transparency. With a dark background the covered areas contrast well in a photograph.

3.4.2 Accuracy of the measurements

The accuracy of the aperture measurement method was tested by carrying out measurements on eight points several times. The whole measurement procedure was repeated each time with new drops. The test was mainly done to check whether the load applied by the plexi glass frame could be regarded as identical if the specimen was opened and reloaded. The test was performed on sample S3 with a water drop volume of 50 µl.

The result from this test gives the total variation in determined aperture due to:

1 volume error

2 point error

3 load error

4 evaluation error

Volume error was checked with a balance which gave an accuracy of ± 0.5 mg (= 0.5 µl) for all sizes of pipette. This means an accuracy of 5 % for a 10 µl drop and of 1 % for a 50 µl drop. An accuracy of 0.9 % is specified by the producer of the pipette.

By point error it is meant the aperture variations due to the fact that the drop is not put exactly at the same point in the repeated measurements in this test. The point error can be large when the point is close to a big change in aperture. Figure 3.10 shows an example of two aperture measurements on sample B (drop volume 10 µl). The drops were intended to be placed in the same points. Note that the size of the areas are not very sensitive to the location of the drops unless the aperture is large at the point.

With evaluation error it is meant the variation in the drop area calculation. The evaluation error has been estimated by repeated evaluation on identical photographs and the comparison shows that this error is maximum 8 % for smaller apertures but up to 20 % for bigger apertures. In a case when a small drop is placed in a point with big apertures the covered area becomes very small and the calculation of it is less accurate.

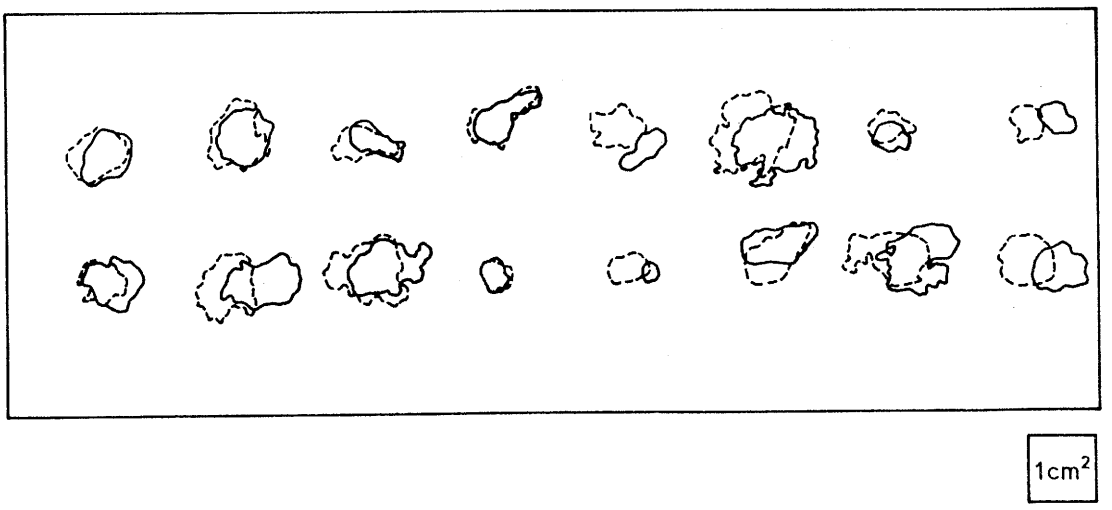

Figure 3.10 The contours from the drop areas from a repeated aperture measurements on sample B. The areas marked with solid lines correspond to one measurement and the dashed lines correspond to a second measurement.

The total variation in determined aperture was maximum ± 15 % in the test serie. Since this level of accuracy is of the same order as the sum of the errors 1, 2, and 4 for the test serie, it was concluded that the load error should be comparatively small and that the same deformation of a joint replica can be achieved by subsequent loadings.

3.4.3 Presentation and interpretation

To give a good picture of the general shape of the void geometry, the collected aperture measurements can be presented with isocurves as in Figure 3.11. The calculation is based on 89 points of measurement and is conducted with a three dimensional digital terrain model (TERMOS, Toppe (1987)). Note that the pattern of the isocurves becomes influenced by the grid pattern especially when the grid is coarse.

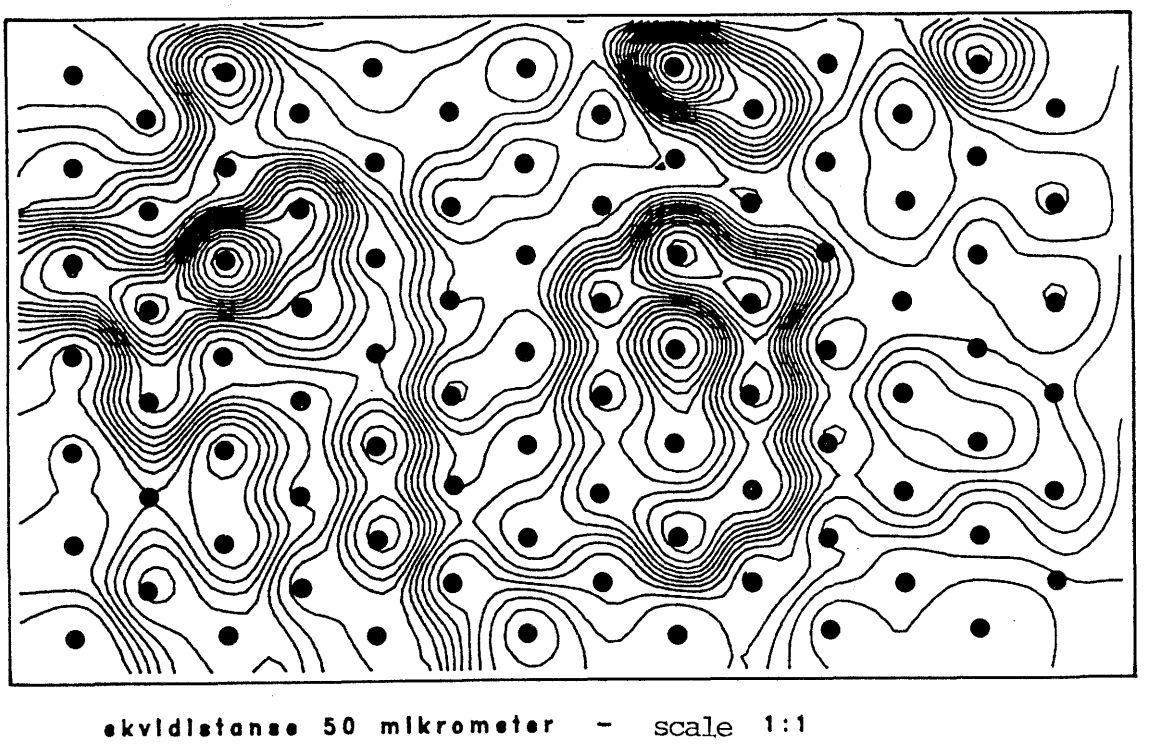

Figure 3.11 Isocurves of the apertures of sample S2 (148X88 mm). The void geometry of the whole surface is determined based on measuremants in the 89 point marked on the isoplot. The calculation is conducted with a digital terrain model (TERMOS).

The results can also be shown as a 3D-plot of the terrain model as in Figure 3.12. The higher parts of the plotted surface correspond to larger aperture values. Note that the modelled geometry is that of the void inside the joint and should not be confused with similar plots of joint surfaces.

An important feature of this method is that it only gives the average values of the apertures over the area covered by the small drop of water, even if these areas are small compared to the whole joint area. This means that the extreme pointwise values of the true aperture distribution will not be directly measured. However, since there is a spatial correlation between the values of aperture in the joint plane (see Brown (1987)) the averages from different small areas of the joint surface will still have a considerable spread. This correlation is also illustrated in the Figure 3.10 where the areas are fairly insensitive to small changes in location.

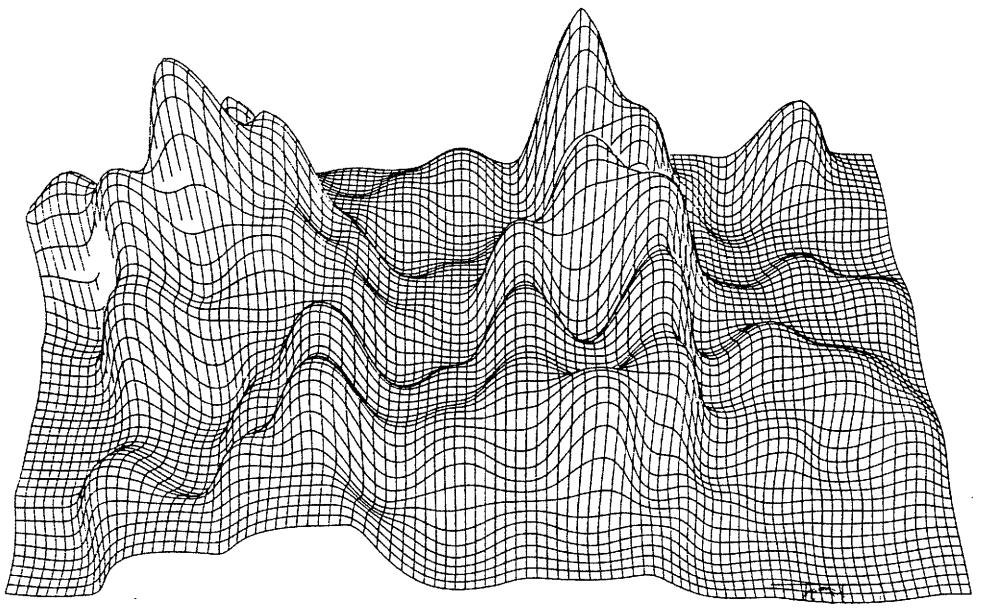

Figure 3.12 A terrain model showing the topography of the void space inside sample S2. The scale for the apertures are exaggerated for the sake of clarity. The higher parts correspond to areas with larger opening.

An advantage with the this way of measuring is that there is no need to get the average aperture value via point wise measurements, nor via models relating profile and 3D distributions.

The aperture distribution can also be illustrated by a frequency histogram of the measurements, Figure 3.13. The histogram is plotted with a computer package for statistical analysis (STATGRAPHICS). Using this package many different analytical distribution functions can also be fitted to the experimental data. In the Figure 3.13 the best fit log-normal function is plotted together with the histogram.

Generaly the aperture distribution from a well mated joint takes on a sharply peaked shape while the distribution of an unmated joint is broad and flat. The distribution may also show a skewness towards one side or the other.

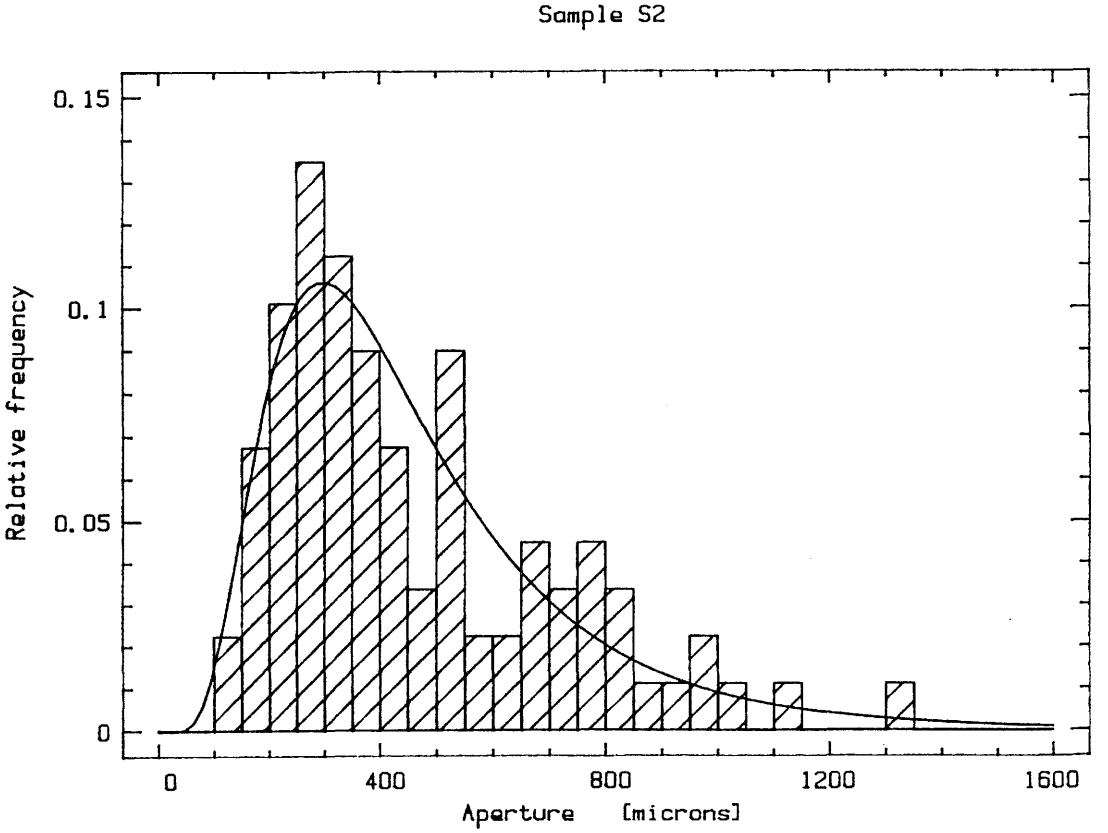

Figure 3.13 Frequency histogram of aperture values measured on sample S2. The fitted curve is a log-normal distribution function ($\bar{x}$ = 464 μm, σ = 273 μm).

3.5 Flow experiments

3.5.1 Experimental set-up

The sides of the joint replica are sealed off with a silicon rubber. A water pressure is then applied at the inflow side via an "intake box" made of plexiglass which is glued to the smaller side of the specimen and is connected to the water pipe, Figure 3.14. It is assumed that the water pressure is constant along the width of the specimen since the flow velocity is low. A similar arrangement is made at the outflow side of the specimen where the water pressure is zero.

The water pressure is built up by the level difference between the specimen and the water container. A constant water pressure from the container is arranged by a "double-bowl-system" shown in Figure 3.15. The inflow to the inner small bowl is kept bigger than the outflow, which enters the joint specimen, so that there is always an overflow and the water level is constantly at the edge. The inflowing water is supplied from a big container where it is de-aired.

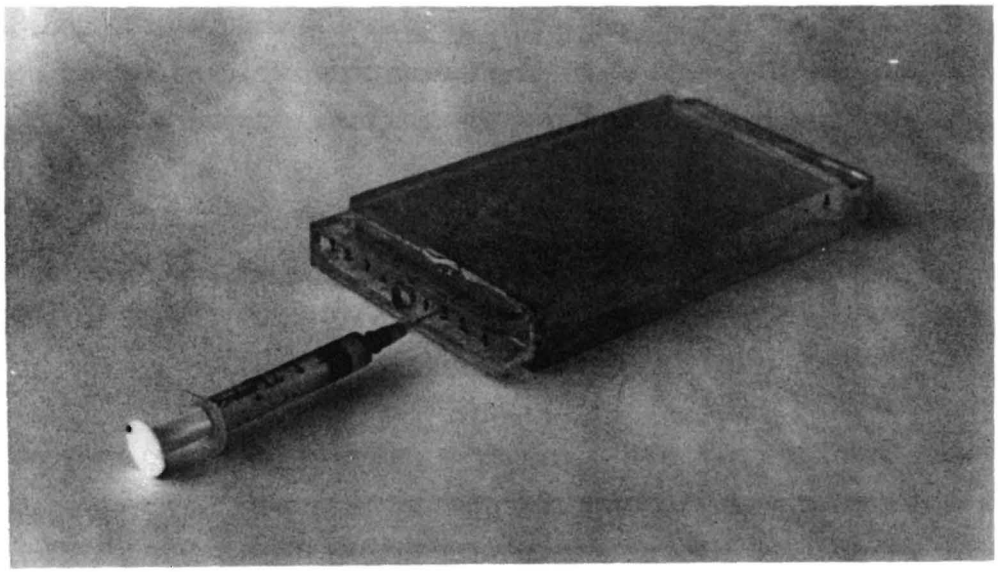

Figure 3.14 An "intake box" made of plexi glass is glued to the specimen. Colour injections along the opening of the joint is possible through small rubber-filled holes. The water pipe is connected to the central hole.

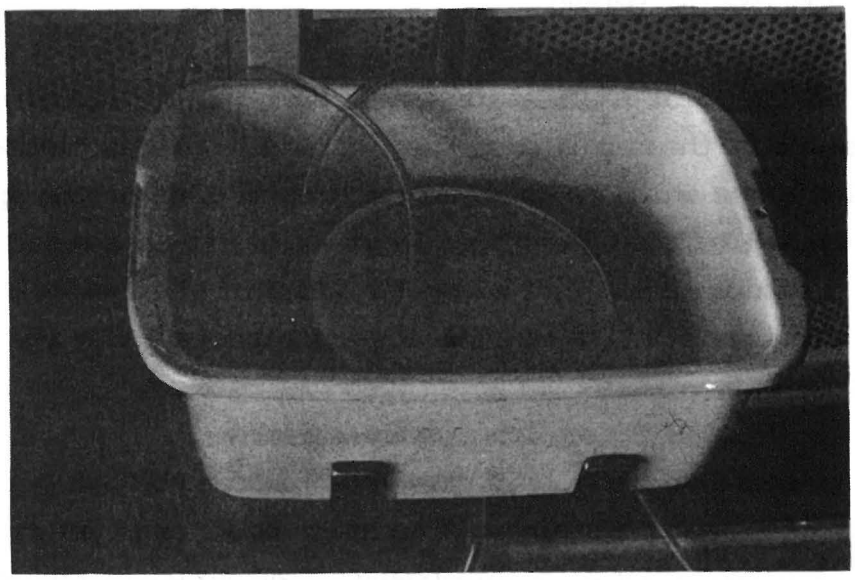

Figure 3.15 A constant water pressure is arranged by a "double-bowl-system". The inner bowl is always kept full.

During the flow tests the joint specimen is placed in the same frame as was used during the aperture measurements, see Figure 3.8, and under the same loading condition. The water pressure gradient is regulated by changes of the elevation of the fixture, Figure 3.16.

Before the joint is filled with water, a small amount of liquid soap is added to the water pipe to reduce the surface tension. With less surface tension of water the risk that air bubbles get stuck inside the joint during filling is reduced.

The flow of water through the joint is measured by weighing the outflow collected during a certain time period.

The temperature of the water is measured during the experiment in order to have the right value of the viscosity v used in the evaluation.

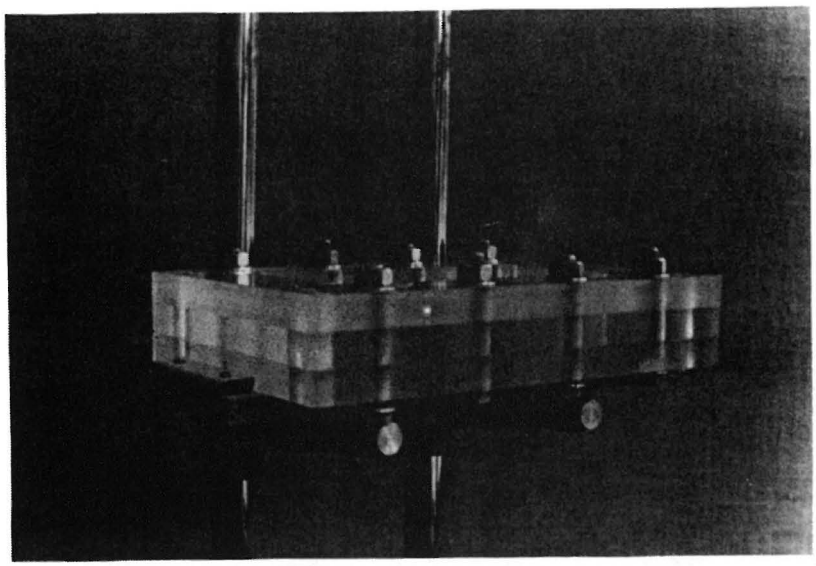

Figure 3.16 Arrangement for obtaining different water pressure gradients. The position of the fixture may be selected as required.

3.5.2 Velocity measurement

To visualize the water flowing through the joint a colour dye (methylene blue) is injected at the inlet of the flow. A syringe is filled with the dye and the needle is pushed through rubber-filled holes on the "inlet box" so that a very small amount of dye can be injected at different points along the width of the joint opening, Figure 3.14.

The velocity of the flow along the visible stream line is determined by measuring the time needed for the colour front to move between two reference lines. Figure 3.17 shows a colour injection at the moment when the front has reached half-way through the joint.

In some cases the flow from the injection point may be too small to be measured accurately. The access to some central parts of the joint opening in front of the connected pipe may also be poor because of the unavailability of the injecting points. The accuracy of the velocity measurements, therefore, might vary between different injection points. In the experiments the time was normally measured 3 - 10 times

at each point and the spread of the values was about ± 5 %. The average flow time value was used in the evaluation and it was estimated in some cases.

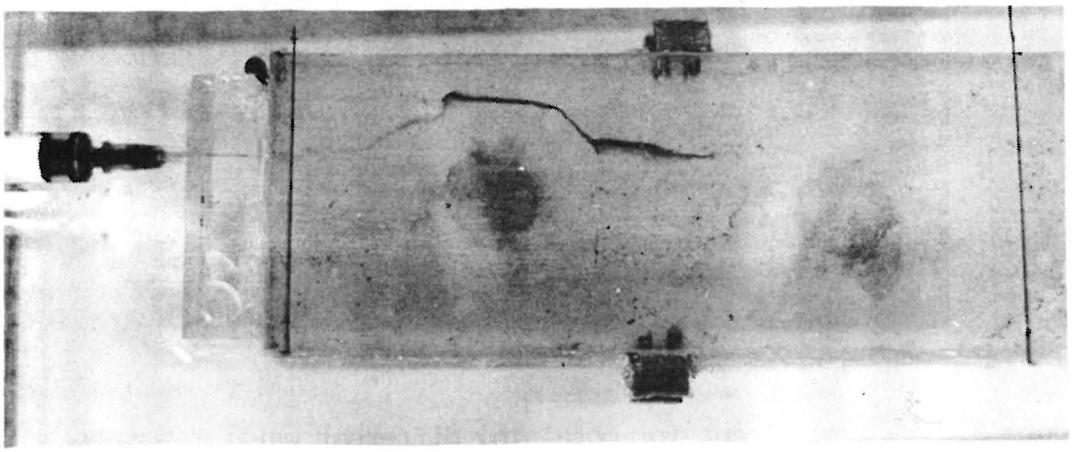

Figure 3.17 Colour injection into the flow inside a joint replica. The time needed for the colour front to move between the two reference lines. Notice how the stream widens in some areas.

A photograph is taken from each injection point which shows the path of the dye. The dye is continously injected to give a clear picture over the whole path length.

The length of the stream lines observed in the photographs may be measured for example by using a computer program, the input data of which are closely digitized points along the flow path. The quotient between the length of each stream line, l, and the length of the joint, L, is a measure of the tortuosity of the flow.

Flow in a narrow slot, such as a joint, is laminar for lower gradients but can become turbulent for high gradients. Figure 3.18 shows the transition zone between laminar and turbulent conditions of flow. One can see that laminar flow is what takes place with normally existing in-situ gradients and apertures. Our experiments were performed within the ranges of gradients and apertures indicated with the hatched area in the figure.

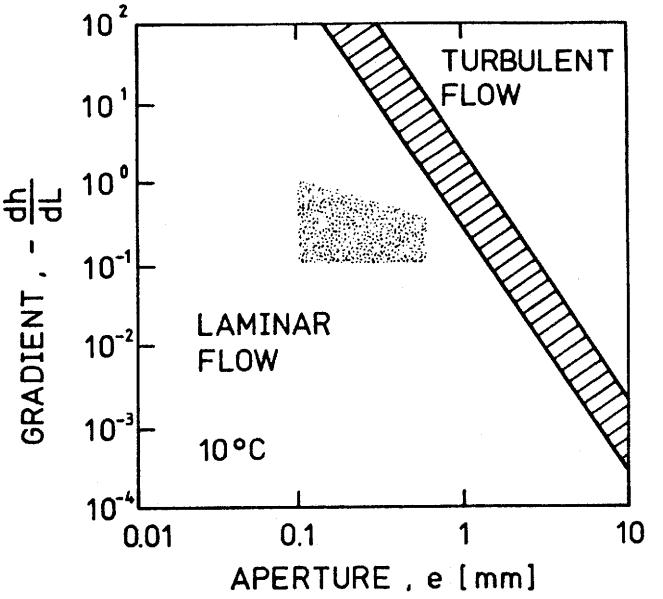

Figure 3.18 Flow regimes in rock joints. Gustavsson (1986). The hatched area corresponds to the conditions during the experiments in this study.

3.5.3 Evaluation

To evaluate the results from the flow and velocity measurements a simplifyed concept of the flow in a joint has to be considered. We assume that the total flow through a joint can be described by flow along a number of channels. Each of these channels is assumed to have a length l, a constant width b, and a constant aperture e. The flow in each channel, q, follows the flow relationship for the parallel plate case (see section 2.3):

$$q_n = \frac{b_n\, g}{l_n\, 12\, \nu}\, \Delta h\, e_n^3 \qquad (5)$$

but also

$$q_n = \bar{v}_n\, b_n\, e_n \qquad (6)$$

where $\bar{v}$ is the real average flow velocity in the channel. The measured velocity v_n along a stream line starting at the injection point is

$$v_n = \frac{l_n}{t_n}$$

where l_n is the distance along the stream line between the reference lines and t_n the time for the colour front to move between them. We then assume that this measure is proportioanl to the average flow in the channel

$$\bar{v}_n = k\, v_n \qquad (7)$$

The stream paths in the velocity measurements can be considered as representative samples of the collection of channels which the joint consists of. An approximation of the flow situation may then be made by dividing the joint into a number of channels based on the aperture and velocity measurements. The total flow can then be calculated with the equations (5), (6) and (7) as

$$Q_{tot} = \sum_n q_n = \sqrt{\frac{12\nu}{\Delta h g}}\; k^{3/2} \sum_n \left(b_n \sqrt{l_n}\; v_n^{3/2}\right) \qquad (8)$$

In the experiments all parameters except b_n and k are measured. The width b_n of the channels constituting the total flow is only conceptual and is not a measurable parameter. If the true length of the flow path l_n is used in the calculation of total flow (equation (8)) the value of b_n must be selected such that the total channel area is equal to the joint area.

However, in our evaluation of the experimental results an "efficient velocity" has been used. The efficient velocity was calculated with flow distance l_n equal to the straight distance. All channels were then assumed to have the same width, that is equal to the joint width divided by the number of channels. In this way the uncertainty in the estimation of b_n was avoided and the evaluation could be made in a fully consistent way. The calculation of total flow is, however, not sensitive to the choice of l_n and b_n since the product $b_n\, l_n$ becomes fairly constant.

Theoretically the maximum velocity of flow between two smooth parallel plates can be calculated with equation (1) (section 2.3) for z = 0. The quotient between the maximum and the average velocity (equation (2)) becomes

$$\frac{v_n^{max}}{\bar{v}_n} = \frac{3}{2}$$

This means that the factor k should lie between 2/3 and 1 if we expect the measured velocity to lie between the average and the maximum velocity. Since the velocity measurements are taken with thenaked eye it is difficult to have an idea about the appropiate value of k and it was therefore decided to conduct a separate experiment to determine the actual k value. This experiment is described in the next section.

3.5.4 Flow test in an ideal joint model

A joint model with an ideal geometry was made out of two plexiglass platens. The length of the platens were 150 mm and the width 60 mm. This size was chosen because it corresponds to the size of the joint sample used during the development of the technique. An open slot between the platen was introduced with a tape of about 0.25 mm thickness which was put along the sides of one platen. The sides were sealed off with silicon rubber.

The flow through such a joint should follow the cubic law (3) since the walls are parallel and smooth. The hydraulic aperture, e, should consequently be equal to the physical aperture in this case. To examine the validity of the cubic law, and the practicability of the experimental set-up, flow tests were perfomed on this ideal joint.

The joint model was fixed in the transparent frame as described earlier in this chapter and the flow through the joint at different water gradients was measured. The result is shown in Figure 3.19. The slope of the fitted line corresponds to a value of the hydraulic aperture of 243 μm. This agrees well with approximate measurements of the real aperture using a feeler gauge which gave 200 μm < E < 250 μm.

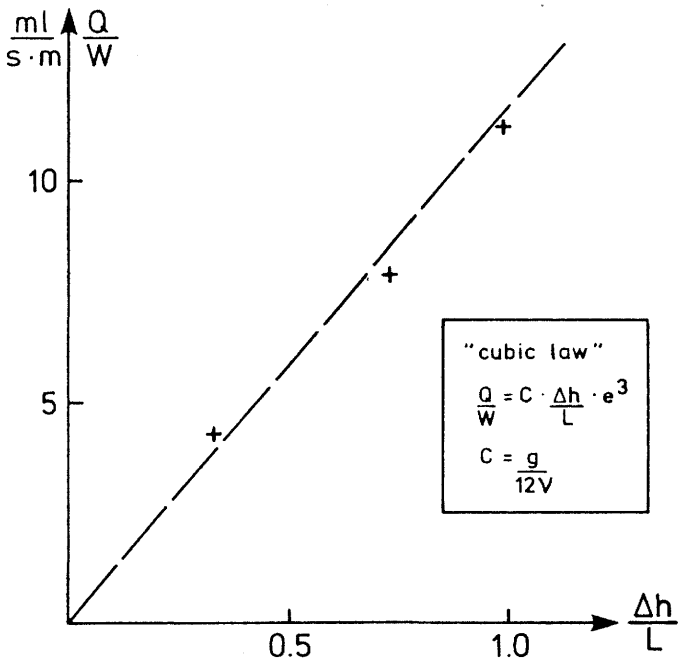

Figure 3.19 Measured flow through the ideal joint model at different gradients.

The velocity measurents taken from four injection points showed, however, that the two platens were not exactly parallel but the aperture varied slightly over the width. This could be due to the soft spacers used, imperfect surface planarity, and due to the load applied by the plexiglass frame.

Using equation (8) (section 3.4.3), assuming four channels with equal width and velocities according to measurements, gave

$$Q_{tot}^{calculated} = 183{,}8\ \mu l/s \quad ; \quad k = 2/3,\ \Delta h = 11{,}2\ cm$$

$$Q_{tot}^{measured} = 182{,}2\ \mu l/s$$

The experiment was repeated with a new loading, giving a slightly different aperture and with a different water gradient. The calculation of flow gave

$$Q_{tot}^{calculated} = 197{,}2\ \mu l/s \quad ; \quad k = 2/3,\ \Delta h = 4{,}8\ cm$$

$$Q_{tot}^{measured} = 198{,}0\ \mu l/s$$

The conclusion drawn from this test was that the proposed method for velocity measurement was feasible for our purpose and that the measured velocity corresponds to the maximum velocity in a cross-section of the joint, i.e. the correct value to be used for k, in equation (8), is 2/3.

4 RESULTS

4.1 Sample description

Five natural joint samples were used in this study. Three of the samples had been taken from Stripa mine. These joint samples were selected from drill-cores (Φ 200mm), drilled especially for the Stripa Project that concerned migration in a single fracture, Abelin et al. (1985). The locations in the drill-cores of sample S2, S3, and S4 indicate that they were taken from a fracture plane named Fracture A in the study by Abelin et al. (1985). These particular Stripa joints have big apertures and the surfaces are unmated. In fact they are minor faults rather than joints but the term joint is used throughout this work for simplicity. The joint surfaces of joint A match very well although they are not fresh. The joint B comes from a road cut and has fairly rough and weathered surfaces. Samples from joint B were used during the development phase of the present technique.

The size of the specimens was made as large as possible. The chosen joint samples had to fulfil the condition of both sides being unbroken and containing no fresh fractures or other visible disturbances.

The characteristics of the joint surfaces can be seen from the surface profiles given in Figure 4.1. The profiles are measured with a profile gauge. The joint roughness coefficients (JRC) (Barton and Choubey, 1977) were also determined for the original rock joints. The properties of the five joints are summarized in Table 4.1.

The joint models were subjected to a cyclic loading up to about 5 MPa in normal stress as described in section 3.3. The load-deformation curve from the larger sample S4 shows a loading cycle up to 3 MPa because of the limited maximum load from the hydraulic testing machine. The results from the different specimens can be compared in Figure 4.2 which shows the third cycle for all specimens.

The normal deformation is determined from the beginning of the third cycle starting at a stress of about 40 kPa. The very low stiffness at

low loads and the uncertainty in total stress on the specimen makes the absolute values of joint deformation unreliable. However, the slope of the curves after the first cycles has a good reproducibility. The stiffness of the joints calculated between 2 and 3 MPa is given in Table 4.2.

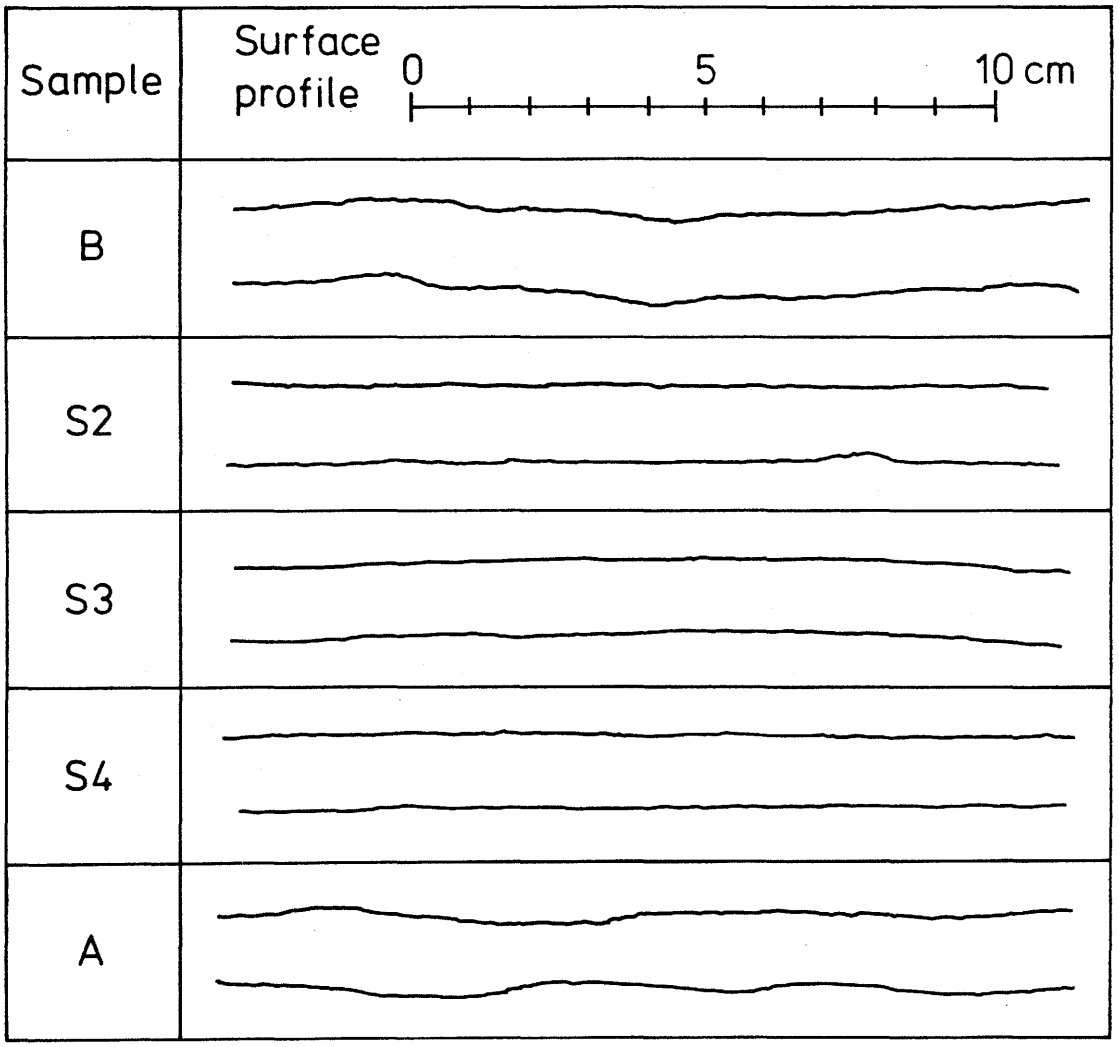

Figure 4.1 Surface profiles from the rock joint surfaces used in the experiments. The profiles are measured with a profile gauge.

Table 4.1 Properties of the natural rock joint samples used in the investigation.

Sample	B	S2, S3, S4	A
Rock type	Leptite	Quartz monzonite	Fine-grained granite
Surface condition	Weathered chlorite coating	Weathered chlorite coating	Slightly stained No filling
Matedness	Mated Apertures ≈ 0.2 mm	Unmated Apertures 0.2 - 0.8 mm	Very well mated Apertures ≈ 0.1 mm
Length x Width [mm]	162 x 59	148 x 88 162 x 82 208 x 159	154 x 54
Area [cm^2]	97	131, 136, 335	83
JRC	6	3	≈ 10

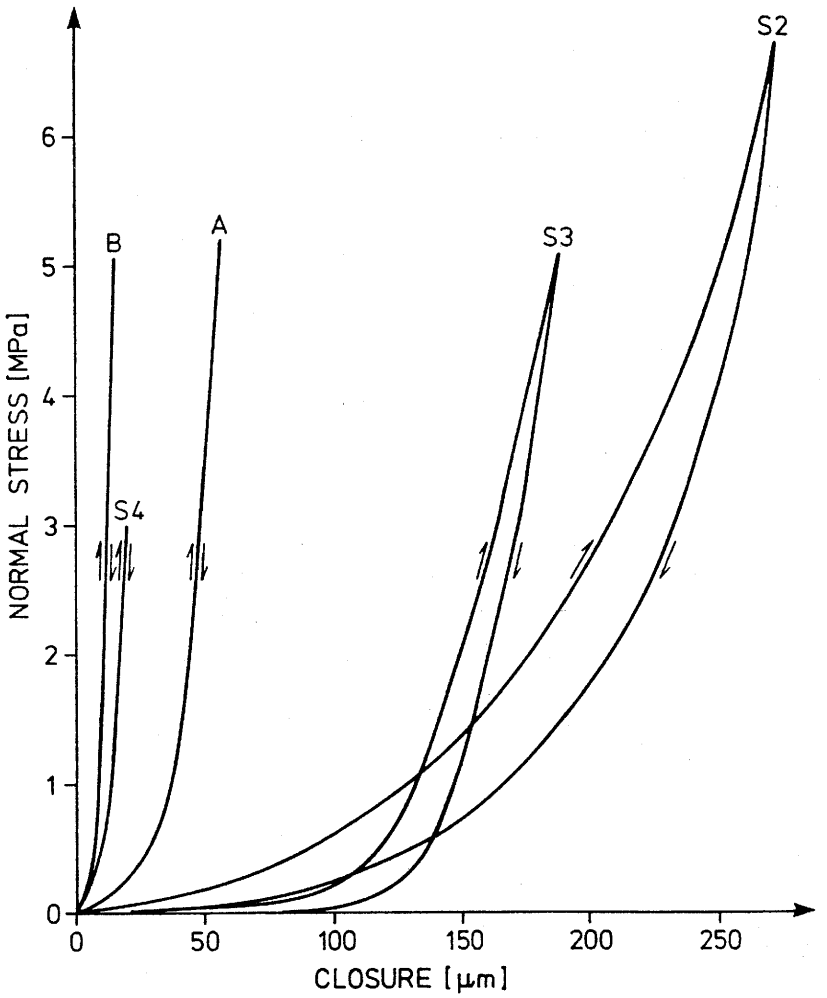

Figure 4.2 Normal stress-deformation curve for the third cycle of the five epoxy joint replicas.

Table 4.2 Normal stiffness of the joint replicas (calculated between 2 and 3 MPa, see Fig. 4.2).

Sample	B	S2	S3	S4	A
Normal stiffness [MPa/mm]	1000	30	70	400	220

4.2 Aperture measurements

Using the technique described in section 3.4 the apertures of the transparent joints were measured. Table 4.3 summarizes the results from the measurements on all specimens and gives the average aperture value and the standard deviation. A log-normal distribution function is fit to the measured apertures using a computer package (STAT-GRAPHICS). The average value and the standard deviation for the best fit is also given in Table 4.3.

Table 4.3 Summary of aperture measurements.

Sample		B	S2	S3	S4	A1	A2
Number of measurement points		182	89	104	284	100	100
Average aperture	$\bar{E}$ [μm]	313	462	417	261	84	161
Standard deviation	σ_E	212	255	449	100	46	75
Best fit log-normal distri-bution	$\bar{x}$ [μm]	309	464	393	261	83	161
	σ_x	193	273	295	98	34	72
	$\sigma_x/\bar{x}$ [%]	62	59	75	38	41	45

One can notice that the average aperture values are much larger than the maximum closure given by the load deformation curves in Figure 4.2. The explanation for this is that the reference load in the loading test is not zero but about 40 kPa which causes a considerabe closure of the joint. The load deformation curves also come from the third loading cycle whereas the aperture measurements were taken after

several "first loadings" at a very low normal stress. Furthermore, the closure measured at maximum stress, even if it was correctly measured from a zero normal stress, should not be as large as the aperture at zero stress since the joint will not close fully.

Figure 4.3 shows an example of a frequency histogram of the aperture measurements on specimen S4 (for the others see Appendix 1). The distributions generally fits well to log-normal functions. The best fit log-normal function for each sample is given in Figure 4.4.

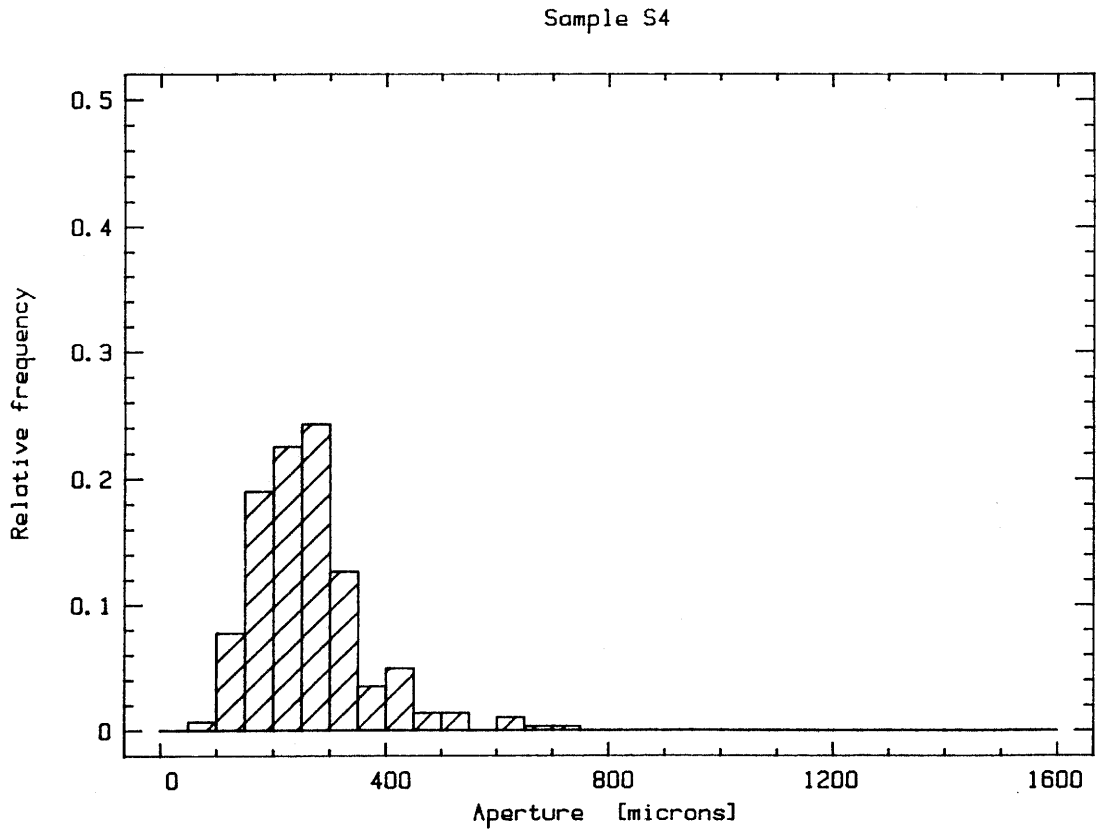

Figure 4.3 Frequency histogram of the aperture measurement on sample S4.

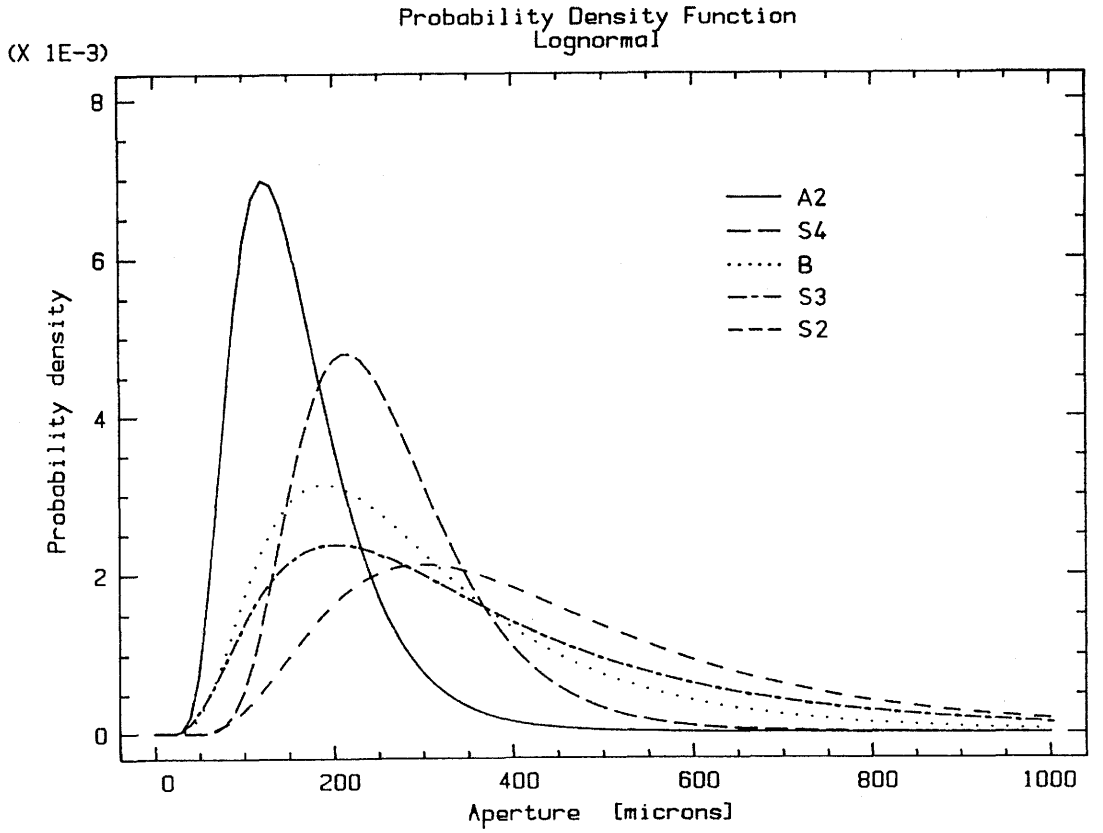

Figure 4.4 Best fit log-normal functions to the aperture distribution of the joint replicas used in the study.

The apertures of specimen A were measured two times under different normal stress. The first measurement was done with the load exerted by the tightened bolts as described earlier (A1) and the second one (A2) with only the weight from the plexi glass plate of the frame. Measurements in both cases were taken at the same points. The results from these two measurements illustrates the change in aperture distribution due to closure of a joint, Figure 4.5. The best fit log-normal distribution to both sets of the measurement are given in Figure 4.6.

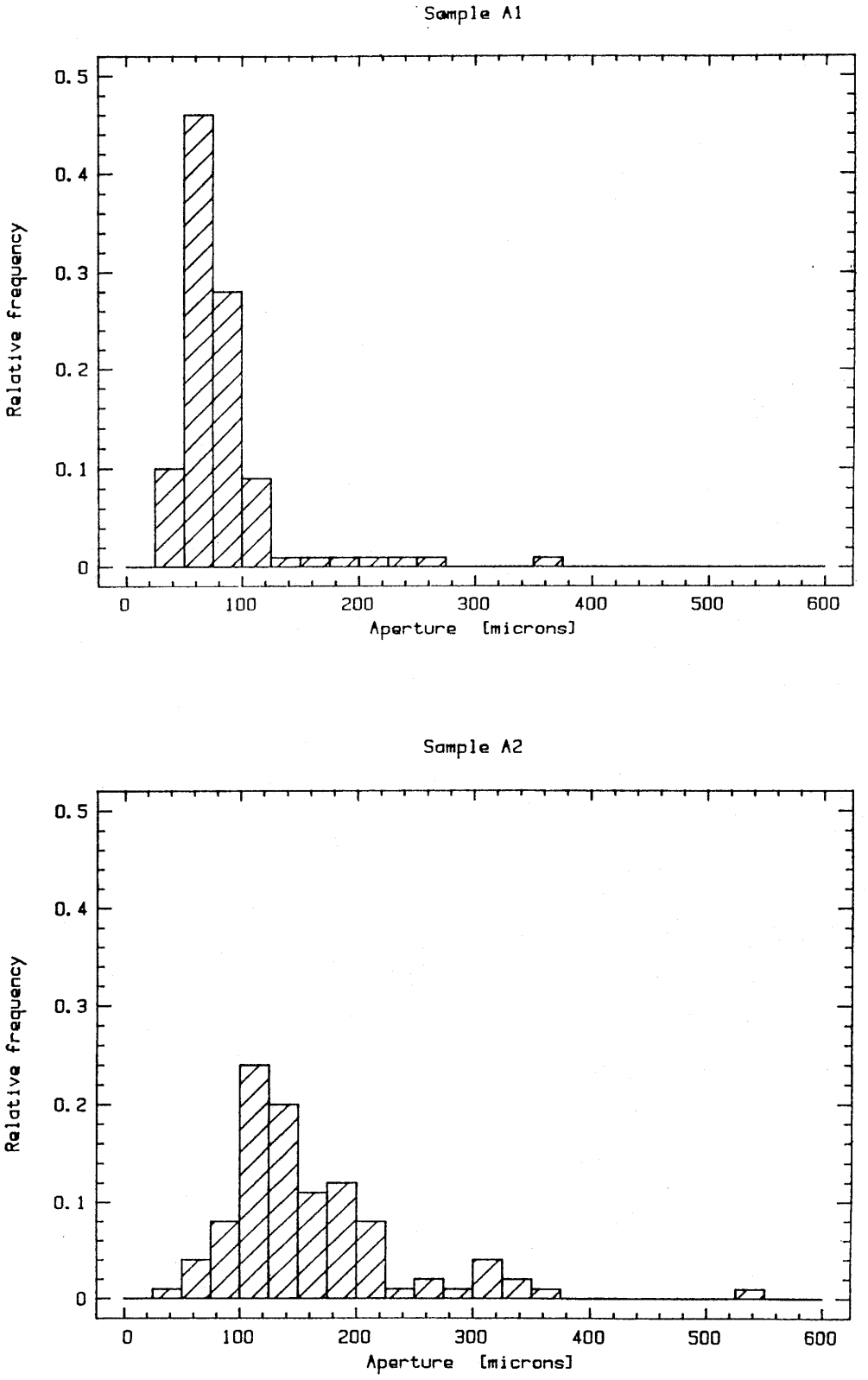

Figure 4.5 Frequency histograms from aperture measuremnt A1 and A2, corresponding to two different levels of compression of joint sample A.

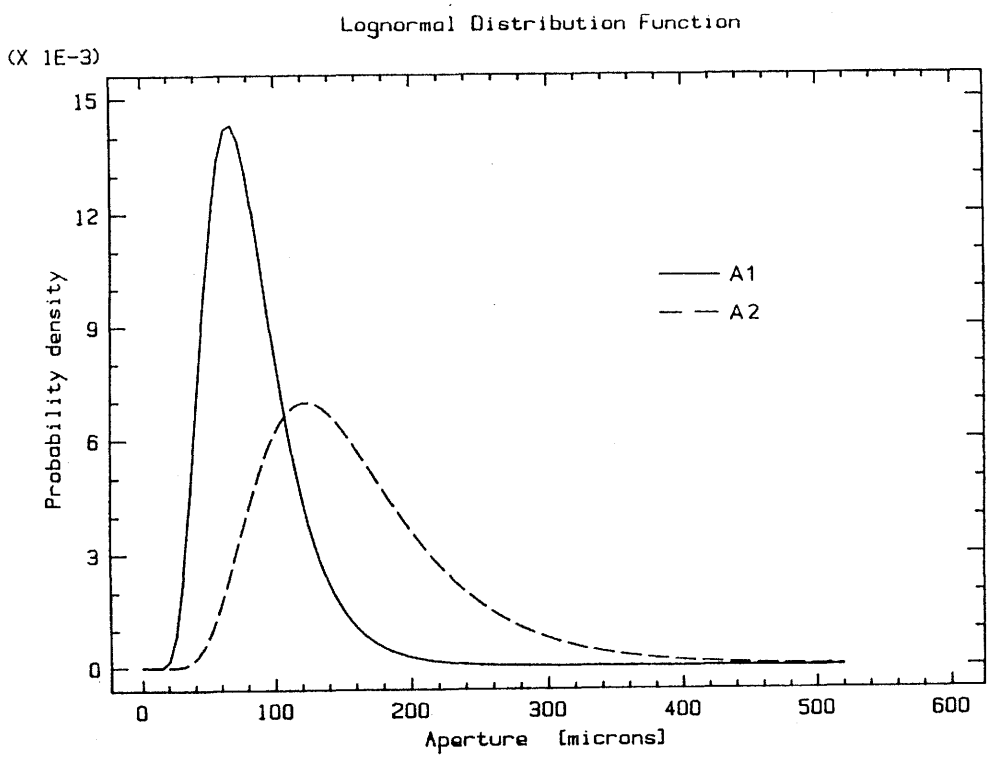

Figure 4.6 Best fit log-normal functions to the aperture distributions A1 and A2 shown in Figure 4.5.

A comparison of the two distribution curves shows that the average aperture is lower for A1 as expected. Also, the spread of the distribution is less. This is explained by the fact that closure is not constant over the joint surface but is obviously larger at points with larger initial aperture, where the joint surfaces do not come into contact with each other. At points where the joint surfaces are initially in contact the closure is zero. This can also be illustrated as in Figure 4.7 showing a frequency histogram of the closure values. The closure is obtained from the difference in aperture measurements at each point of A1 and A2. The closure distribution shows the same general shape as the aperture distribution itself, Figure 4.5.

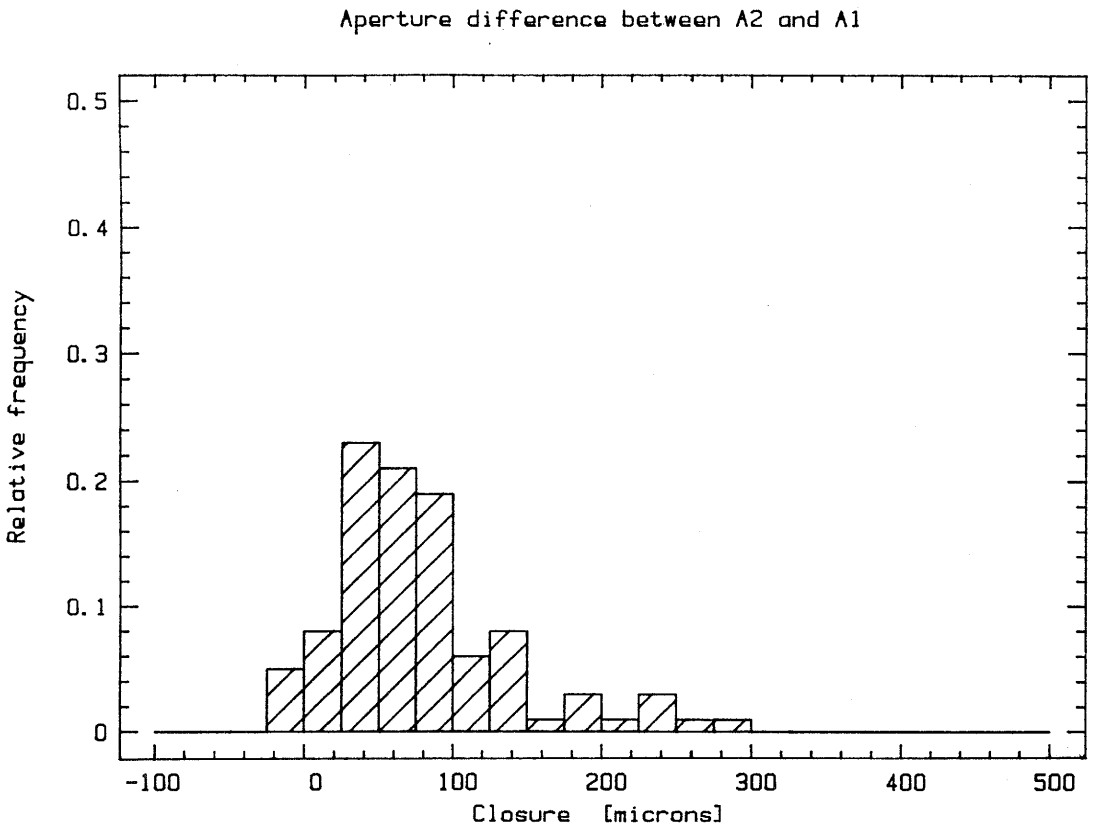

Figure 4.7 Frequency histogram of the closure of the joint apertures due to compression (A2-A1).

The differences in void geometries of the samples are most easily seen from the three dimensional plots, Figure 4.8. Sample A, from a well mated joint, shows a very even void geometry compared to sample S3, taken from an unmated joint. In sample A there is only one area with slightly larger aperture. Note that the scale in the z-direction is exaggerated for the sake of clarity.

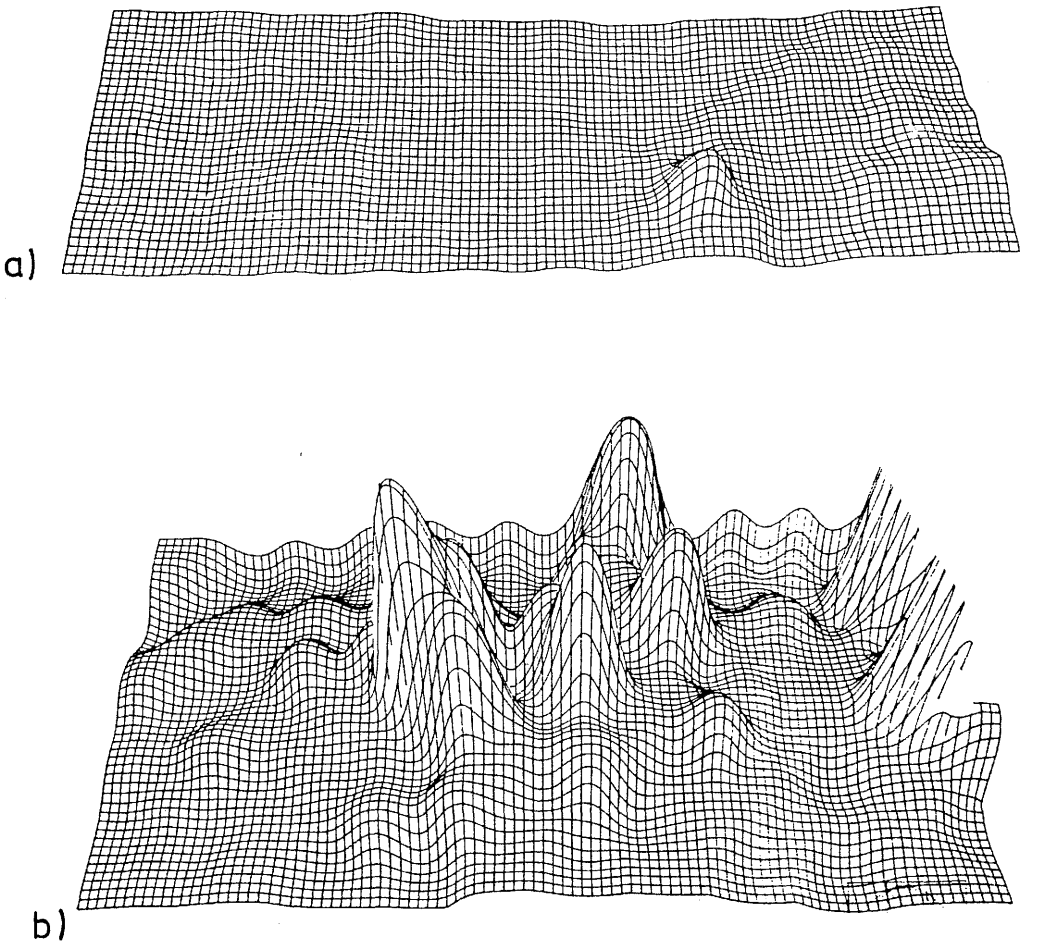

Figure 4.8 DTM-plots of the void geometries of the joint sample a) A and b) S3.

The void geometry of the joint can also be illustrated with an isoplot of the measured apertures (see section 3.4.3). Figure 4.9 shows the isocurve calculation from sample S4 and S2. The equidistance is 50 μm for both samples. The hatched areas correspond to areas with apertures smaller than 250 μm. It can be seen that the hatched areas, where the contact points also are expected to occur, are less in the sample S2 than in sample S4. The void space of S2 is also more unevenly distributed over the surface compared with S4.

Terrain models and isoplots from the aperture measurements on all samples are given in Appendices 2 and 3. The flow experiments, presented in the next section, were performed with the water flowing from the left to the right side of the specimens in all figures.

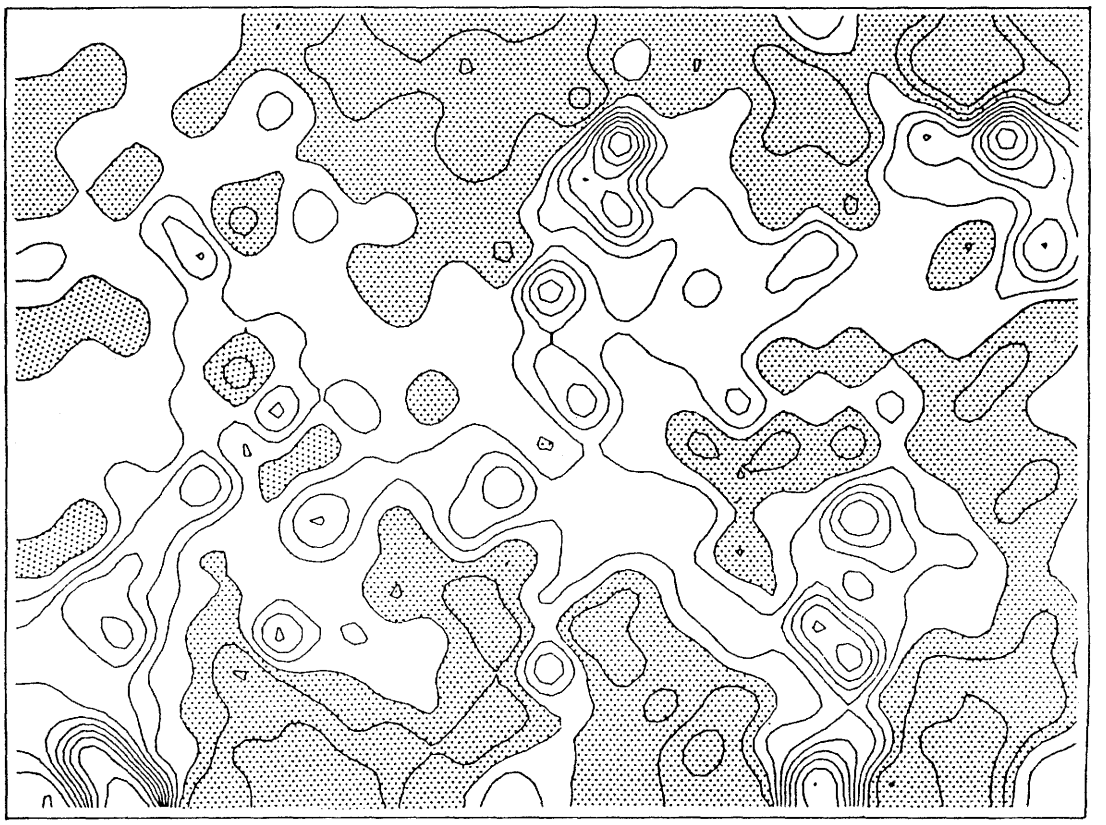

a)

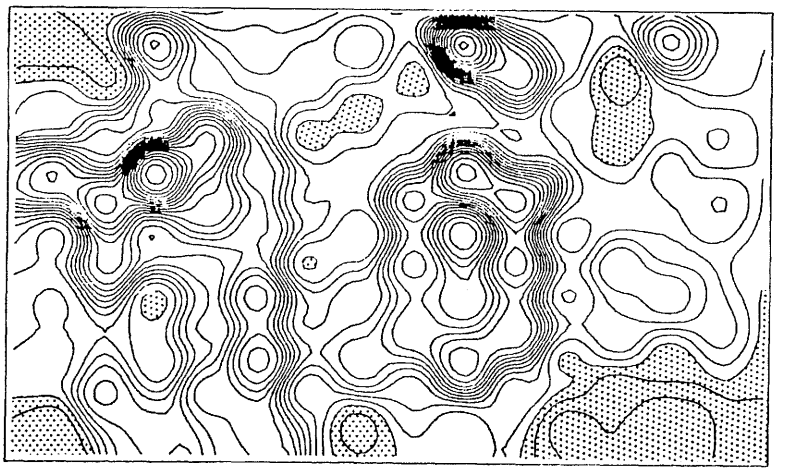

b)

Figure 4.9 Isoplots of the apertures of sample a) S4 and b) S2. The hatched areas correspond to apertures smaller than 250 μm. Equidistance 50 μm. Scale 1:1.5.

4.3 Flow experiments

The total flow through each joint was measured using a range of water gradients. The water gradients were selected such that the flow became large enough to be measured accurately without having any risk of turbulent conditions. The results from the measurements from all samples are given in Figure 4.10. The flow per unit width is plotted against the average water pressure gradient over the joint length. The real water pressure gradient will naturally vary over the joint surface because of the aperture variation.

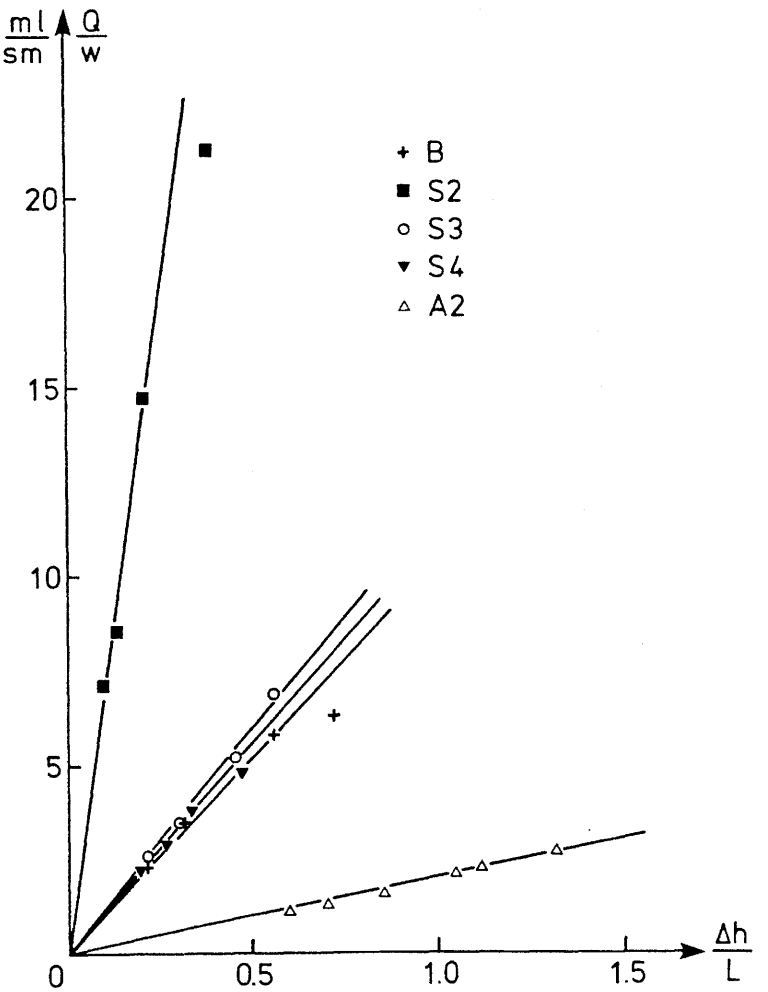

Figure 4.10 Flow experiments on the joint replicas. Measured flow per width is plotted against the water pressure gradient. The lines show the linear function fitted to the data points.

The equivalent hydraulic aperture for a joint is calculated from the slope of the linear flow-gradient relationship which was fitted to the measurement points. The quotient between the average mechanical aperture (E) and the hydraulic aperture (e) of a joint is a measure of the difference between real void geometry and the equivalent parallel plate concept of the joint. The results are summarized in Table 4.4.

Table 4.4 Summary of flow experiments.

Sample	B	S2	S3	S4	A1	A2
Average aperture $\bar{E}$ [μm]	313	462	417	261	84	161
Hydraulic aperture e [μm]	236	428	244	237	< 5	134
$\bar{E}/e$	1.33	1.08	1.71	1.10	> 16	1.20

As described in section 3.5.2, velocity experiments were performed using colour injections at several points along the inlet of the joints. A compilation of stream lines from each sample is given in Appendix 4. For sample B both boundaries of the coloured stream is drawn to illustrate the fact that the width of the stream varies along the joint. For the other samples a single line indicates the flow path.

Figures 4.11a and b shows examples of stream lines from sample S4 and B. In the figures the stream lines are overlayed on the calculated isoplots from aperture measurements to illustrate how the apertures influence the flow pattern.

Example: 1) The stream lines converge into areas with larger apertures.

2) The stream lines diverge from the tighter areas.

3) The stream lines bend such that they cut the isocurves perpendicularly, i.e. in the probable direction of maximum gradient.

4) A stream broadens when it passes a tighter area.

The velocities are measured and calculated as described in section 3.5.3 and the result for each sample, at two different gradients, is given in Appendix 5. Generally there is no difference in the results at different gradients on the same joint sample. Since the flow was kept laminar any changes in flow pattern or velocity distribution was also not to be expected.

The velocity was observed to vary between flow paths and also along each flow path. A comparatively tight area may in some cases have a big gradient which will give rise to a higher velocity. Example 4) above was such a case and the colour front was seen to move fast over that area. Generally the velocity is proportional to the aperture squared and a path with bigger aperture on average will also have the fastest flow. The velocity along the stream line number 7 in sample S2 is, for example, higher than the velocity along stream line number 8, Figure 4.12. From the isoplot of apertures in Figure 4.13 one can also notice the difference in apertures in the areas along path 7 and 8 respectively.

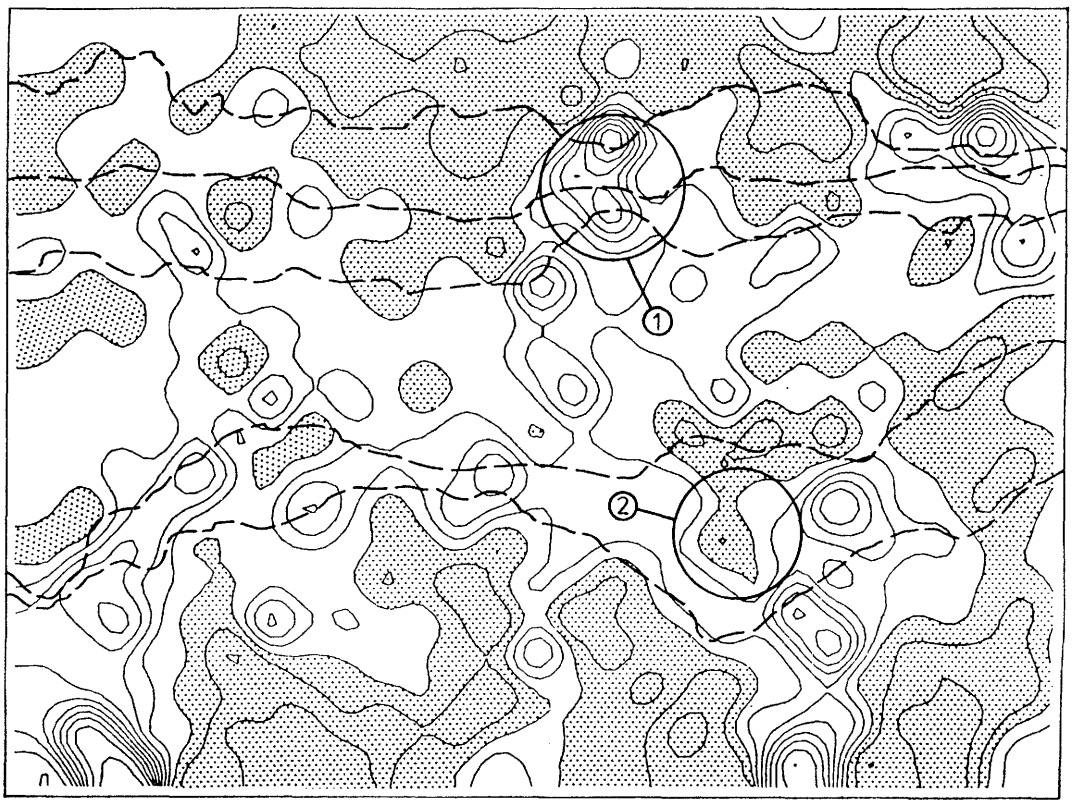

a)

b)

Figure 4.11 Observed stream lines of the flow overlayed the aperture isoplots for a) sample S4, and b) sample B.

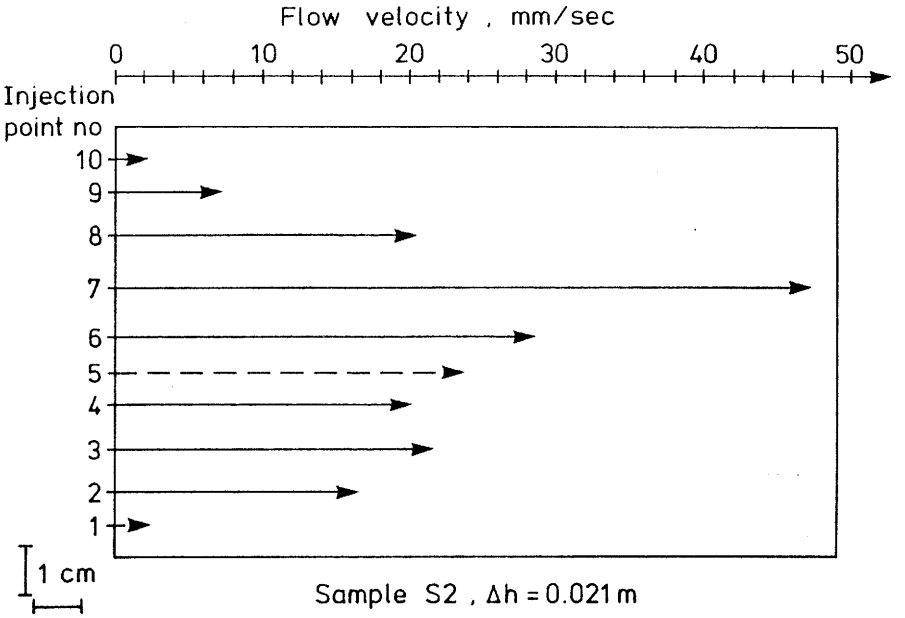

Figure 4.12 Results from velocity measurement on sample S2.

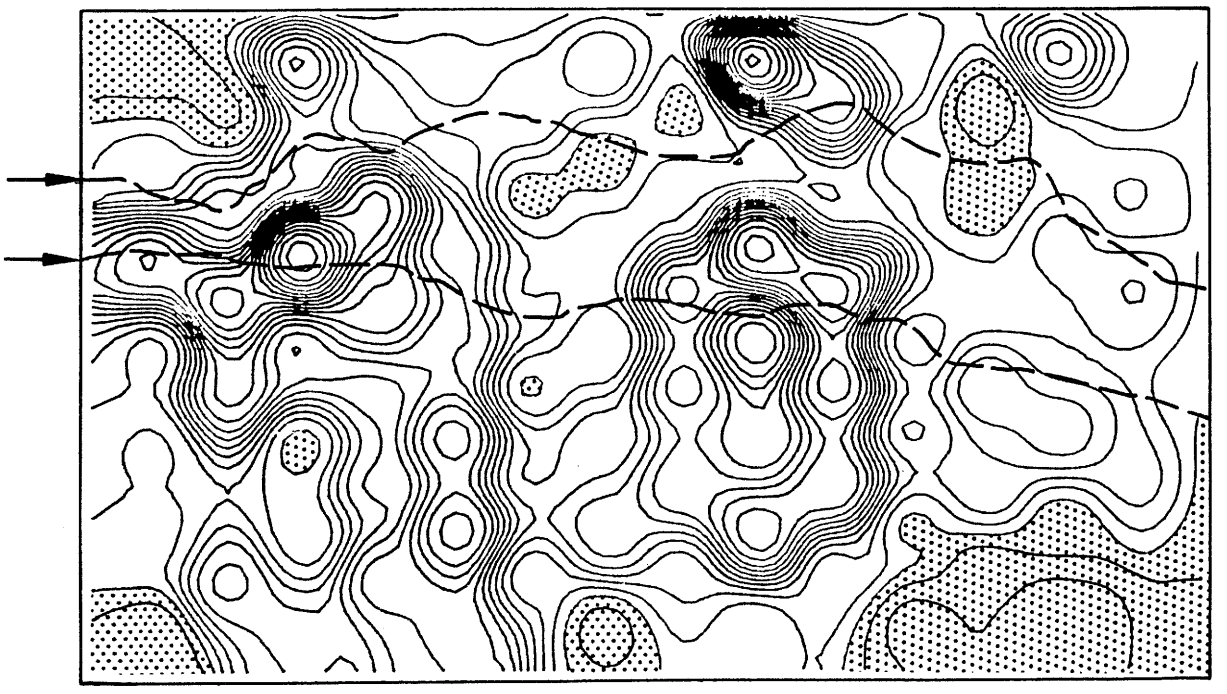

Figure 4.13 Stream paths corresponding to injection point 7 and 8 of sample S2. The lines are derived from photographs of colour injections and overlayed the isoplot. The hatched areas correspond to apertures smaller than 250 μm. Scale 1:1.

Similar comparisons between aperture measurements, photographs and velocity measurements can be done on all samples leading to similar results. In the cases when a stream line does not follow the expected path, this may be due to the coarse grid of measurement points used in the aperture measurements and the errors in the aperture determination (see sections 3.4.2 and 5.1), which results in a calculated void geometry different from the true void geometry.

In some cases the stream lines may bend because of air-bubbles that are trapped inside the joint. Since this was mainly observed in the narrow areas, the distinction between tortuosity due to air and due to points in contact could be difficult to make.

The most obvious result from the colour injection is the difference between the different joint types. The three Stripa joints show the same general features. The flow paths change direction several times along the joint. The sample A shows, however, a different flow pattern. Apart from one area with comparatively big apertures, which deflects the flow, the stream lines through this joint are almost parallel. Figure 4.14 shows a photograph of sample A when a bigger amount of colour was injected into the water flow. Notice how the surface of the joint is covered quite evenly by the flow. From this observation it can be expected that the contact area between the joint surfaces of sample A is small.

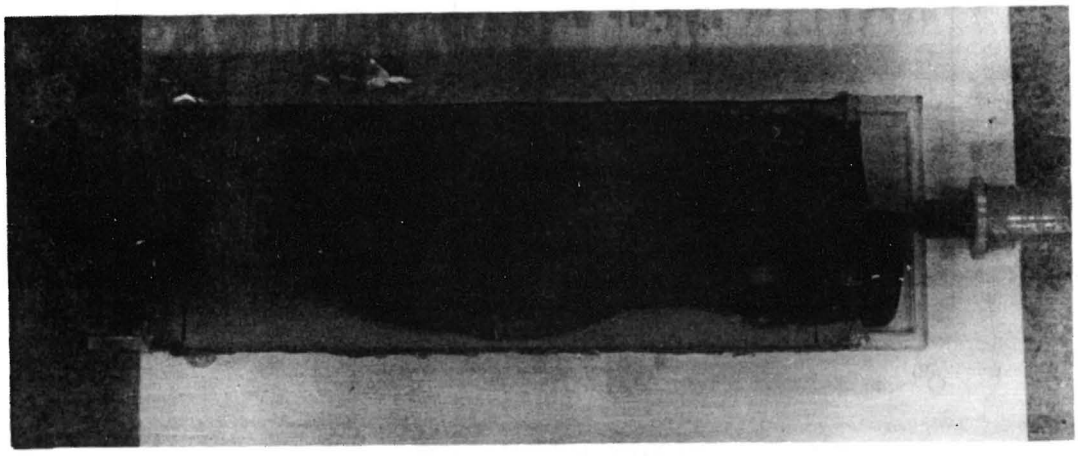

Figure 4.14 Photograph of a colour injection in the water flow through sample A.

The tortuosity of the flow varies between the samples as well as along different flow paths on each sample. The result from the tortuosity measurements is given in Table 4.6.

The total flow through the joints can be approximately calculated based on the velocity measurements using equation (8) (p. 56) as explained in section 3.4.3 ($k = 2/3$). This flow estimate is denoted Q^v.

The flow can also be calculated using the aperture measurements. The average aperture value $\bar{E}$ is used in the "cubic law" (equation (3), p. 19). This equation is based on the parallel plate assumption.

These two flow estimates Q^v and q were calculated for each experiment and are given together with the measured flow Q^m in Table 4.5.

Table 4.5 Compilation of flow estimates and measured flow (for further explanation see text).

Sample No.	Gradient $\Delta h/L$	$\frac{Q^m}{W}$ $\left[\frac{ml}{s \cdot m}\right]$	$\frac{q}{W}$ $\left[\frac{ml}{s \cdot m}\right]$	$\frac{Q^v}{W}$ $\left[\frac{ml}{s \cdot m}\right]$
B	0.32	3.48	7.76	1.69
B	0.56	5.03	13.57	2.14
S2	0.14	9.03	12.10	4.77
S2	0.21	11.51	17.52	5.20
S3	0.31	2.22	23.80	0.95
S3	0.60	5.92	35.35	2.55
S4	0.18	1.43	2.67	1.30
S4	0.20	2.18	3.03	2.31
A	0.70	1.28	2.46	0.87
A	1.05	2.00	3.69	1.19

Q^m measured flow

q cubic law calculation of flow

Q^v calculated flow from measured velocities

In Figure 4.15 the measured flow Q^m and the estimated flow based on velocity measurements Q^v are given relative to the flow estimate q from cubic law. Q^m varies between 10 and 75 % of q. Q^v lies between 5 to 75 % of q. Notice that Q^v is in almost all cases smaller than Q^m. An explanation to this may be that the assumptions made in the evaluation were too rough. They might have caused a systematic underestimation of the flow.

Because of the variation in velocities along different flow paths the contribution to the total flow will vary between different parts of of the joint surface. In the calculations of the total flow Q^v, based on the velocity measurements, the contribution from each "channel" is added together. Since the number of colour injection points was limited, and consequently was the avaliable information on actual velocities, the contribution to flow could only be roughly estimated.

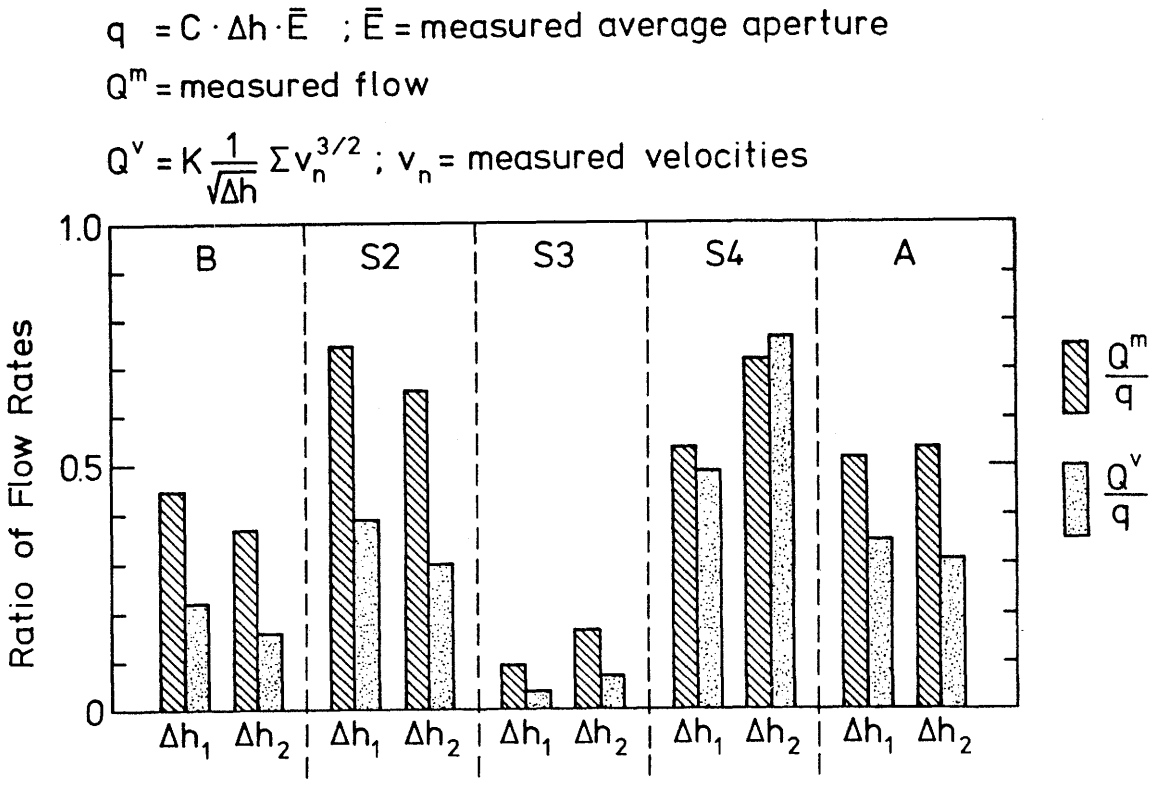

Figure 4.15 Comparison between measured and estimated flow rates given in Table 4.5. The bars show the magnitudes of the ratios $\frac{Q^m}{q}$ and $\frac{Q^v}{q}$ for each flow experiment.

The largest contributions to flow, corresponding to the fastest channels were successively added together until the sum was about 75 % of the total flow Q^V. The number of channels needed to give this percentage of total flow was compared to the total number of channels. This quotient provides an indication of how much of the joint surface area that contributes effectively to the total flow. The results from our experiments are given in Table 4.6.

The flow is most unevenly distributed on sample S3. About 80 % of the flow results from three out of ten channels corresponding to 30 % of the joint surface area. For the sample A about 75 % of the flow results from seven out of ten channels, corresponding to about 70 % of the joint surface. This implyes that for sample A almost the whole surface area is effectively contributing to the flow.

Table 4.6 Estimations of flow distribution and results from tortuosity measurement (for further explanation see text).

Sample	B		S2		S3		S4		A2	
Δh [cm]	5.2	9.1	2.1	3.1	5.0	9.7	3.8	4.2	10.8	16.2
% of Q_{tot}	82.4	83.1	71.5	75.2	78.6	77.6	75.8	76.0	76.2	76.8
No. channels / Tot. No. ch.	$\frac{2}{4}$		$\frac{4}{10}$		$\frac{3}{10}$		$\frac{12}{21}$		$\frac{7}{10}$	
Tortuosity 1/L min - max	1.05-1.12		1.05-1.15		1.03-1.34		1.05-1.21		1.01-1.06	

5 DISCUSSION

5.1 Experimental technique

The epoxy replicas of natural joints cannot fully model all mechanical and hydraulic aspects. The strength of the asperities, especially the variation in strength between different areas where the joint has been weathered or is covered with coating materials, is obviously not reflected in the epoxy models.

The mechanical properties of epoxy are different from those of rock. Elasto-plastic deformation will occur at the contact points of the model in contrast to crushing which is expected from brittle rocks. The ratio between the elastic modulus and the compressive strength is also much lower for epoxy than rock.

However, in this study where the specimens are used several times, and the idea is to conduct flow experiments for a known aperture situation, it is advantageous to have a joint model made of a strong elastic material. Under the low stresses used for the experiments there will not occur any irreversible deformation after the initial cycles up to 5 MPa. Although the absolute stress levels will be different for the epoxi joint model the general change of aperture distribution of a rock joint can be studied with the presented technique.

Natural joints with very soft fillings cannot be studied with this technique. Loose particles may possibly exist inside the natural joints and influence the conductivity. This case can normally not be considered in any laboratory study since the joint specimens are easily destroyed and become disturbed already during sampling. Small differences between the original real joint and the epoxy replicas could also appear due to imperfect copying procedure and hardening effects such as shrinking or warping of the specimen. Nevertheless the joint model obtained will provide a void geometry that could exist in nature and can well serve as a sample for the purpose of studying flow through a natural joint.

The main advantage of this technique is the visibility that allows us to study the flow by actually observing its features. Conclusions should therefore be drawn, regarding the void geometry of a joint as the main concern and how it influences the flow.

There are, to our knowledge, two other studies which combine information about the void geometry of a joint sample with results from flow experiments on the same specimen. These studies have been conducted by Gale (1987) and Pyrak-Nolte (1977), (see section 2.1). The difference between our technique and the techniques employed by them is again, as discussed in section 2.3, a matter of how to simplify the complex three-dimensional problem. Pyrak-Nolte connected the flow results to the situation of contact or "dead" areas while they had no information on apertures. Our technique gives no information about contact areas but provides a picture of the aperture variation. Gale (1987) compared the measured average mechanical apertures with the calculated apertures based on flow tests on the same joint, which is similar to what was done in this work.

The sample size of the joint specimens in this study is of the same order as the specimen used by for example Gale (1987) but around ten times bigger than those of Pyrak-Nolte (1987). This size is still small compared to joints in-situ. Studies of the fractal nature of joint surfaces, Brown and Scholz (1985b), shows, however, that the roughness is almost scale independent which argues in favour of studies on the laboratory scale.

Since an aperture value determined by the method presented here is an average from the small area covered by a water drop the most extreme values from the population will not be detected. Therefore the presented method will result in an aperture distribution which is more peaked than the actual pointwise aperture distribution.

The areas over which the values are averaged, will also vary depending on the actual apertures. This might lead to a slight increase in skewness of the aperture distribution, in favour of larger values.

The accuracy of these aperture measurements may also be questioned. The different sources of error were discussed in section 3.4.2. The total error was estimated to about 20 % for 10 µl drops. Any similar estimation of the accuracy of the techniques used in other studies has not been avaliable for comparison. In this stage of developing different investigation techniques, a fairly low accuracy level must be expected.

Since the techniques of aperture measurements so far employed by different workers are quite different, it would make a comparison between them specially interesting. A combination of many methods applied on the same joint samples should be a fruitful approach for future investigations.

The experimental set-up allows for flow tests with water pressure levels up to only about two meters. This still gives higher gradients than normally exists in the bedrock in-situ, exept from some locations close to rock excavations. If greater gradients are applied in flow tests the flow might become turbulent.

Due to this limitation of the experimental set-up the flow test through the tightest joint replica could not be conducted (A1). The flow through the joint became two small to be measured. The corresponding velocities of the flow would, however, also become so small that the chemical diffusion of the colour injected to the water must be considered and might overshadow the spread due to the pressure gradient.

Already at the lowest flow velocities that could be measured in this study the trace of the colour became diffused at the outlet end of the specimen. The time measurement therefore is less accurate in this case and may represent better the average velocity, in a cross section of the joint (Fig. 2.13), rather than the maximum velocity. This implies that the correct value of the factor k is not certain (see sections 3.5-3.4).

During the flow tests we experienced the problem of airbubbles getting trapped inside the joint samples. This is a problem which may also be present in flow tests on real rock joints although it is more difficult to detect. The air problem could possibly be overcome if a way of sealing the joint under water could be found. A closed flow system with an air-bleeding arrangement, which has been used in some other studies (Iwai (1976) and Elliot et al. (1985)), would make tests with high pressure gradients possible, and would also improve the possibilities of controlling the air-content of the flowing water.

In the analysis of the velocity measurements, each measurement is assumed to represent the flow in a channel of rectangular cross section (see section 3.5.3). The shape of the actual channels (if there is still enough basis for using the term channel) is not rectangular and this is a difficulty when we want to attribute an equivalent width and aperture to each channel. The assumption used in the analysis reduces the true three-dimensional problem to a one-dimensional problem, and the magnitude of the errors involved is not known.

In the performed experiments 4 to 21 velocities were determined on each sample. The value of the information from the velocity measurements will, however, be enhanced with increasing the number of injection points along the width of the joint inlet. Having increased the number of injection points, the contribution of flow from different parts of the joint can be studied in more detail and the chance increases that the fastest flow path is found and measured.

If the individual velocities were measured over parts of the flow path down-stream of the inlet the value of information would be further enhanced. This requires, however, that the tests are documented on film so that the flow velocities can be evaluated later with the aid of the film.

One clearly advantageous feature of the present technique is that it shows the paths of flow and make direct measurements of tortuosity possible. Such information is not provided by other techniques. The necessarily tortuous character of the flow is clear from studies of

contact points, for example Iwai (1986) and Pyrak-Nolte (1987), but the extent of tortuosity cannot be actually measured by their techniques.

5.2 Results

5.2.1 Mechanical properties

The load-deformation curves from the normal loading of the epoxy replicas show a great difference in stiffness between the samples (Fig. 4.2). Since the material of the replica surfaces is the same for all samples the difference in stiffness must be only due to the different geometries of the joints. The samples S2 and S3 are clearly most compliant. This was also expected since these two joint samples are the most open, as can be seen from the aperture measurements, and the area of contact in them should be comparatively small. The sample S4 has a smaller average aperture than S2 and S3 and is also stiffer than them. This joint can be expected to have a larger contact area. More points of contact will decrease the actual stress levels in a joint at the contacts and give less total deformation.

According to the study by Hopkins et al. (1987) (see section 2.2) the stiffness will also be influenced by the mere configuration of the contacts. The spread of apertures is less for sample S4 than for S2 and S3 (see Figs. 4.4 and 4.9). This is a further explanation to why sample S4, which is derived from the same type of unmated joint, is stiffer than samples S2 and S3.

Aperture and conductivity predictions based on stress-displacement measurement is an appealing approach which has been suggested by Tsang and Witherspoon (1981). However, many factors influence the final shape of a load-deformation curve, such as the mechanical properties of the joint surface material, the degree of correlation between the two opposite joint surfaces, and the experimental details during the deformation test. The differences between load-deformation curves caused by various factors are very difficult to separate.

5.2.2 Aperture measurements

The results from the aperture measurements are in agreement with the results of earlier investigations. Gentier (1986) and Gale (1987) present histograms of measured aperture distributions with the same general shape as in this study, Figures 2.2 and 2.4.

The average apertures measured on the samples from Stripa are comparable to the calculated apertures from in-situ tracer tests in Stripa mine, Abelin et al. (1985) and Abelin (1986). For sampling holes S2-6 and S2-8 at the main test site, the aperture was determined to be 240 μm and 280 μm respectively. This calculation was done assuming linear flow from the injection hole, mixing of the tracer at the injection hole and using the mass balance conditions. For calculations based on assumptions different to what was mentioned, the apertures were smaller.

The fit to a log-normal function of the aperture distributions are generally good. This function has also been suggested by others, for example Gale (1987). A problem when applying a theoretical distribution to the calculations of flow, is the long theoretical tail. The actual distributions have an upper limit of the aperture and the applied distribution should therefore be truncated at some level. Since the flow is sensitive to the largest apertures, a correct shape of the tail and a correct truncation is important for the result.

Neuzil and Tracy (1981) assumed a log-normal distribution of the apertures in their theoretical model of a joint. Figure 5.1 shows their calculation of the change in aperture distribution due to compression. The result from our measurment on sample A, for different degrees of closure, agrees well with their calculation, Figure 4.5. The mean aperture of A1 is about half of that of A2 and the relative frequency for the peak value of A1 is double compared to A2.

According to their model the change in aperture at any location is proportional to the original aperture at that location, Figure 5.2. This simple model of a complex deformation process is supported by our

results. If the isoplot of the calculated void geometry for A2 is compared with the isoplot of the closure (A2-A1), Figure 5.3, this correlation can be noticed.

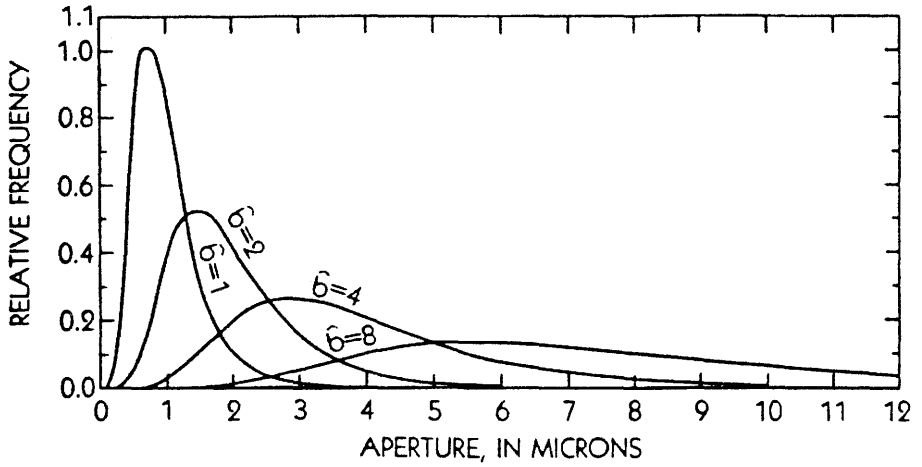

Figure 5.1 Theoretical changes in a log-normal distribution describing aperture frequency in a fracture undergoing compression. As compressive stress increases, mean aperture b decreases. Neuzil and Tracy (1981).

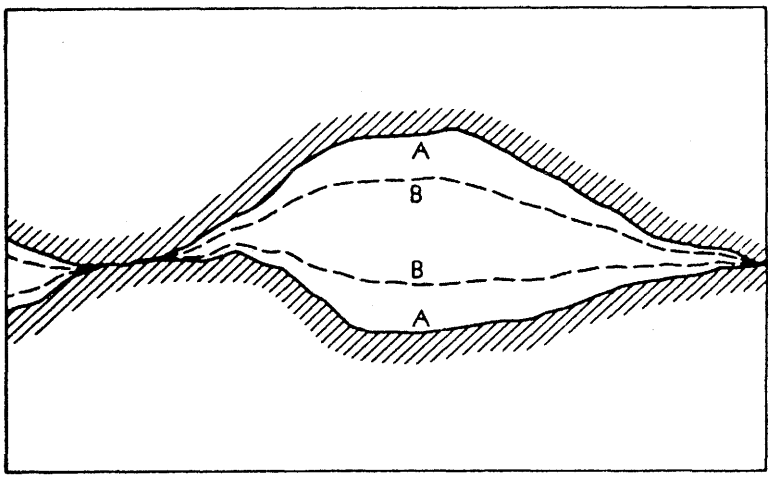

Figure 5.2 Model of aperture change due to elastic compressional deformation of fracture walls. Contours A and B correspond to two different stress levels. Neuzil and Tracy (1981).

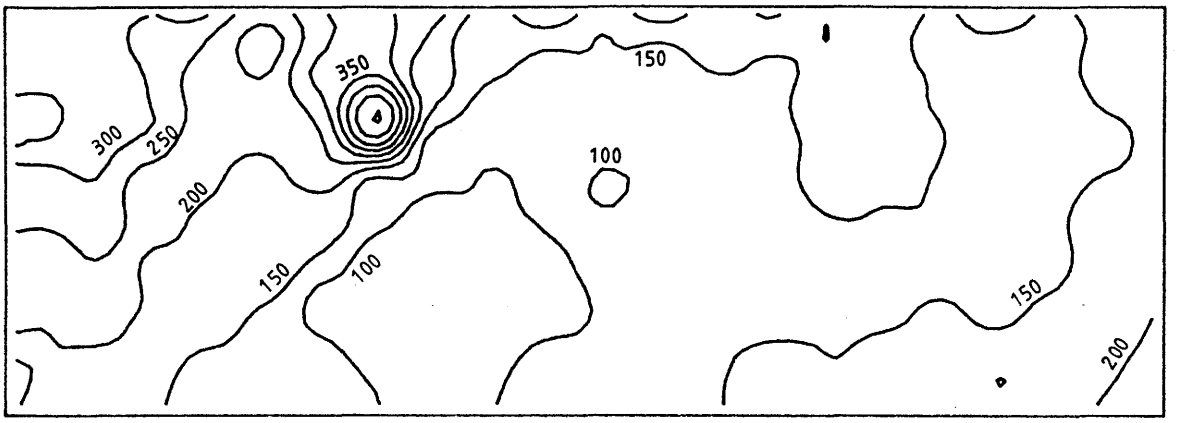

A2 - ekvidistanse 50 mikrometer scale 1:1

a)

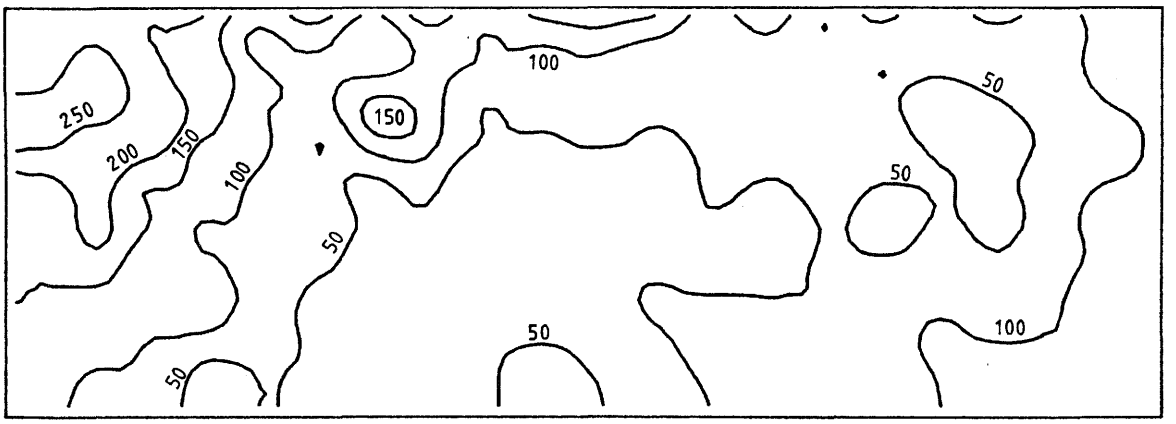

b)

Figure 5.3 a) Isocurves of the aperture measurements from sample A at a low normal stress (A2).
b) Isocurves of the change in aperture when the normal stress on the sample A is higher (A1). The closure is calculated as the difference in aperture measurement at each point for A2 and A1.

5.2.3 Flow experiments

A detailed comparison with the results from the study by Brown (1987) (see sections 2.1-2.3) cannot be done easily. His calculations are based on uncorrelated surfaces and the parameter σ, which is the standard deviation for the surface height distribution on the uncorrelated

scale, is important in the presentation of the result. This parameter is difficult to estimate for the joint samples in our study that are expected to mate to some degree, at least in the case of samples A and B. For the joint replicas derived from joints in Stripa granite a rough comparison can be made assuming that they consist of uncorrelated surfaces.

The results from the velocity and tortuosity measurements agrees in general character with the numerical results by Brown (1987) (see Fig. 2.19). The variation of the velocities for the Stripa samples are of the same order as for the modeled joint in his study. A surface separation of $d_m = 4\sigma$, corresponding to surfaces that are just touching, should be the degree of contact most comparable with the conditions in our study where the normal stress was very low.

The comparison of cubic-law flow estimates q, with actual measured flow Q^m, Figure 4.15, also shows ratios of the same order of magnitude as those calculated by Brown, Figure 2.20. The standard deviation of the topography should be approximately of the same order as of the aperture which gives the rough estimation of σ = 0.1 - 0.4 mm for the Stripa samples. The mean separation d_m can be approximated with the average aperture E. With these assumptions the standardized separation d_m/σ, on the x-axis in Figure 2.20, lies between 1 and 2 for sample S2, S3 and S4. The aperture value used in the cubic law in our study is the arithmetic average. Therefore Q^m/q should correspond to the filled circular data points in Figure 2.20. It can be seen that the values from the calculations by Brown agrees with the result in this study.

Tsang (1984) used an electrical analog to study the effect of tortuosity of flow through joints and concluded that this effect on the total flow through a joint could be of several orders of magnitude. This may seem contradictory to the result in our study where the cubic law estimation, although it gives a larger flow, is of the same order of magnitude as measured flow. However, the degree of contact considered in the study by Tsang is in some cases very high, about 30 % and higher. For fractional contacts of 1, 3 and 5 %, which is of the same

level as expected in our experiments, Tsang calculates the tortuous flow to be between 30 to 99 % of the non-tortuous flow.

Tsang (1984) also showed that a more peaked aperture distribution gave smaller effects of tortuosity than a broad distribution. This agrees with our result where sample A and S4 have the most peaked distribution (Table 4.3) and the velocities of different flow paths also varies less than for the other samples.

Tsang also compared a skewed aperture distribution, having the tail before peak, with the symmetric Gaussian distribution. The comparison shows less tortuosity effects for the skewed distribution. The aperture distributions measured in our study is skewed but with the tail after the peak. Stronger tortuosity effects should therefore be expected for our distribution than for the Symmetric Gaussian distribution. However, as discussed earlier, the aperture distribution will become more peaked during closure which is a compensating factor on the tortuousity effect. Tsang used a pure truncation of the distribution to account for the changes due to closure (see section 2.2).

The ratios between the mechanical and hydraulic aperture E/e calculated from the flow experiments lies between 1.1 and 1.7 for joints with hydraulic apertures between 134 μm and 428 μm. According to the empirical equation suggested by Barton et al. (1985), the ratio should be 1 for these apertures when JRC is as low as 3 - 9. However, this relationship is built on a compilation of data from mated joints and should therefore be applied to this type of joints.

Among the five studied joint samples the sample A is clearly mated. For the sample A JRC ~ 10. The flow test on A2 gives a datapoint in agreement with the curves in Figure 2.14, suggested by Barton. The flow test on A1 indicated a value on $E/e > 16$ and $e < 5$ μm. This point also plots in rough accordance with the suggested relation.

A comparison of the result in Table 4.6, concerning the distribution of the flow over the surface areas, with the result from aperture measurement in Table 4.3 shows that a more even flow corresponds to

smaller apertures and also to smaller spread in aperture distribution. An explanation to this trend, given by our experiments, could be that matedness is correlated with aperture such that well mated joints, i.e. with well correlated surfaces, have generally smaller average aperture than unmated joints.

This tendency can be understood physically simply because two almost identical, opposite surfaces subjected to normal stress should close better than two surfaces with uncorrelated topographies. At depth in the rock mass, rock joints are normally subjected to considerable normal stress.

Joints showing some shear displacement, in particular the joints which have a large dilation angle, should be responsible for the major part of flow. An exception would be the cases where extensive filling material, subsequent to earlier shearing, has partly sealed the joints.

In the interpretation of in-situ tracer tests the major channels of transport should therefore be expected to be found on the most unmated and open joints and to be unevenly spread over these surfaces. However, on a larger scale of tracer tests, channels of transport may be found along geological structures other than the so called single joints. These channels could be responsible for a considerable part of the transport depending on the actual rock mass.

The technique developed has so far been applied to five different joint replicas. The aperture and flow measurements were performed for one state of compression on each sample, apart from sample A, on which the apertures were measured for two different compressions. The data collected is therefore limited and does not allow for extensive conclusions. However, the available results and evaluations do provide ideas and suggestions for further research. Observed trends may then be confirmed or modified.

6 CONCLUSIONS

- Carefully fabricated transparent replicas of rock joints have been shown to provide useful subjects for hydromechanical studies. The techniques developed during this work give the possibility to measure both aperture and flow characteristics of natural rock joints.

- Five different joint samples have been replicated and their void geometries were studied by aperture measurements. The average mechanical aperture, E, varied between 84 and 462 μm. The aperture distribution of the studied joint samples can be statistically described with a log-normal function.

- The equivalent hydraulic aperture, e, of the samples were determined from flow experiments. The quotient E/e was shown to vary between 1.1 and 1.7 for samples with apertures larger than 0.1 mm.

- Estimates of the flow through the joints were made using the measured apertures, E, in the cubic law. The flow actually measured in the experiments were 10 to 75 % of the estimates.

- The velocities along several different flow paths over the joint surface were measured. The result shows that through some channels of a joint the flow velocity can be up to about twenty times higher than through other channels. The channeling character differed between the joint samples.

- The determination of the hydraulic aperture, e, was not sufficient to explain the different channeling characters between different joints. Among the studied joint samples were examples of similar e values on joints with different channeling character.

- Also the quotient E/e was alone not sufficient to fully describe the hydraulic character of a joint. The value of this quotient is influenced both by actual aperture value and by the degree of matedness.

- When the variation in aperture value was large the part of the joint surface area, effectively contributing to the total flow, was small compared to the whole joint surface area. Well mated joints were, on the other hand, shown to conduct the water more evenly over the whole surface.

- The degree of matedness is therefore an important factor influencing the conductive properties of a joint. The spread of the aperture distribution reflects the matedness. The ratio between the average aperture and the standard deviation of the aperture distribution could be a possible matedness parameter.

- The joint matedness property, alternatively the degree of mismatch between joint surfaces, should be considered in hydrogeological surveys, in particular when the velocity of the water flow is of importance. Practical and objective methods for the determination of aperture and matedness are needed to improve the possibilities of good hydromechanical modelling of the rock mass.

7 ACKNOWLEDGEMENT

I would very much like to thank Dr. Nick Barton for his supervision and encouragement during the course of this work. I would also like to thank Professor Ove Stephansson for giving me the opportunity to work on this project.

I am grateful to Josef Forslund and Tove-Heidi Mortensen for their help with the experimental work and to Monica Leijon for drawing the figures.

Financial support provided for this work by the Luleå University of Technology and the Stripa Project is acknowledged.

8 REFERENSER

Abelin, H. (1986): Migration in a single fracture. Ph.D. Thesis, Royal Institute of Technology, Stockholm.

Abelin, H., Neretnieks, I., Tunbrant, S. and Moreno, L. (1985): Final report of the migration in a single fracture - Experimental results and evaluation. Stripa Project, Technical Report 85-03. Swedish Nuclear Fuel and Waste Management Co., Stockholm.

Bandis, S.C. (1980): Experimental studies of scale effects on shear strength and deformability of regularly jointed rock. Ph.D. Thesis, Univ. of Leeds, 385 p.

Bandis, S.C., Lumsden, A.C. and Barton, N.R. (1983): Fundamentals of rock joint deformation. Int. J. Rock Mech. Min. Sci. & Geomech. Abstr., Vol. 20, No. 6, pp. 249-268.

Barton, N.R. (1986): Deformation phenomena in jointed rock. Geotechnique, Vol. 36, No. 2, pp. 147-167.

Barton, N. and Choubey, K. (1977): The shear strength of rock joints in theory and practice. Rock Mechanics, Vol. 10, pp. 1-54.

Barton, N. and Bakhtar, K. (1983): Rock joint description and modelling for the hydrothermomechanical design of nuclear waste repositories. Contract Rept., Subm. to CANMET, Min. Res. Lab., Ottawa, Parts 1-5, 378 p.

Barton, N., Bandis, S. and Bakhtar, K. (1985): Strength, deformation and conductivity coupling of rock joints. Int. J. Rock Mech. Min. Sci. & Geomech. Abstr., Vol. 22, No. 3, pp 121-140.

Barton, N. and Makurat, A. (1988): Modelling excavation responses in jointed rock. OECD/AECL Workshop on "Excavation Responce in Deep Radioactive Waste Repositories", April 1988, Toronto, Canada.

Brown, S. (1987): Fluid flow through rock joints: The effect of surface roughness. J. Geoph. Res., Vol. 92, No. B2, pp. 1337-1347.

Brown, S.R. and Scholz, C.H. (1985a): Closure of random elastic surfaces in contact. J. Geoph. Res., Vol. 90, No. B7, pp. 5531-5545.

Brown, S.R. and Scholz, C.H. (1985b): Broad bandwith study of the topography of natural rock surfaces. J. Geoph. Res., Vol. 90, No. B14, pp. 12,575-12,582.

Brown, S.R. and Scholz, C.H. (1986): Closure of rock joints. J. Geoph. Res., Vol. 91, No. B5, pp. 4939-4948.

Carlsson, A. and Olsson, T. (1977): Water leakage in the Forsmark tunnel, Uppland, Sweden. Geological Survey of Sweden, Ser. C, No. 734.

Elliot, G.M., Brown, E.T., Boodt, P.I. and Hudson, J.A. (1985): Hydro-mechanical behaviour of joints in the Carnmenellis granite, S.W. England. Proc. Int. Symp. on Fundamentals of Rock Joints, Björkliden, Sweden, 15-20 September 1985, Centek Publ., Luleå, pp. 249-258.

Gale, J.E. (1982): The effects of fracture type (induced versus natural) on the stress-fracture closure-fracture permeability relationships. Proc. 23rd US Symp. on Rock Mecanics, Berkeley, California, pp. 290-298.

Gale, J.E. (1987): Comparison of coupled fracture deformation and fluid flow models with direct measurements of fracture pore structure and stress-flow properties. 28th US Symp. on Rock Mechanics, Tucson, Arizona, June 29-1 July, pp. 1213-1222.

Gentier, S. (1986): Morphologie et comportement hydromechanique d'une fracture naturelle dans une granite sous contrainte normale. Ph.D. Thesis, L'Universite d'Orleans.

GEOVAL 87 (1987): A symposium of verification and validation of geosphere performance assessment models. April 7-9, 1987, Stockholm, Swedish Nuclear Power Inspectorate, Stockholm.

Greenwood, J.A. and Williamson, J.B.P. (1966): Contact of nominally flat surfaces. Proc. R. Soc. London, Ser. A 295, pp. 300-319. *

Greenwood, J.A. and Tripp, J.H. (1967): The elastic contact of rough spheres. J. Appl. Mech., March, 1967, pp. 153-159.

Gustavsson, G. (1986): Geohydrologiska förundersökningar i berg. Bakgrund - metodik - användning. BeFo 84:1/86, Swedish Rock Engineering Research Foundation, Stockholm (in Swedish).

Hopkins, D.L., Cook, N.G.W. and Myer, L.R. (1987): Fracture stiffness and aperture as a function of applied stress and contact geometry. 28th US Symp. on Rock Mechanics, Tucson, Arizona, June 29-1 July, pp. 673-680.

Iwai, K. (1976): Fundamental studies of fluid flow through a single fracture. Ph.D. Thesis, Univ. of California, Berkeley.

Maini, Y.N.T. (1971): In situ hyraulic parameters in jointed rock - Their measurement and interpretation. Ph.D. Thesis, Imperial College of Science and Technology, Univ. of London.

Moreno, L. (1985): Analysis of some laboratory tracer runs in natural fissures. Water Resources Res., Vol. 21, No. 7, pp. 951-958.

Neuzil, C.E. and Tracy, J.V. (1981): Flow through fractures. Water Resources Res., Vol. 17, No. 1, pp. 191-199.

Nolte, D.D., Pyrak-Nolte, L.J. and Cook, N.G.W. (1987): The fractal geometry of the flow paths in natural fractures in rock and the approach to percolation. Accepted by PAGEOPH on 8/19/87.

Pyrak-Nolte, L.J, Myer, L.R., Cook, N.G. and Witherspoon, P.A. (1987): Hydraulic and mechanical properties of natural fractures in low permeability rock. Proc. 6th Int. Cong. on Rock Mechanics, Montreal, Canada, Vol. 1, pp. 225-231.

Raven, K.G. and Gale, J.E. (1985): Water Flow in a Natural Rock fracture as a function of stress and sample size. Int. J. Rock Mech. Min. Sci. & Geomech. Abstr., Vol. 22, No. 4, pp. 251-261.

STATGRAPHICS, Statistical Graphics System by Statistical Graphics Corporation, User's Guide

Swan, G. (1983) Determination of stiffness and other joint properties from roughness measurements. Rock Mech. Rock Eng., Vol. 16, pp. 19-38.

Toppe, R. and Stabell, L-E. (1987): TERMOS Terrain Modelling System - A new concept in computer based maphandling. NGI Report, No. 51520-2, Norwegian Geotechnical Institute, Oslo.

Tsang, Y.W. (1984): The effect of tortuosity on fluid flow through a single fracture. Water Resources Res., Vol. 20, No. 9, pp. 1209-1215.

Tsang, Y.W. and Witherspoon, P.A. (1981): Hydromechanical behavior of a deformable rock fracture subject to normal stress. J. Geoph. Res., Vol. 86, No. B10, pp. 9287-9298.

Tsang, Y.W. and Tsang, C.F. (1987): Channel model of flow through fractured media. Water Resources Res., Vol. 23, No. 3, pp. 467-479.

Tsang, Y.W., Tsang, C.F., Hale, F.V., Moreno, L. and Neretnieks, I. (1987): Channeling characteristics of flow and solute transport through a rough-surfaced fracture. LBL-23195 UC-11, Lawrence Berkeley Laboratory, Berkeley, California.

Witherspoon, P.A., Wang, J.S.Y., Iwai; K. and Gale, J.E. (1980): Validity of cubic law for fluid flow in a deformable rock fracture. Water Resources Res., Vol. 16, No. 6, pp. 1016-1024.

* Reference cited from other sources.

APPENDIX 1 Aperture frequency histograms

Frequency histograms of the aperture distribution showing the results from aperture measurements using the technique described in section 3.4. A summary of the results is given in Table 4.3 (p. 63).

The histograms are calculated and plotted using the computer package for statistical analysis STATGRAPHICS.

Sample B

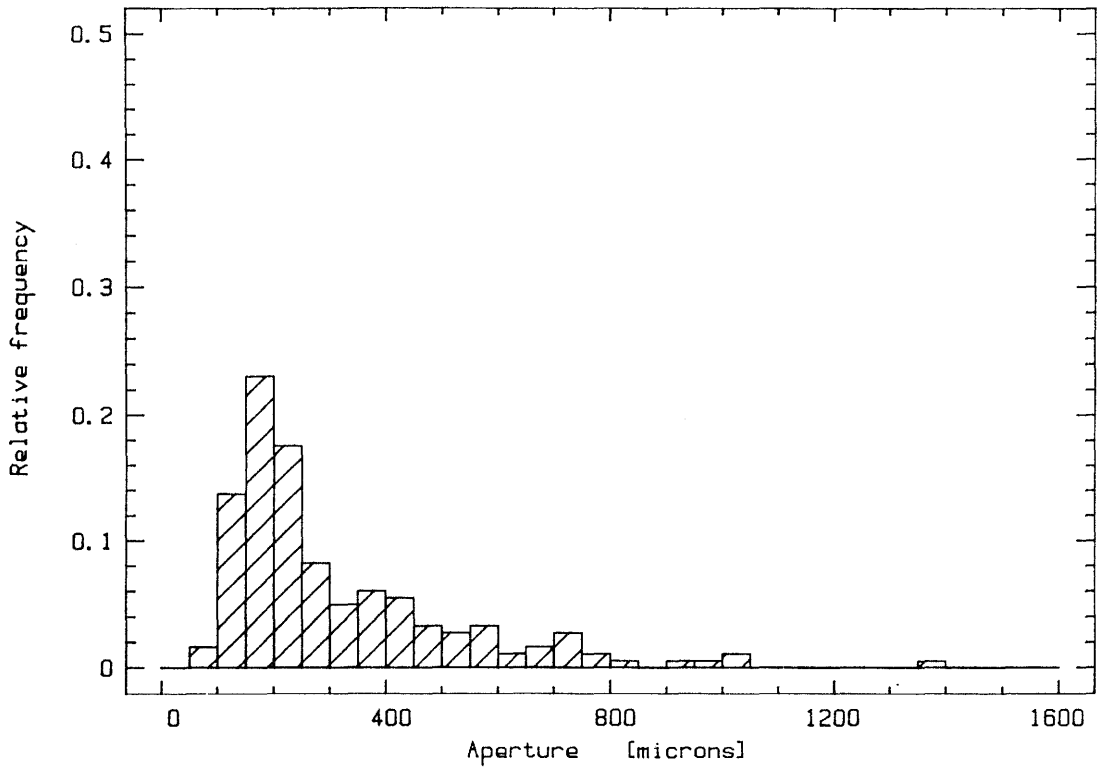

Sample S2

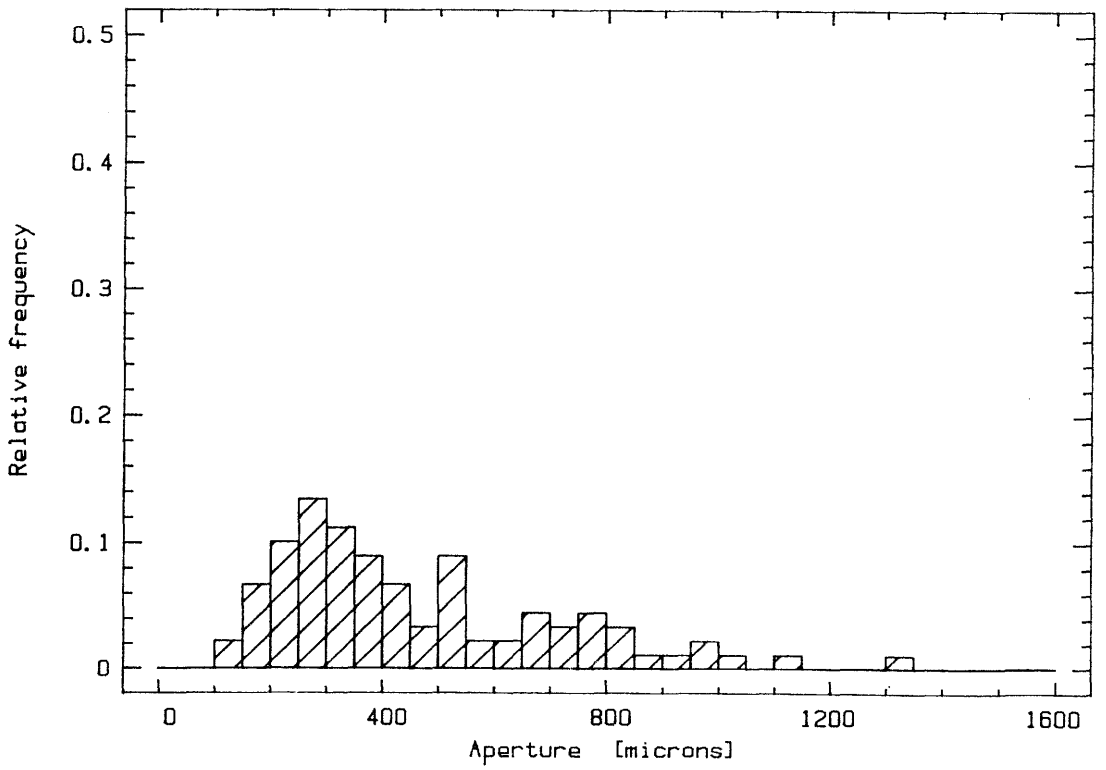

Sample S3

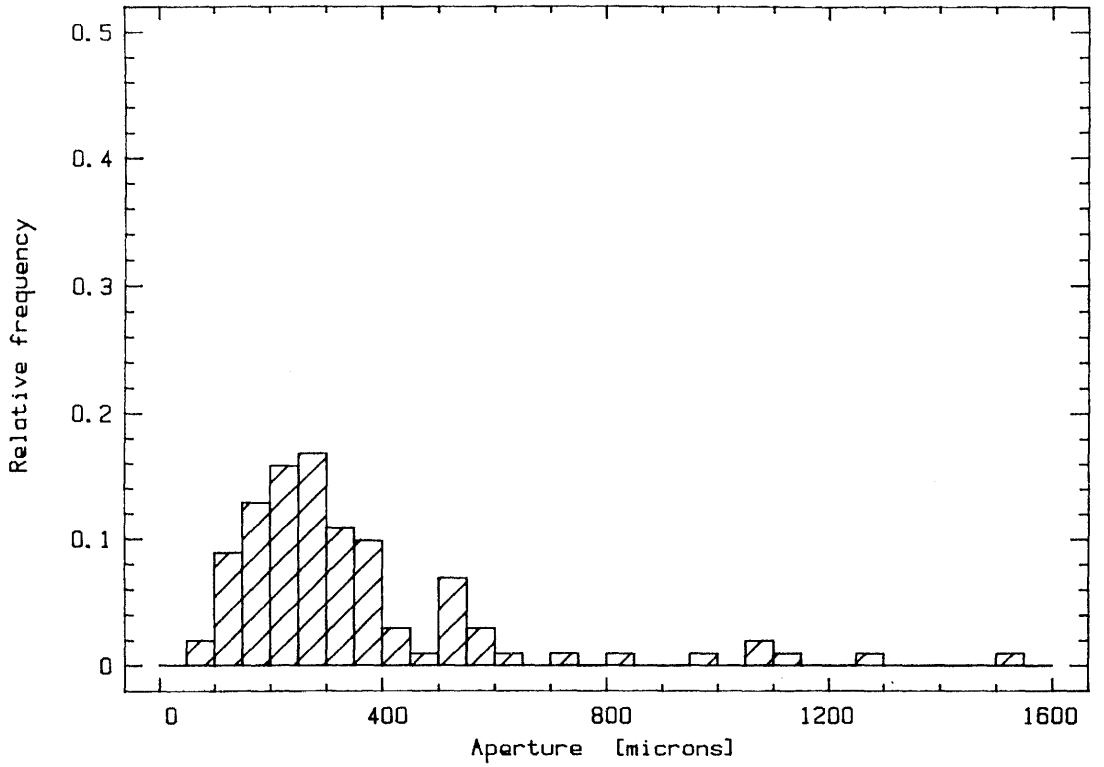

Sample S4

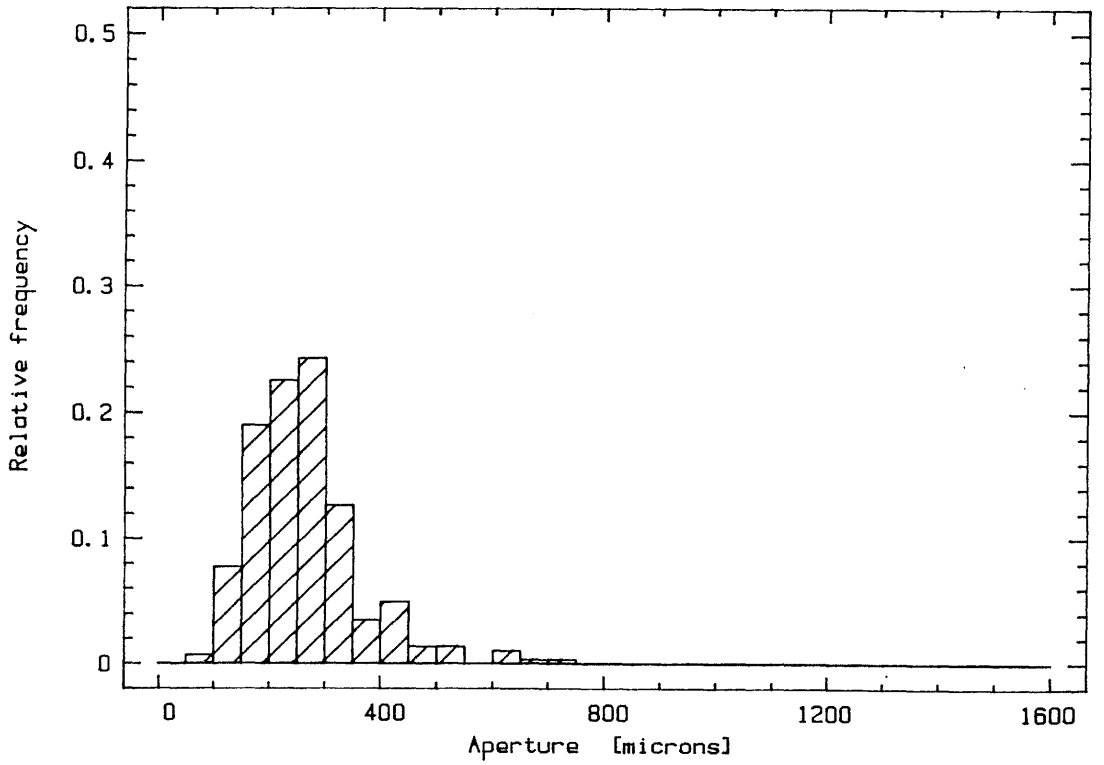

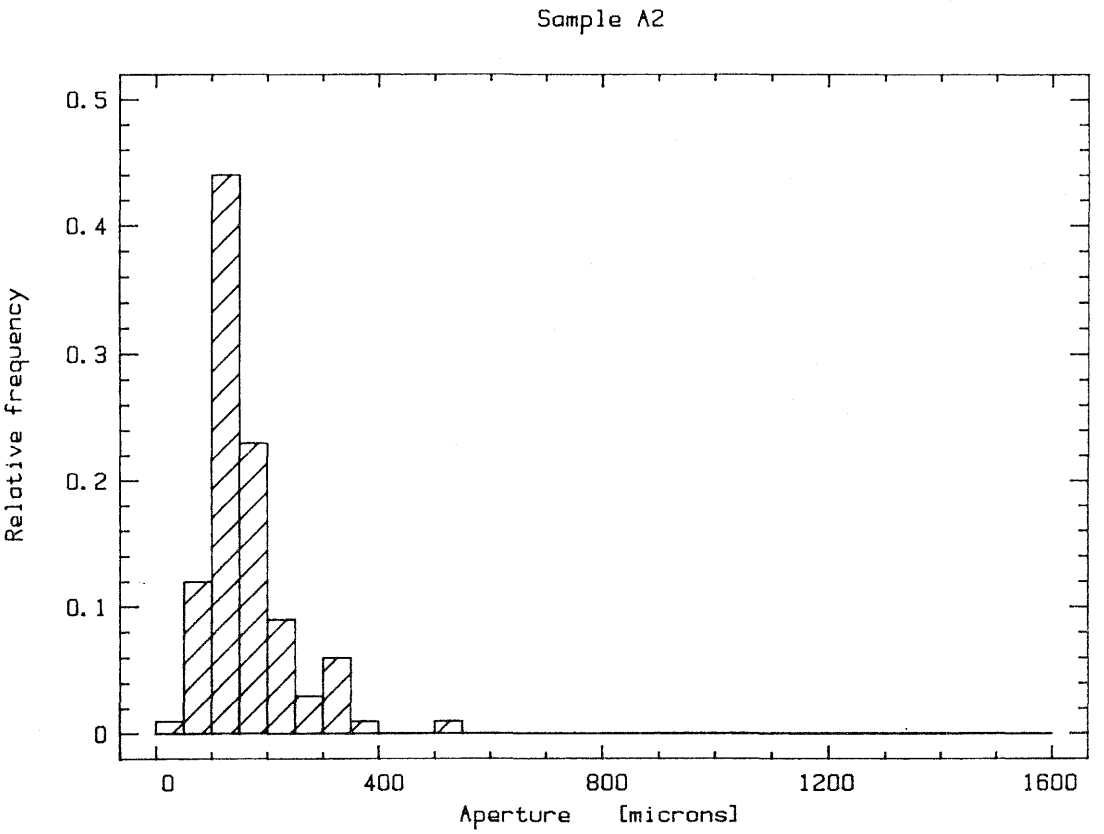
Sample A2
Relative frequency
0.5
0.4
0.3
0.2
0.1
0
0
400
800
1200
1600
Aperture [microns]

APPENDIX 2 Aperture isoplots

Isocurves of the apertures measured over the surface area of the joint replicas. The equidistance between lines is 50 μm and the areas corresponding to apertures smaller than 250 μm, for samples B, S2, S3 and S4, and smaller than 150 μm for sample A, is hatched.

Measurement A1 and A2 is made on the same joint replica, sample A, but under different degrees of compression. Measurement A1 corresponds to the highest level of normal load.

The last isoplot shows the isocurves of the difference in aperture values in each point between loading case A2 and A1, i.e. the closure of the aperture due to the change in normal load. The areas corresponding to closure less than 50 μm are hathed.

The calculation of the spatial aperture distribution is conducted with a digital terrain model program, TERMOS.

Sample B. Scale 1:1

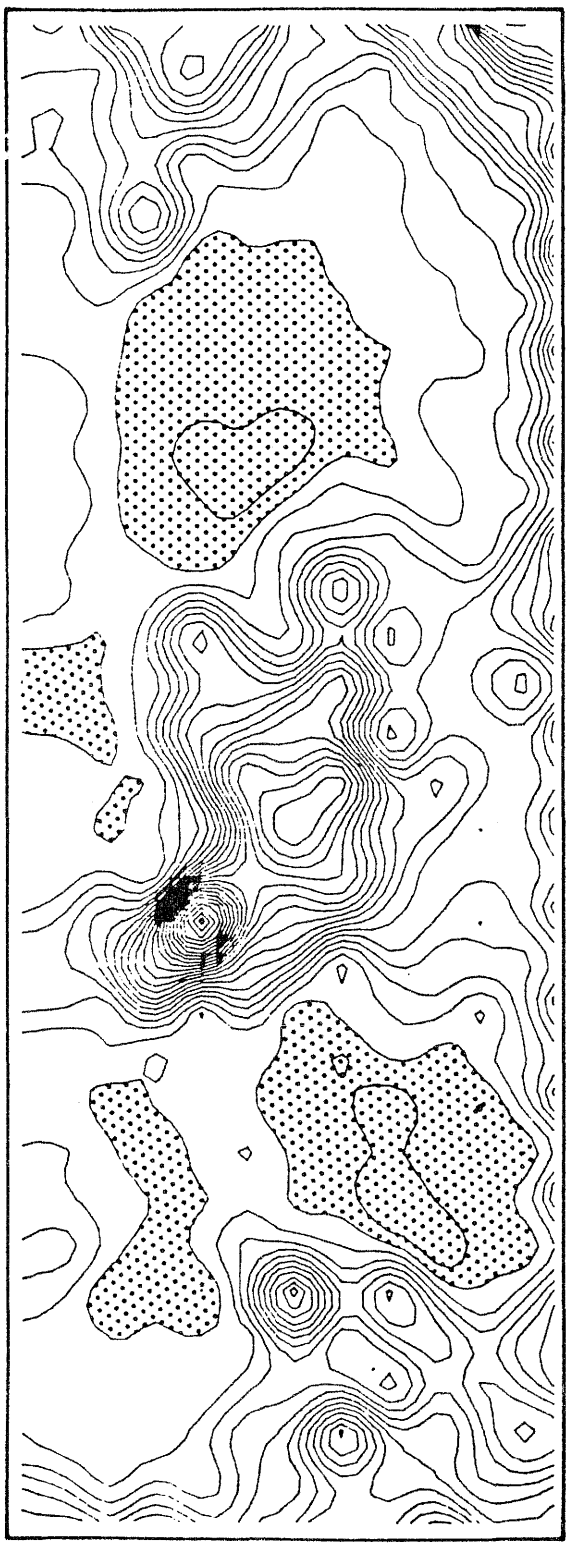

Sample S2. Scale 1:1

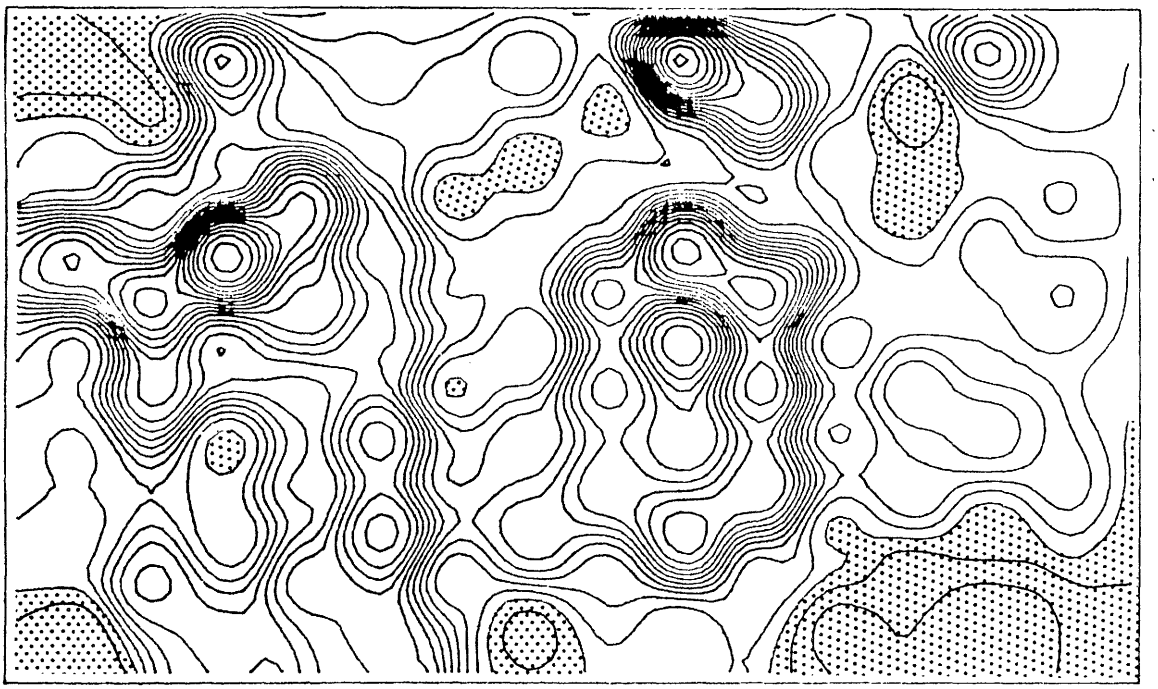

Sample S3. Scale 1:1

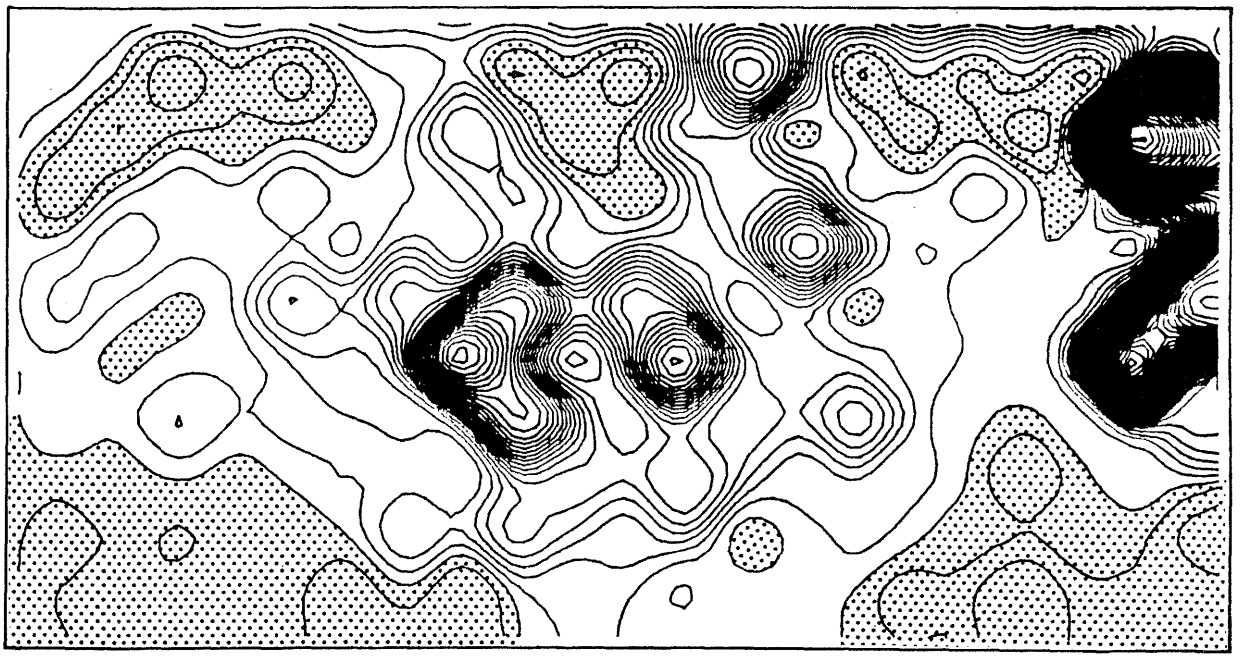

Sample S4. Scale 1:1

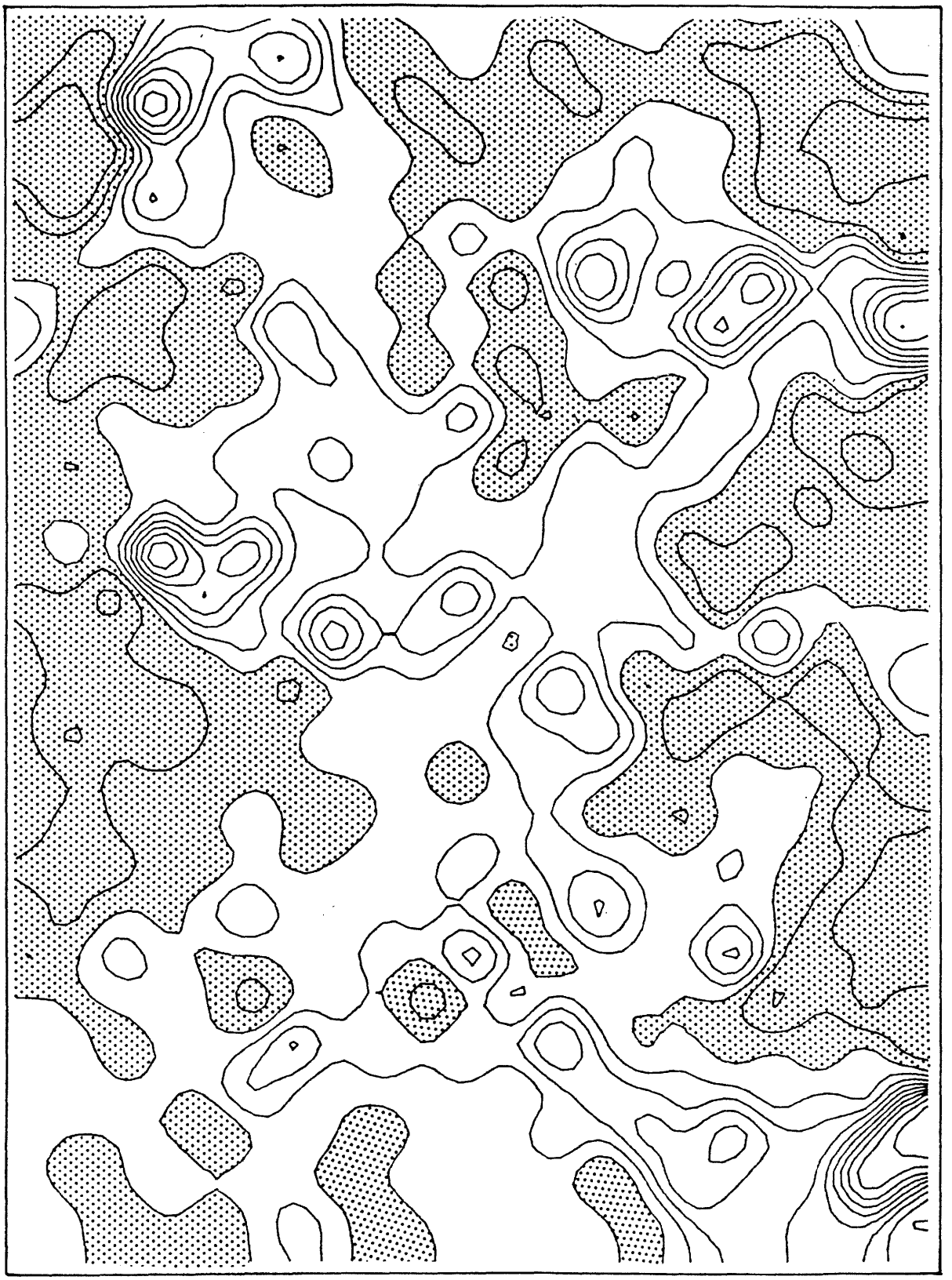

Sample A. Scale 1:1

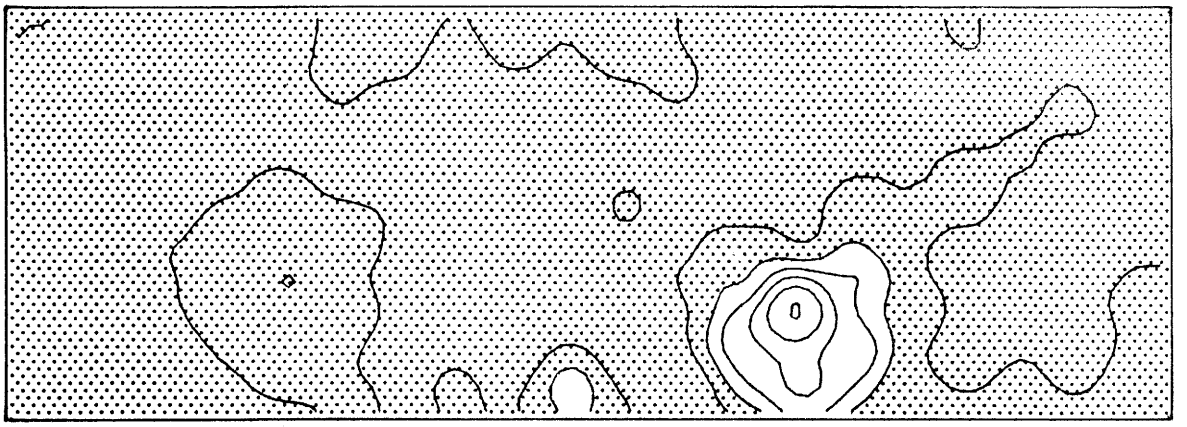

Measurement A1

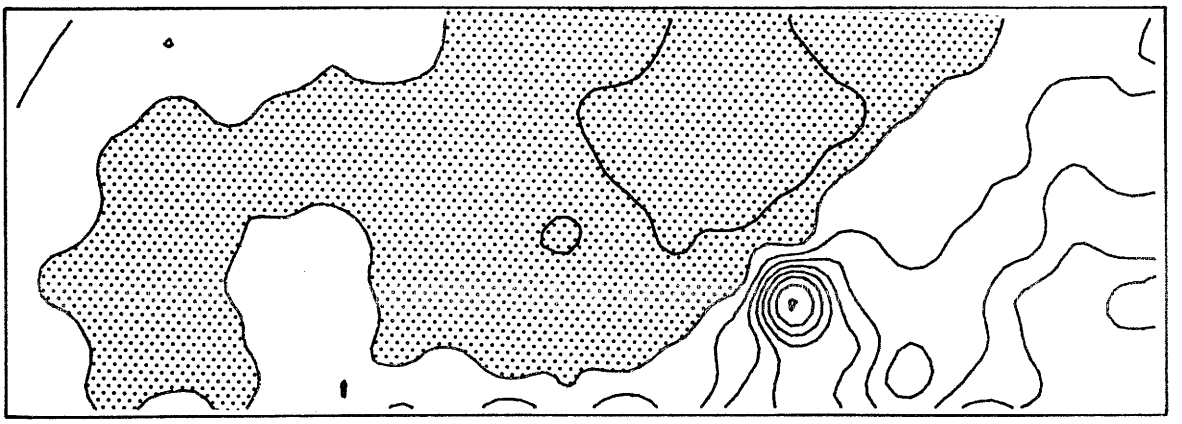

Measurement A2

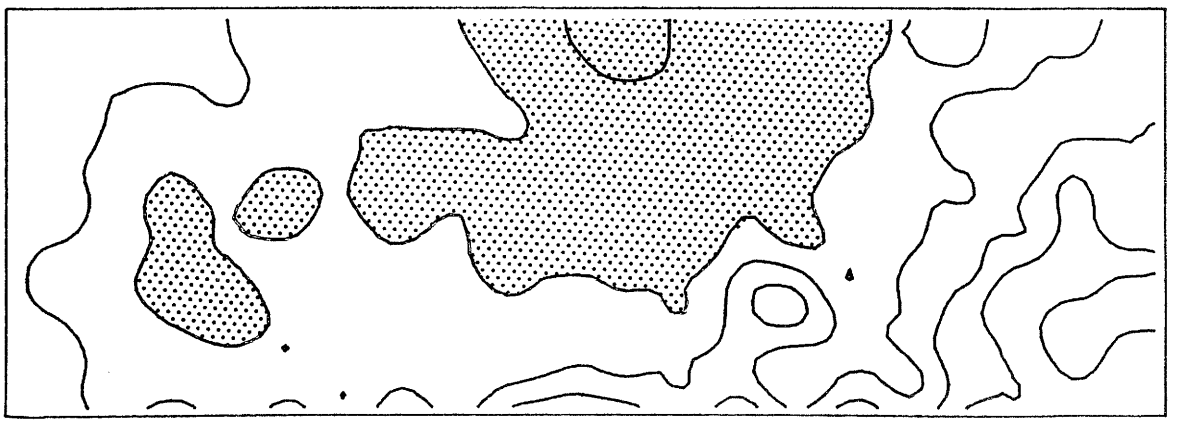

Closure (A2 - A1)

APPENDIX 3 Void geometry terrain models

Terrain models showing the topography of the void space inside the joints. The geometry is calculated using a DTM-package, TERMOS. The indata to the calculation is the aperture measurements described in section 3.4. The scale of the apertures (z-direction) is exaggerated for the sake of clarity.

Sample B

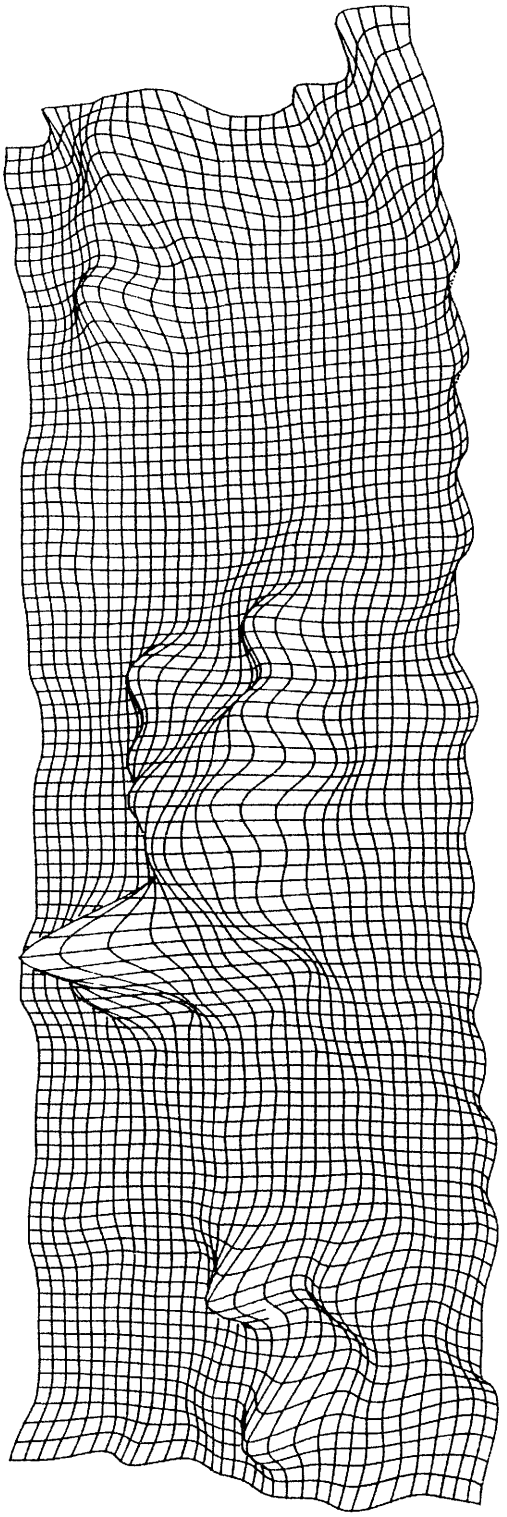

Sample S2

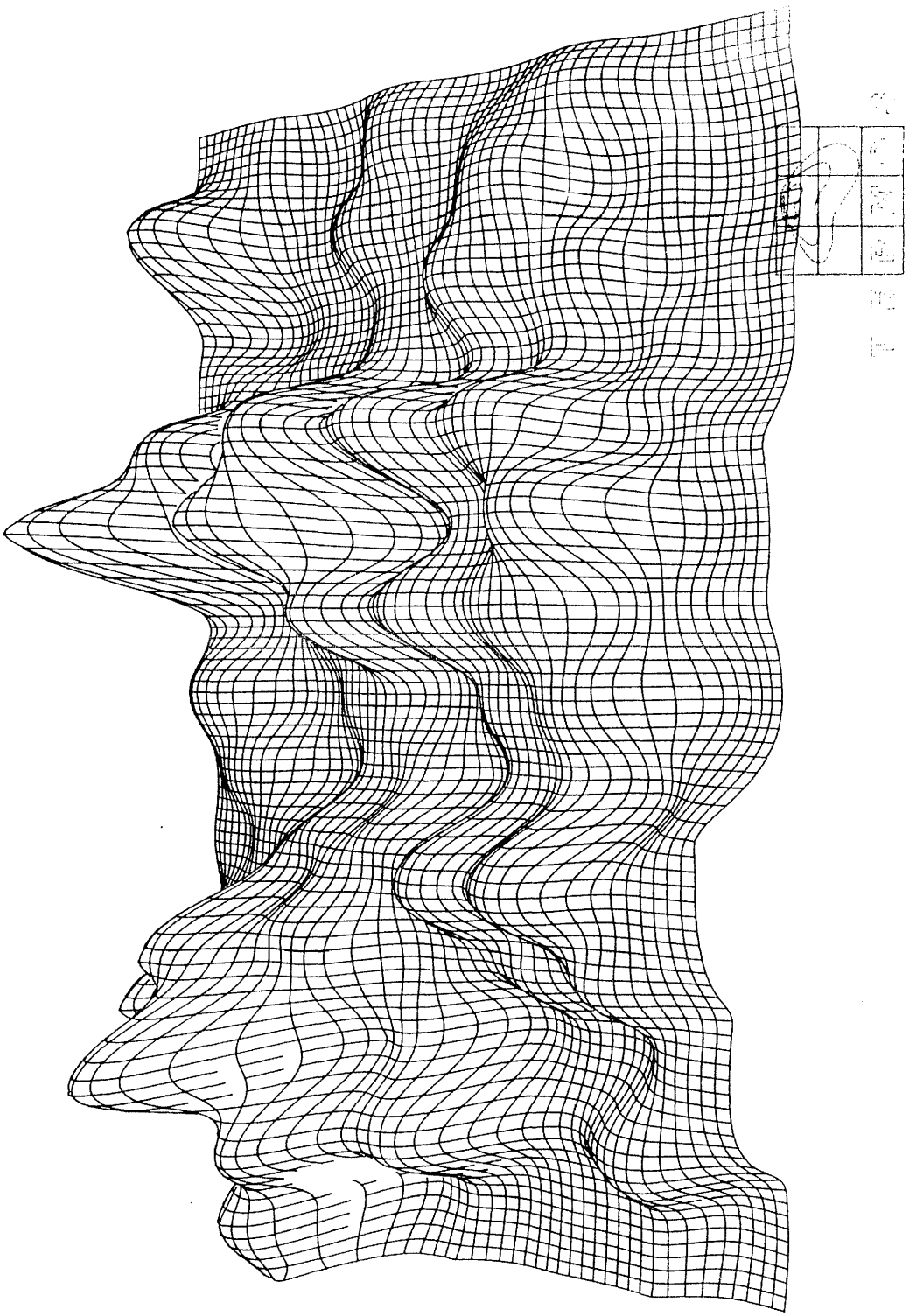

Sample S3

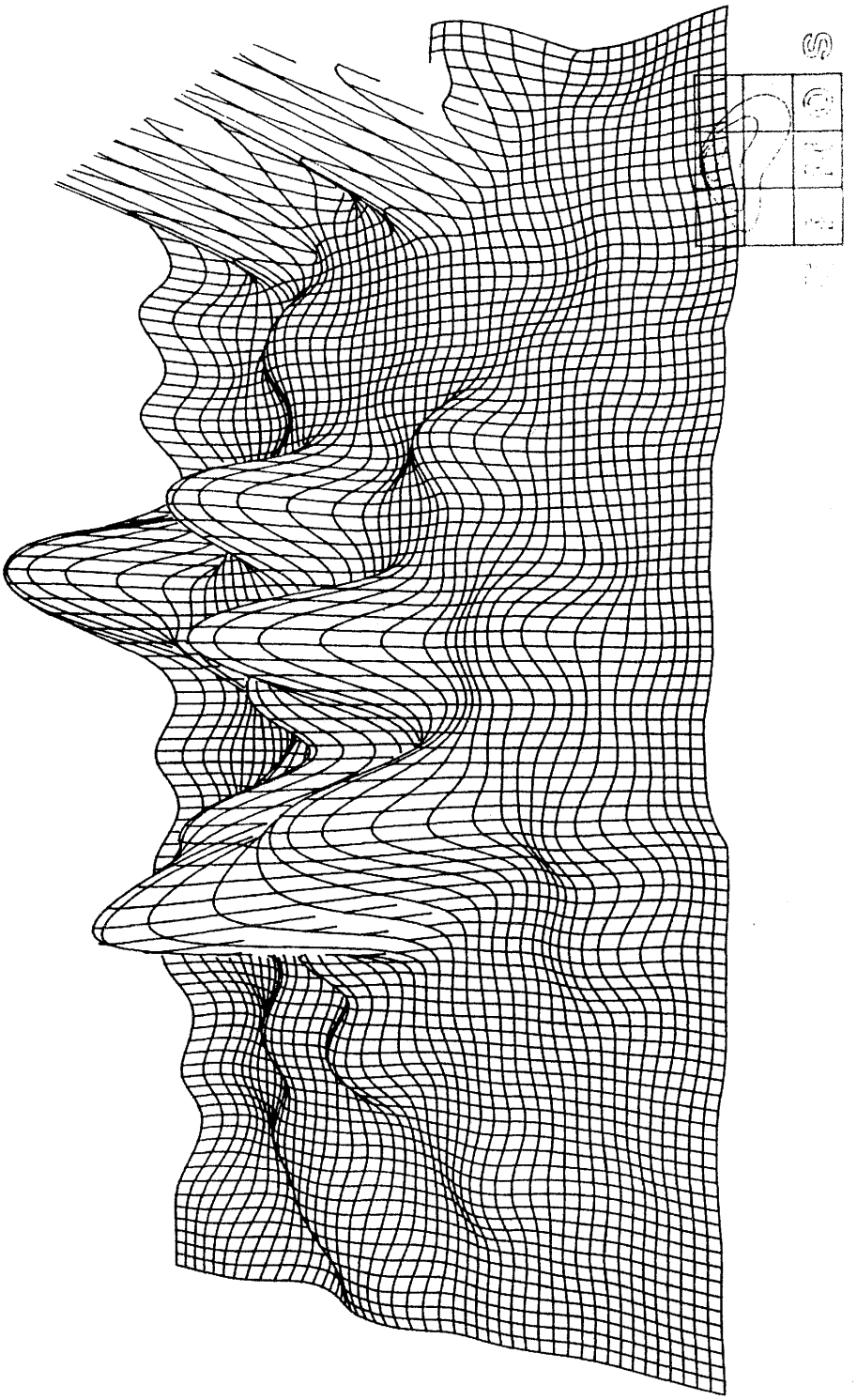

Sample S4

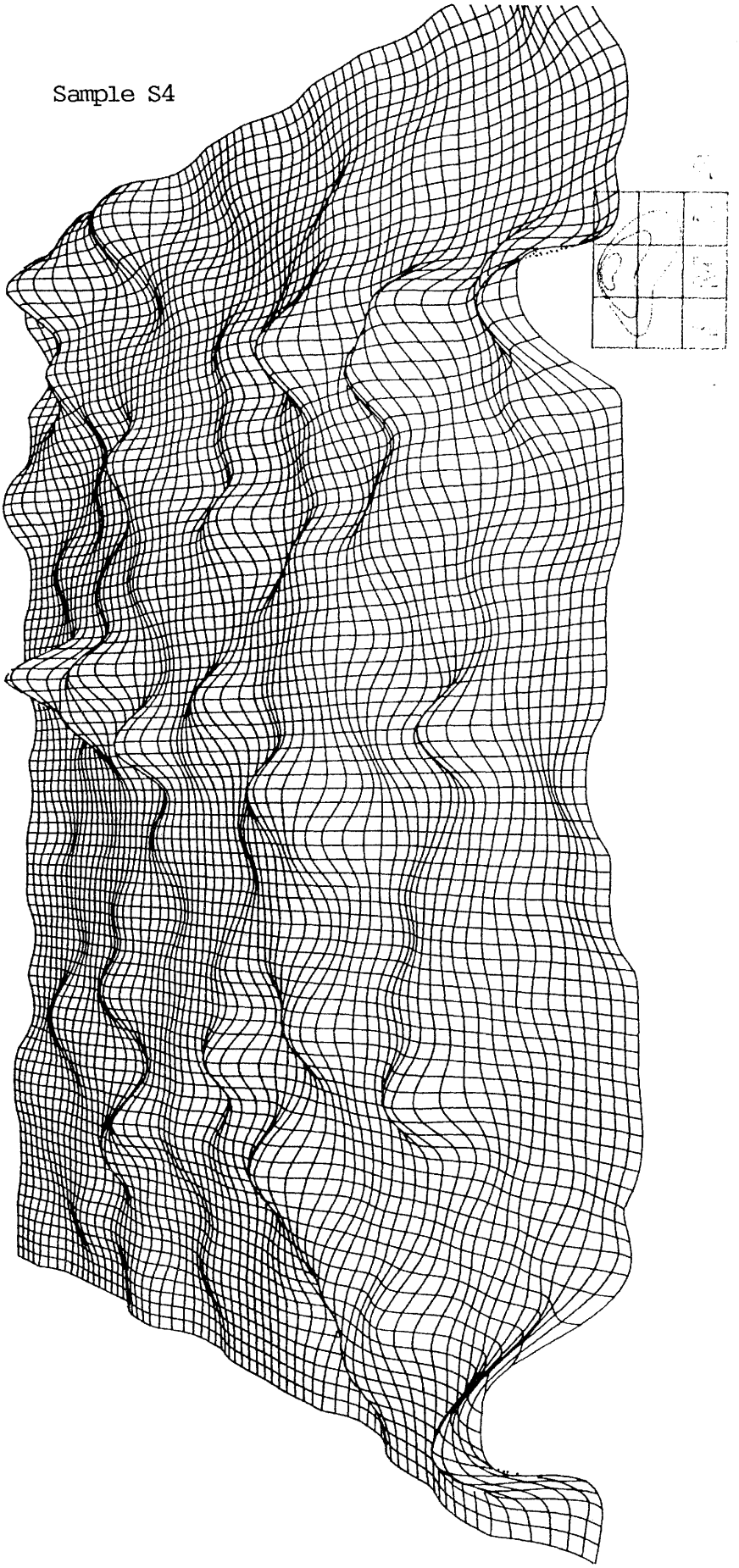

Sample A1

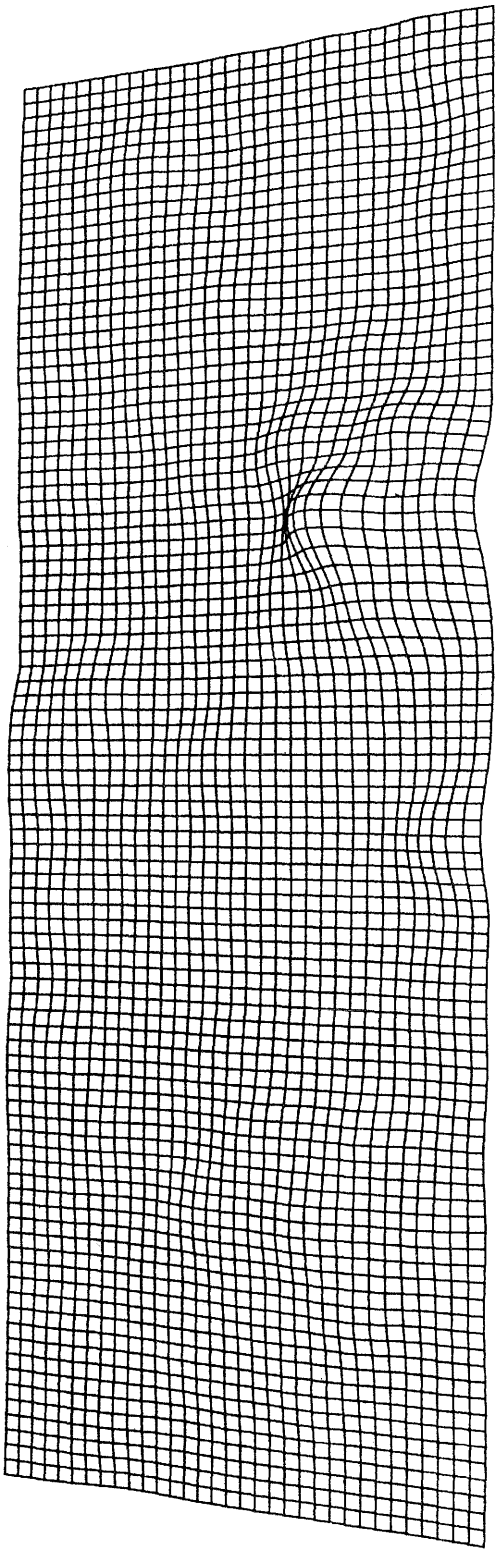

Sample A2

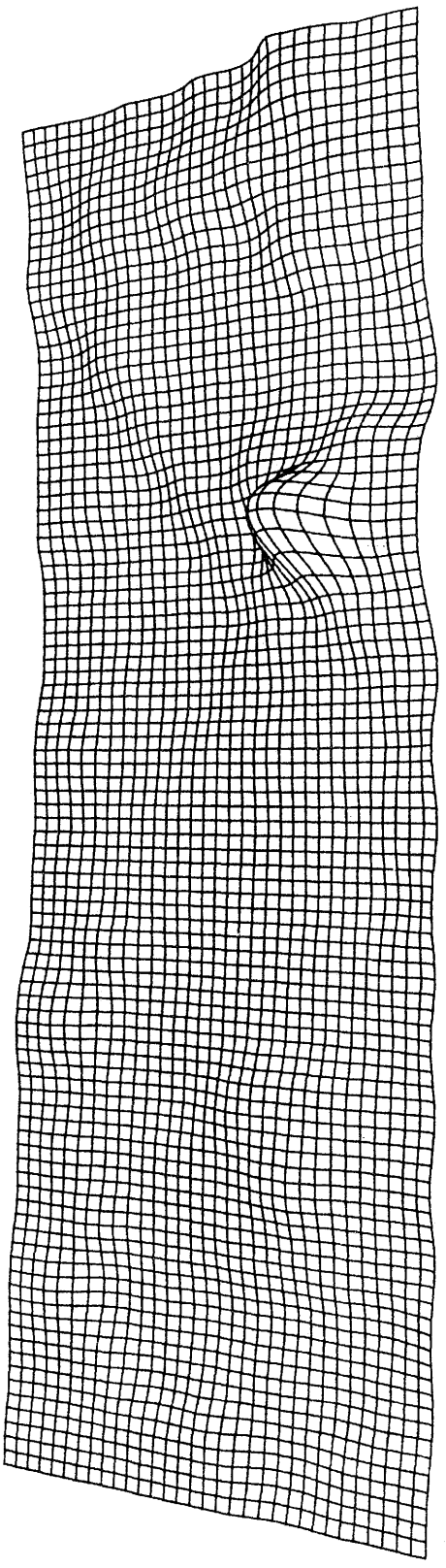

APPENDIX 4 Stream lines of flow

Colour injections into the water flow during the flow tests were recorded with photographs. The following figures shows a compilation of stream lines collected from different photographs on each sample.

The lines should be regarded only as examples of flow paths and are not selected of any specific reason. Unclear stream lines and lines very similar to others were omitted. On sample B both sides of the observed colour stream is given to illustrate that the width of the stream may vary along the path.

The direction of the flow is from bottom to top in the figures for all samples.

Sample B

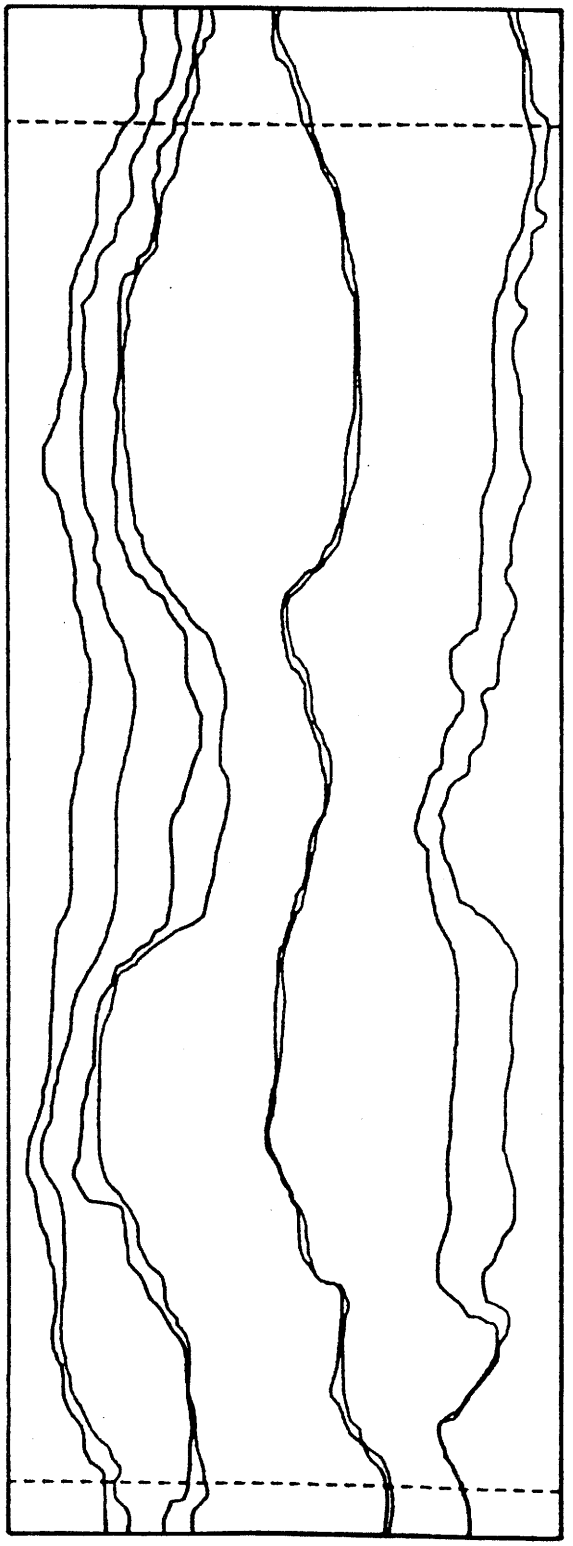

Sample S2

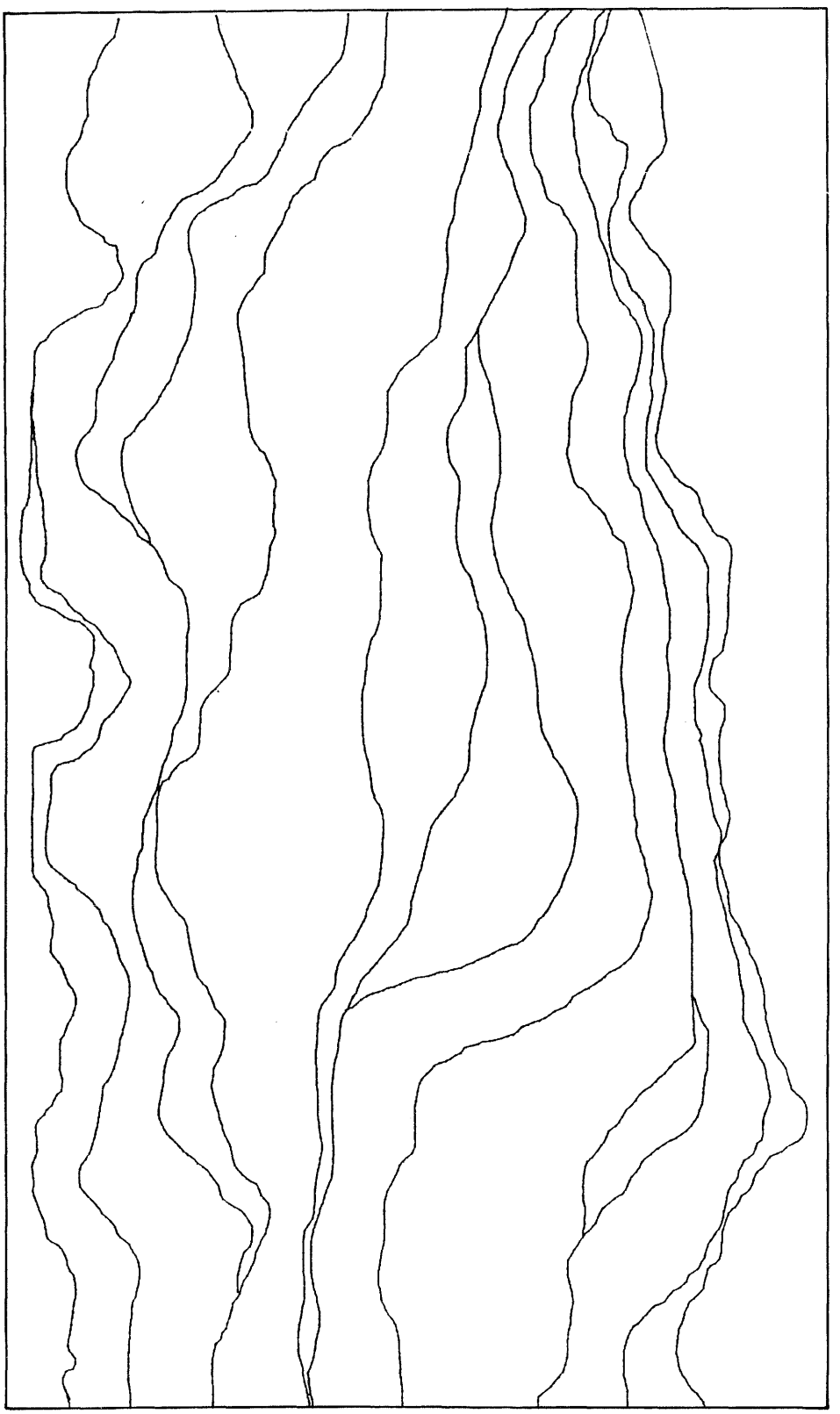

Sample S3

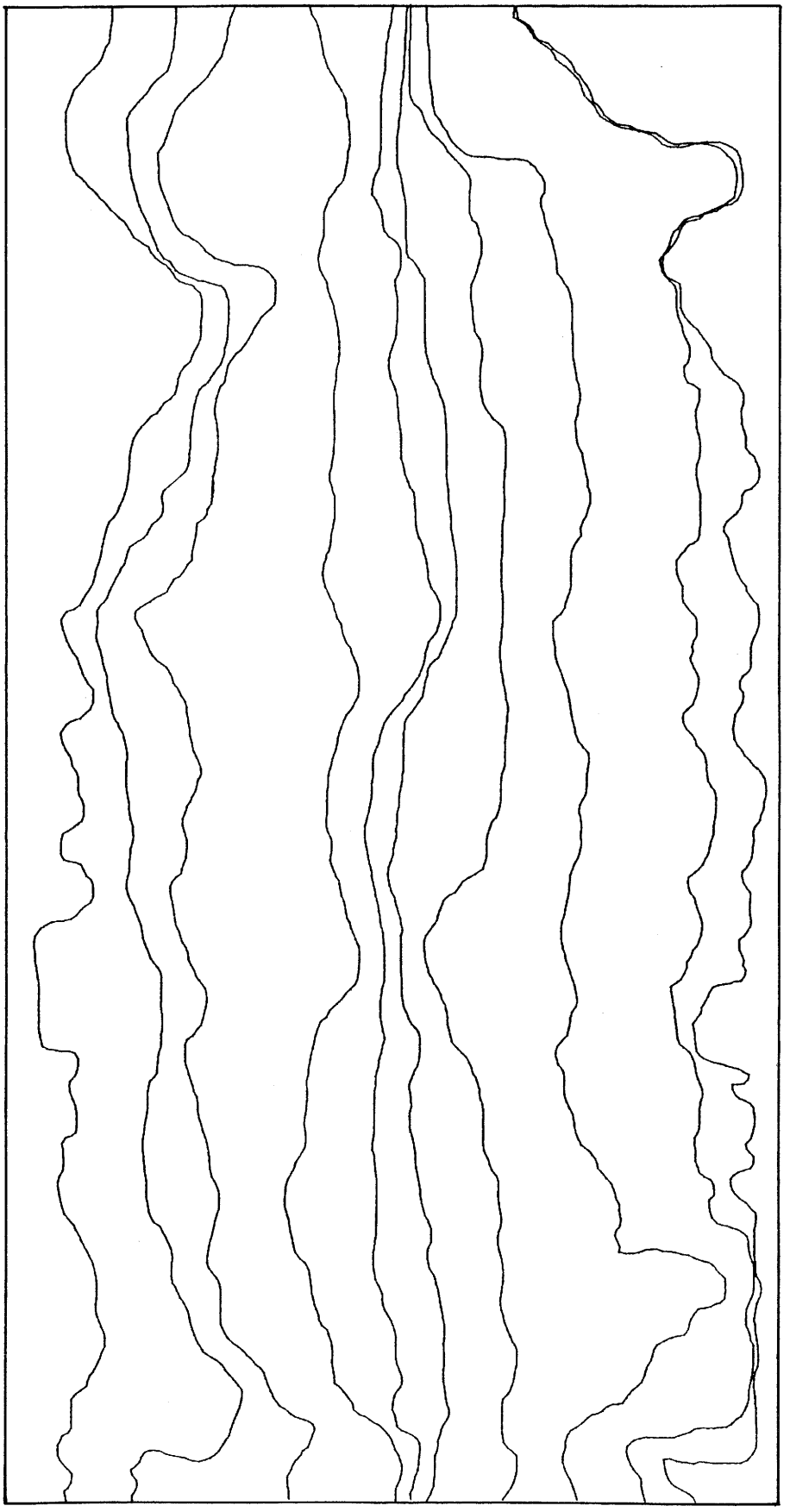

Sample S4

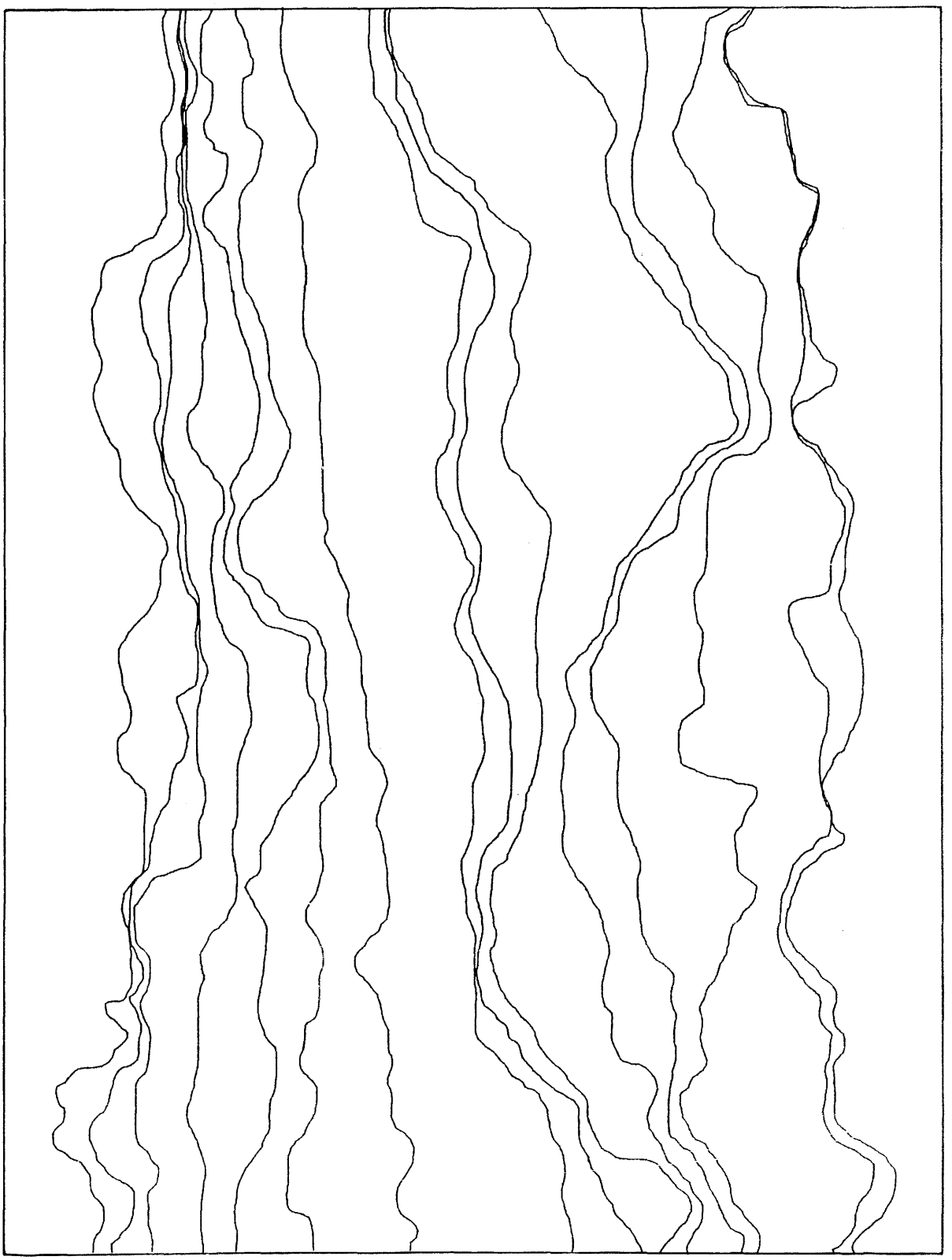

Sample A2

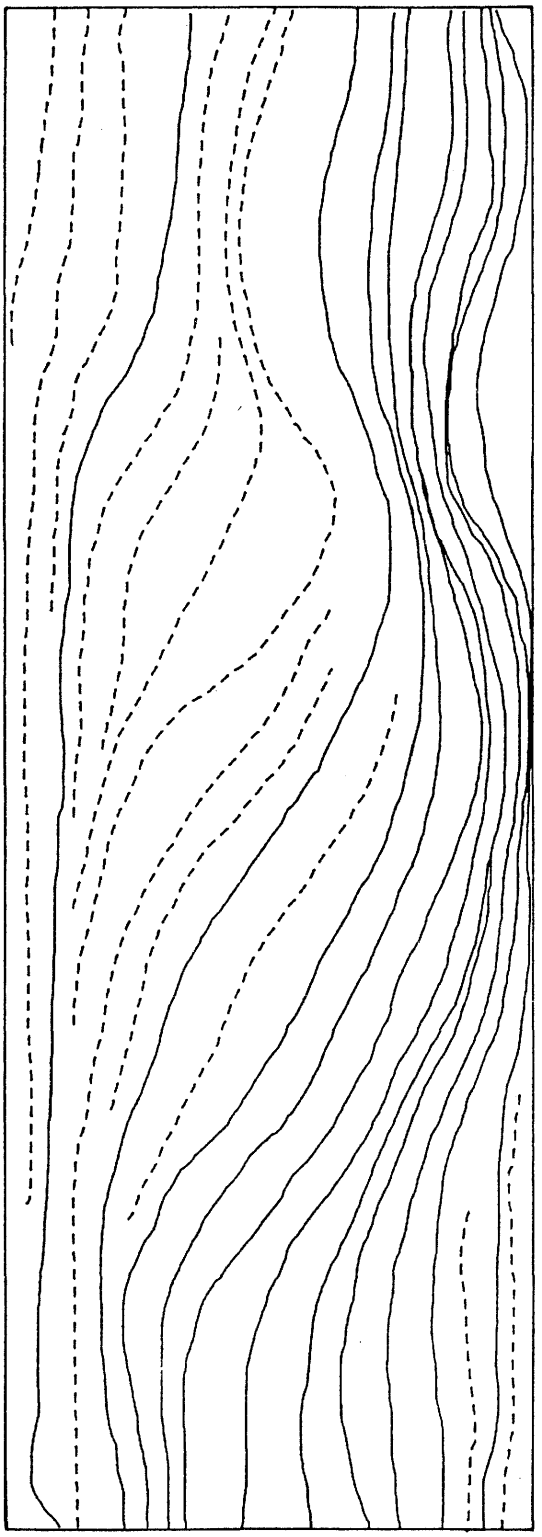

APPENDIX 5 Flow velocity diagrams

The results from flow velocity measurements are presented in the following diagrams. The measurement technique is described in section 3.5.2. The size and shape of the sample is given by the square. The length of the arrows correspond to the effective velocity of the flow determined from the colour injections. The starting point of each arrow is located at the beginning of the colour trace as observed from the photographs.

Dashed arrows shows estimated flow velocities in the cases when the measurements have not been successful.

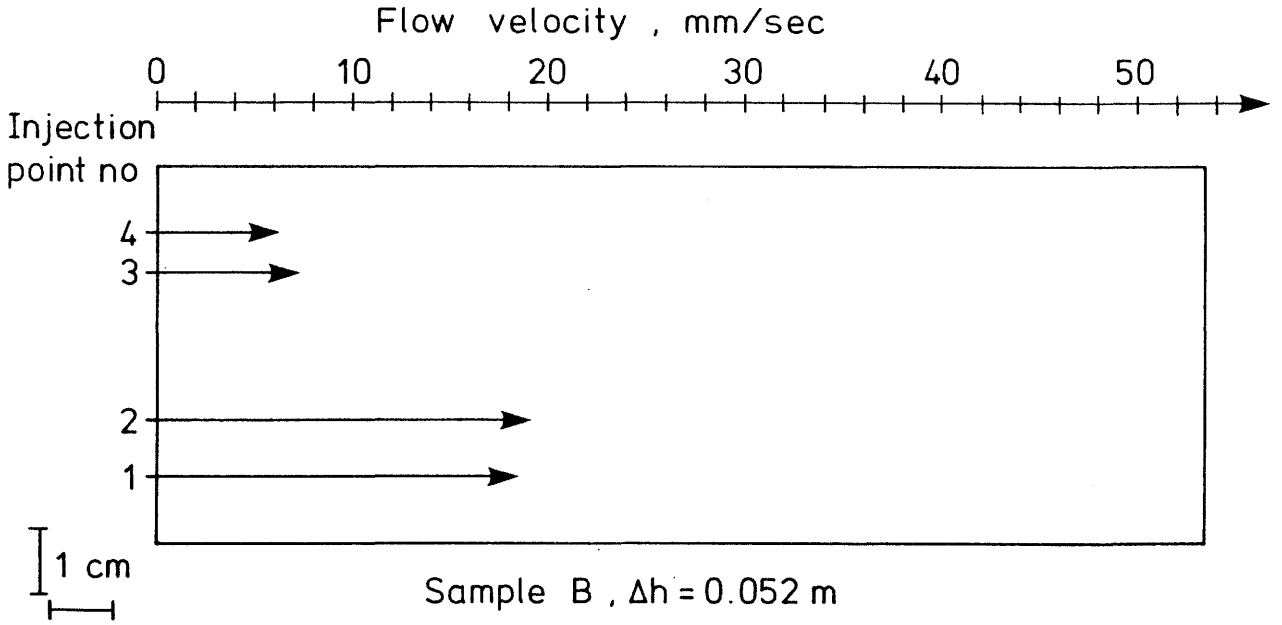

Sample B , Δh = 0.052 m

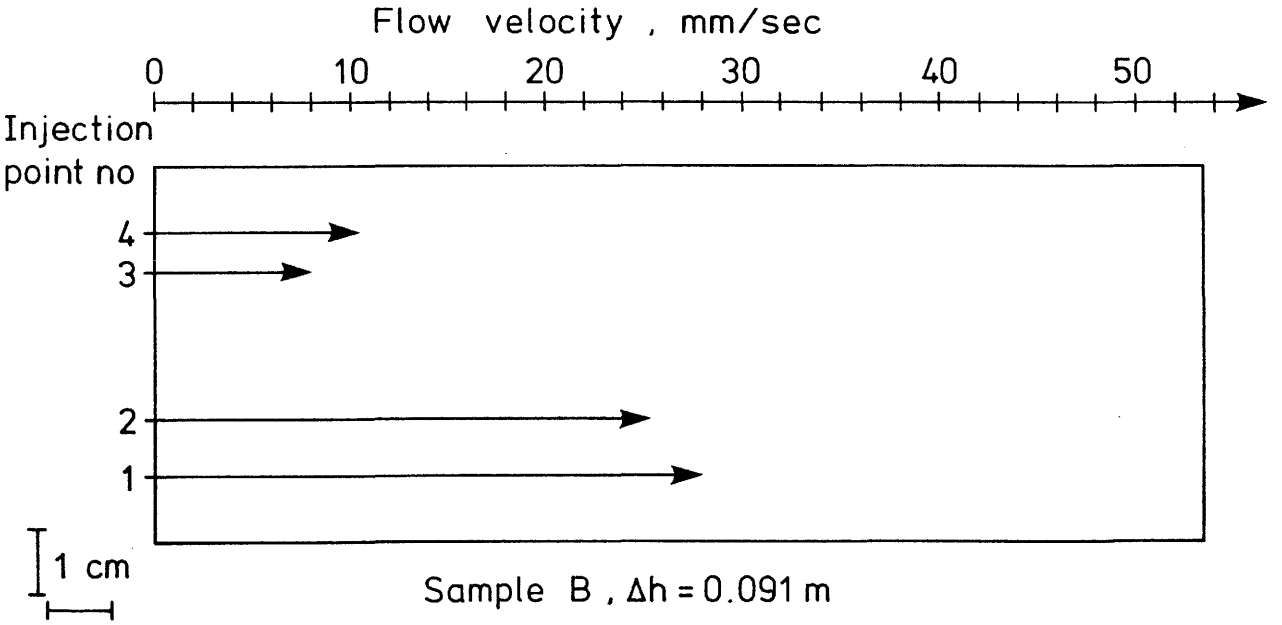

Sample B , Δh = 0.091 m

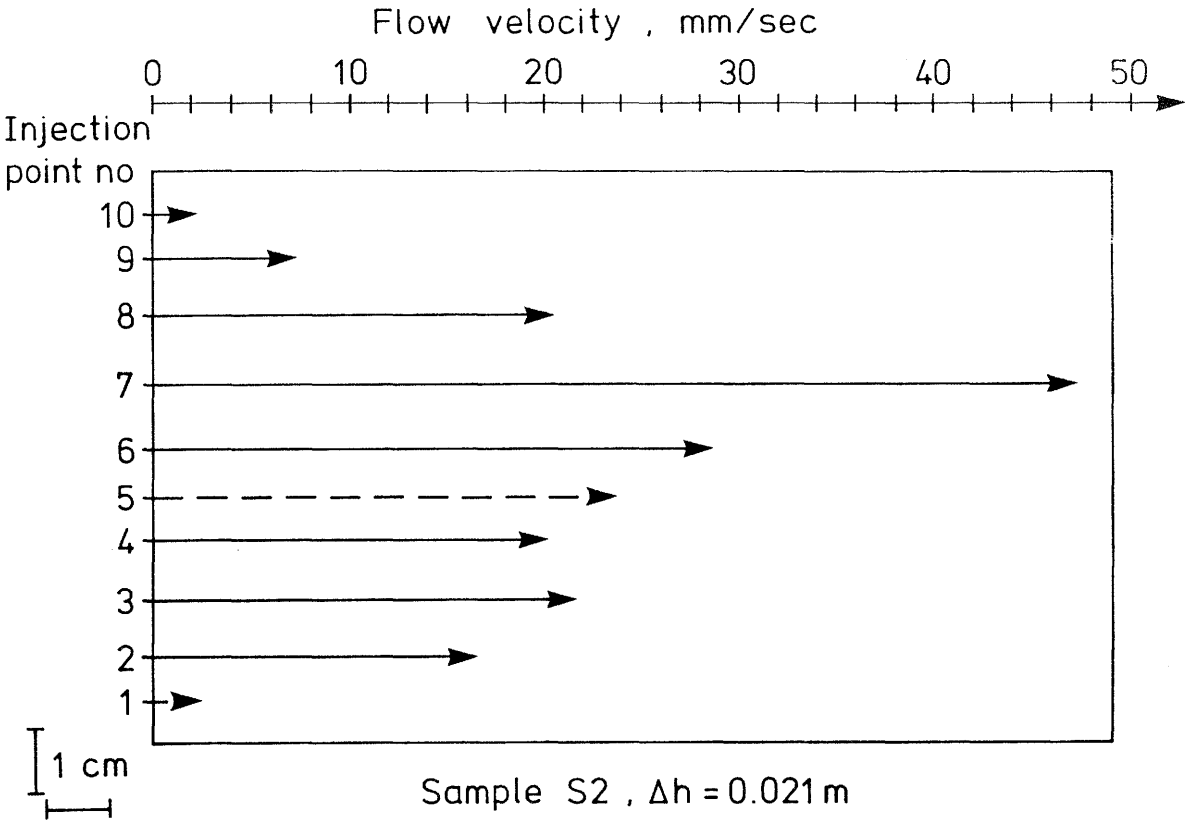

Sample S2 , $\Delta h = 0.021$ m

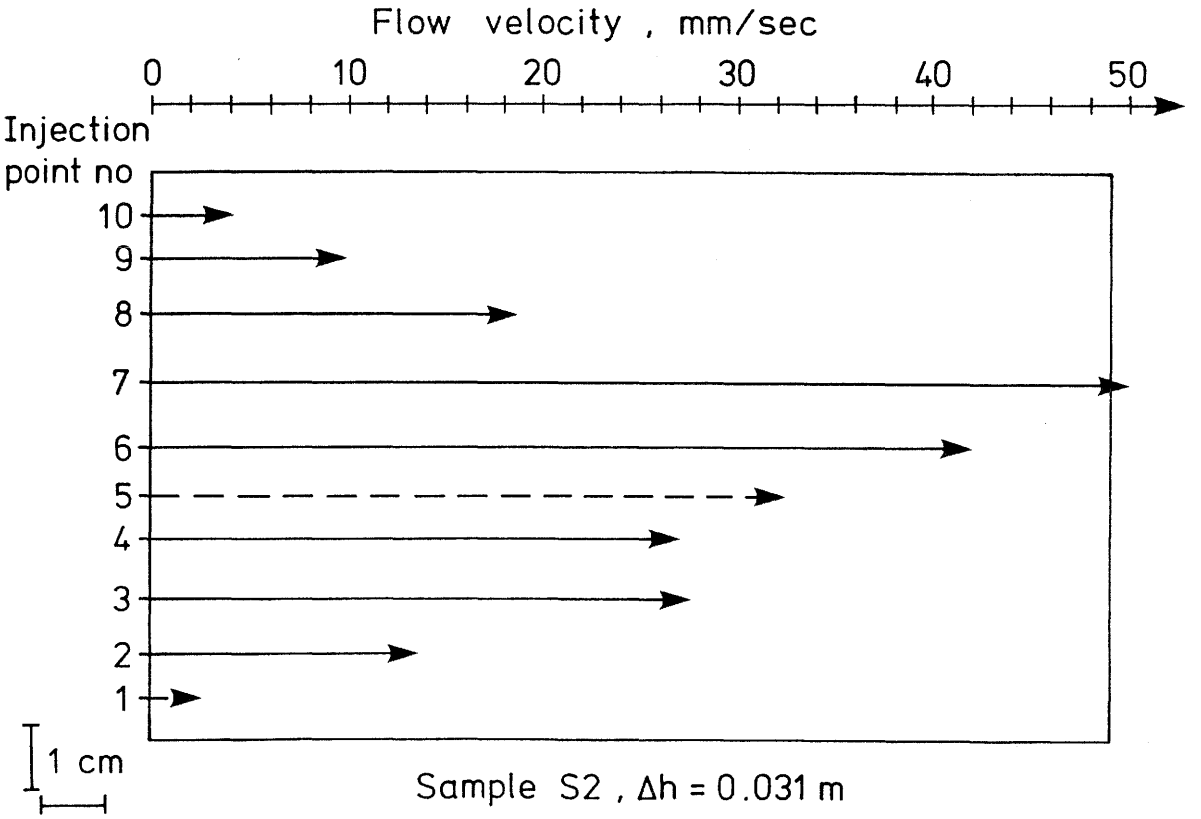

Sample S2 , $\Delta h = 0.031$ m

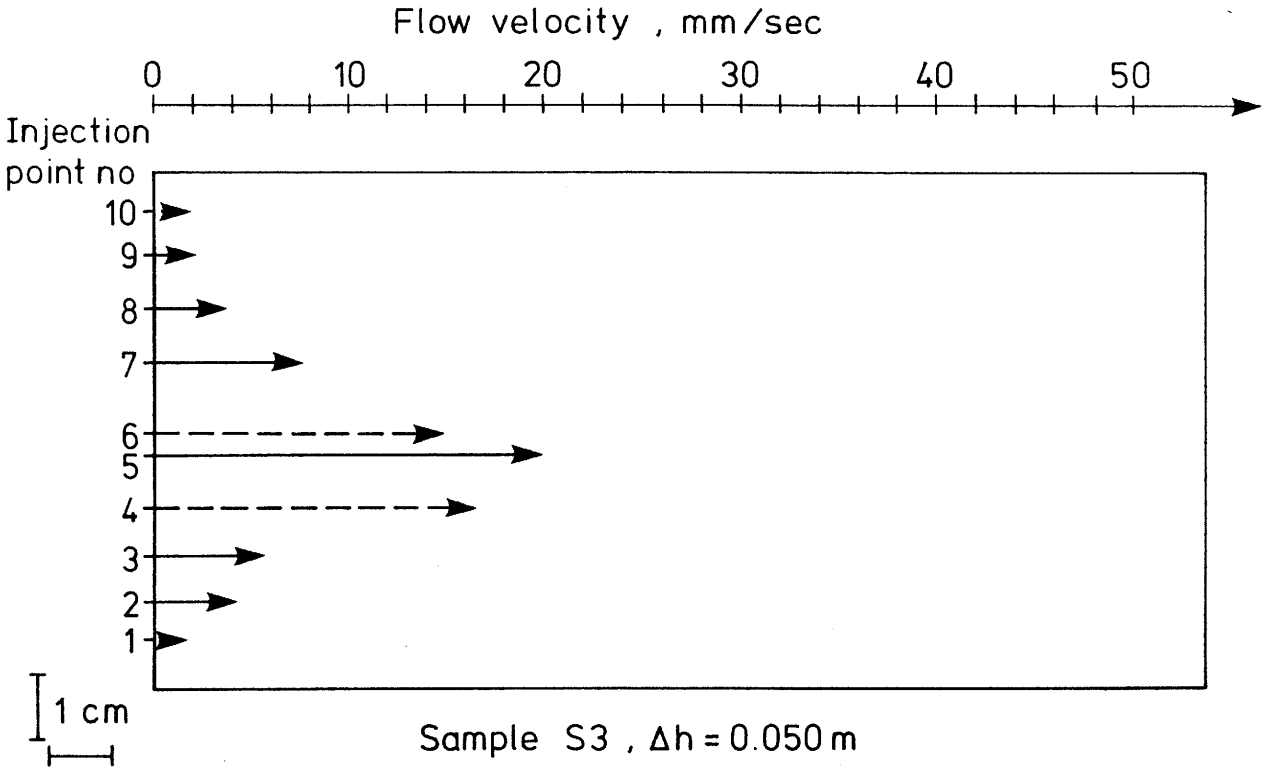

Sample S3 , $\Delta h = 0.050$ m

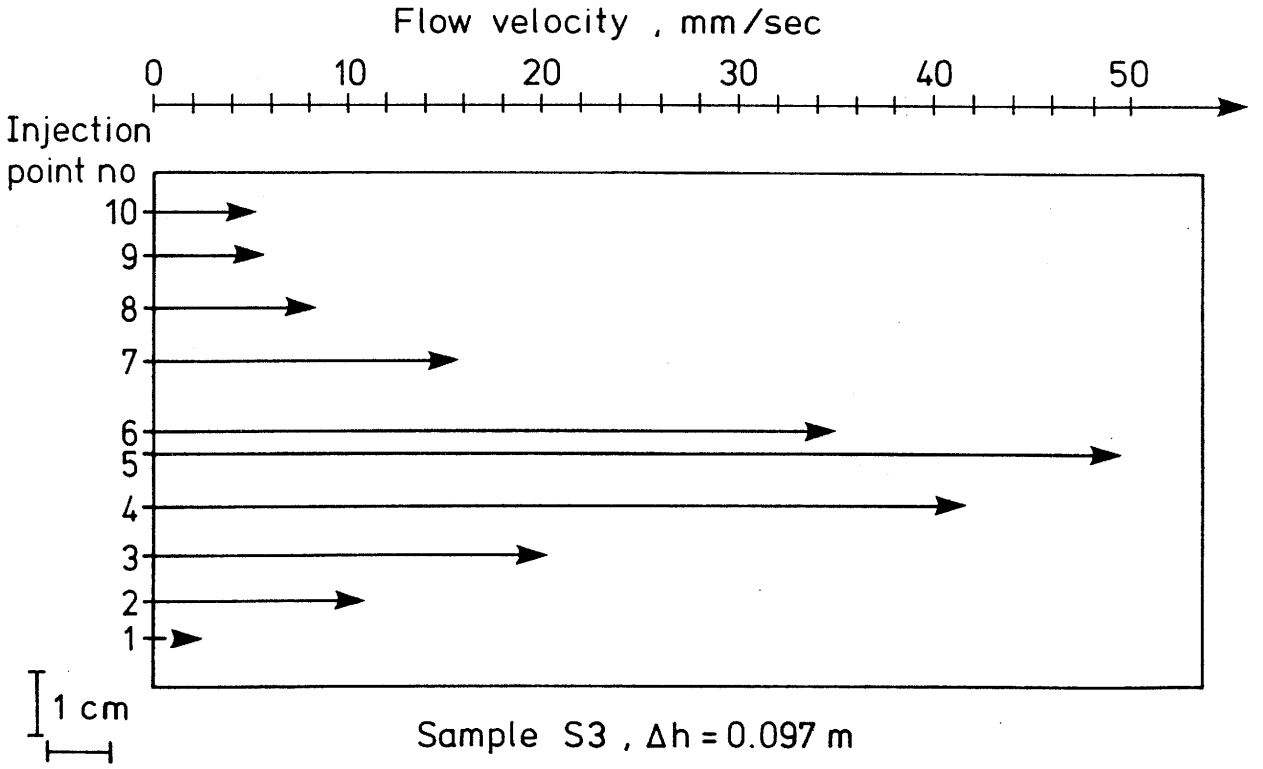

Sample S3 , $\Delta h = 0.097$ m

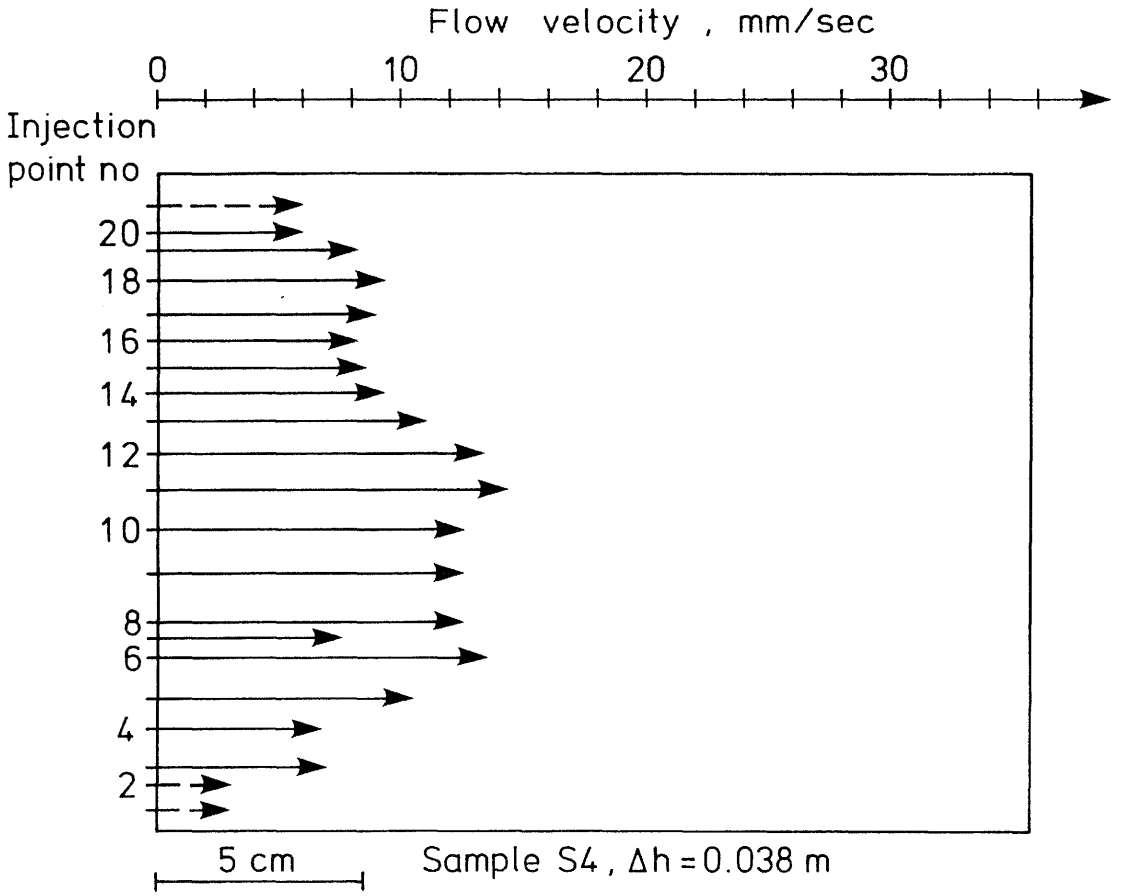
Flow velocity , mm/sec
0
10
20
30
Injection point no
20
18
16
14
12
10
8
6
4
2
5 cm
Sample S4 , Δh = 0.038 m

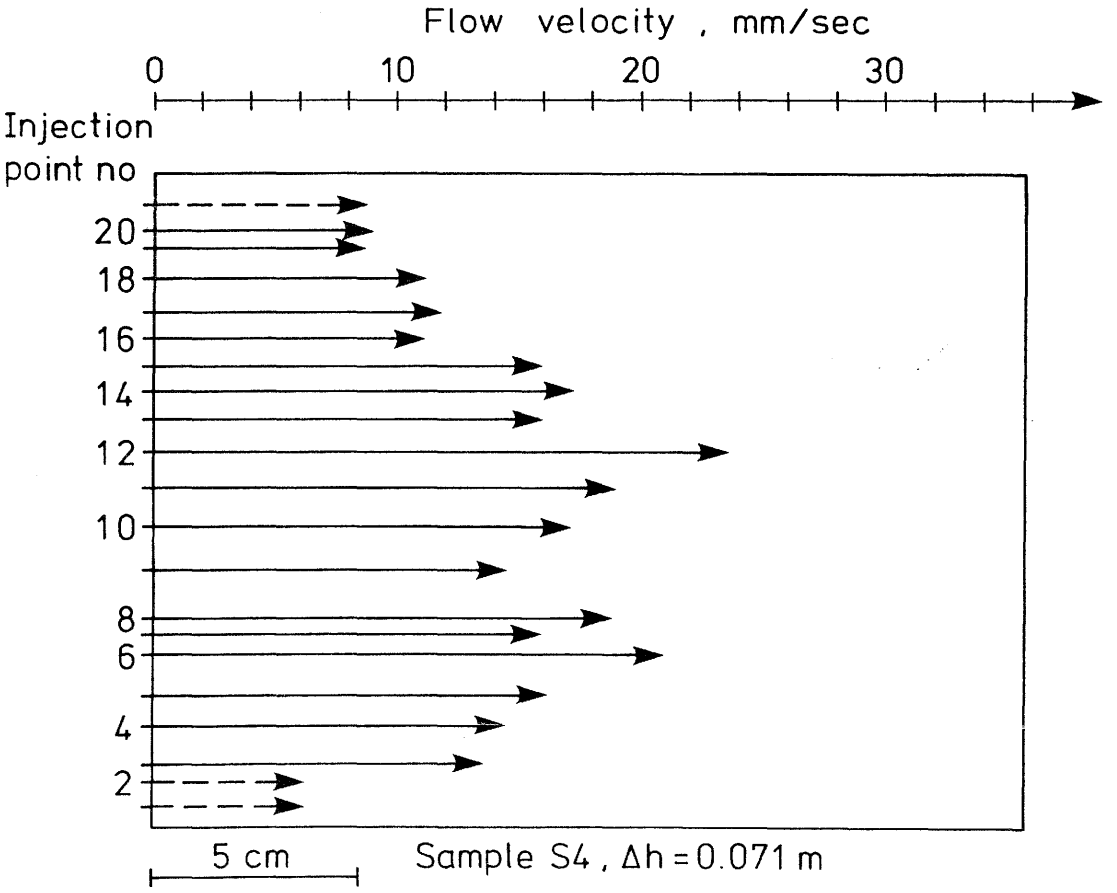
Flow velocity , mm/sec
0
10
20
30
Injection point no
20
18
16
14
12
10
8
6
4
2
5 cm
Sample S4 , Δh = 0.071 m

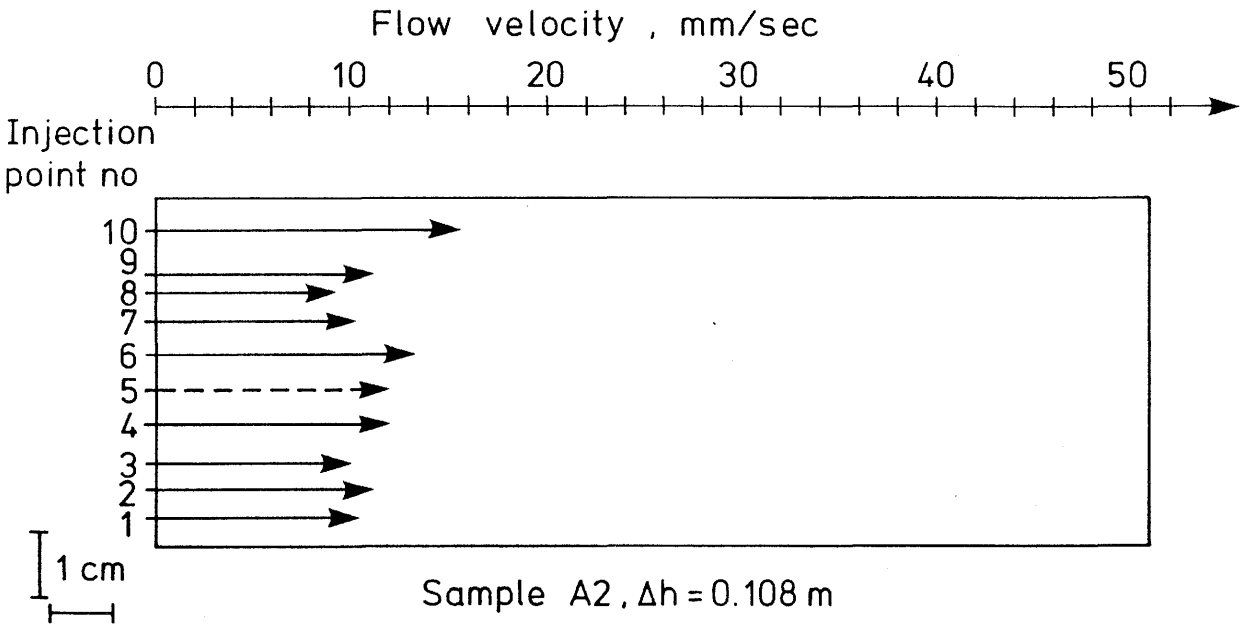

Sample A2 , Δh = 0.108 m

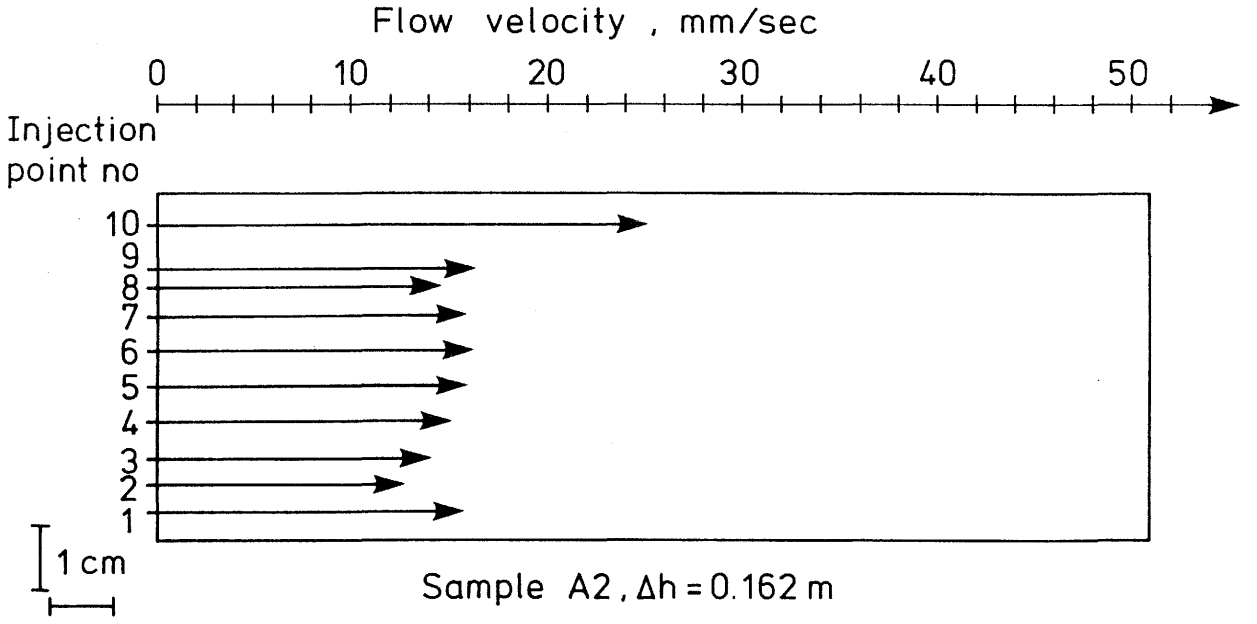

Sample A2 , Δh = 0.162 m

Stripa Project – Previously Published Reports

1980

TR 81–01
"Summary of defined programs"
L Carlsson and T Olsson
Geological Survey of Sweden, Uppsala
I Neretnieks
Royal Institute of Technology, Stockholm
R Pusch
University of Luleå
Sweden November 1980

1981

TR 81–02
"Annual Report 1980"
Swedish Nuclear Fuel Supply Co/Division KBS
Stockholm, Sweden 1981

IR 81–03
"Migration in a single fracture Preliminary experiments in Stripa"
Harald Abelin, Ivars Neretnieks
Royal Institute of Technology
Stockholm, Sweden April 1981

IR 81–04
"Equipment for hydraulic testing"
Lars Jacobsson, Henrik Norlander
Ställbergs Grufve AB
Stripa, Sweden July 1981

IR 81–05
Part I "Core-logs of borehole VI down to 505 m"
L Carlsson, V Stejskal
Geological Survey of Sweden, Uppsala
T Olsson
K-Konsult, Stockholm

Part II "Measurement of Triaxial rock stresses in borehole VI"
L Strindell, M Andersson
Swedish State Power Board, Stockholm
Sweden July 1981

1982

TR 82–01
"Annual Report 1981"
Swedish Nuclear Fuel Supply Co/Division KBS
Stockholm, Sweden February 1982

IR 82–02
"Buffer Mass Test – Data Acquisition and Data Processing Systems"
B Hagvall
University of Luleå, Sweden August 1982

IR 82–03
"Buffer Mass Test – Software for the Data Acquisition System"
B Hagvall
University of Luleå, Sweden August 1982

IR 82–04
"Core-logs of the Subhorizontal Boreholes N1 and E1"
L Carlsson, V Stejskal
Geological Survey of Sweden, Uppsala
T Olsson
K-Konsult, Engineers and Architects, Stockholm
Sweden August 1982

IR 82–05
"Core-logs of the Vertical Borehole V2"
L Carlsson, T Eggert, B Westlund
Geological Survey of Sweden, Uppsala
T Olsson
K-Konsult, Engineers and Architects, Stockholm
Sweden August 1982

IR 82–06
"Buffer Mass Test – Buffer Materials"
R Pusch, L Börgesson
University of Luleå
J Nilsson
AB Jacobson & Widmark, Luleå
Sweden August 1982

IR 82–07
"Buffer Mass Test – Rock Drilling and Civil Engineering"
R Pusch
University of Luleå
J Nilsson
AB Jacobson & Widmark, Luleå
Sweden September 1982

IR 82–08
"Buffer Mass Test – Predicitions of the behaviour of the bentonite-based buffer materials"
L Börgesson
University of Luleå
Sweden August 1982

1983
IR 83–01
"Geochemical and isotope characterization of the Stripa groundwaters – Progress report"
Leif Carlsson,
Swedish Geological, Göteborg
Tommy Olsson,
Geological Survey of Sweden, Uppsala
John Andrews,
University of Bath, UK
Jean-Charles Fontes,
Université, Paris-Sud, Paris, France
Jean L Michelot,
Université, Paris-Sud, Paris, France
Kirk Nordstrom,
United states Geological Survey, Menlo Park
California, USA
February 1983

TR 83–02
"Annual Report 1982"
Swedish Nuclear Fuel Supply Co/ Division KBS
Stockholm, Sweden April 1983

IR 83–03
"Buffer Mass Test – Thermal calculations for the high temperature test"
Sven Knutsson
University of Luleå
Sweden May 1983

IR 83–04
"Buffer Mass Test – Site Documentation"
Roland Pusch
Univeristy of Luleå and Swedish State Power Board
Jan Nilsson
AB Jacobson & Widmark, Luleå,
Sweden October 1983

IR 83–05
"Buffer Mass Test – Improved Models for Water Uptake and Redistribution in the Heater Holes and Tunnel Backfill"
R Pusch
Swedish State Power Board
L Börgesson, S Knutsson
University of Luleå
Sweden, October 1983

IR 83-06
"Crosshole Investigations — The Use of Borehole Radar for the Detection of Fracture Zones in Crystalline Rock"
Olle Olsson
Erik Sandberg
Swedish Geological
Bruno Nilsson
Boliden Mineral AB, Sweden
October 1983

1984
TR 84-01
"Annual Report 1983"
Swedish Nuclear Fuel Supply Co/Division KBS
Stockholm, Sweden, May 1984.

IR 84-02
"Buffer Mass Test — Heater Design and Operation"
Jan Nilsson
Swedish Geological Co
Gunnar Ramqvist
El-tekno AB
Roland Pusch
Swedish State Power Board
June 1984

IR 84-03
"Hydrogeological and Hydrogeochemical Investigations—Geophysical Borehole Measurements"
Olle Olsson
Ante Jämtlid
Swedish Geological Co.
August 1984

IR 84-04
"Crosshole Investigations—Preliminary Design of a New Borehole Radar System"
O. Olsson
E. Sandberg
Swedish Geological Co.
August 1984

IR 84-05
"Crosshole Investigations—Equipment Design Considerations for Sinusoidal Pressure Tests"
David C. Holmes
British Geological Survey
September 1984

IR 84-06
"Buffer Mass Test — Instrumentation"
Roland Pusch, Thomas Forsberg
University of Luleå, Sweden
Jan Nilsson
Swedish Geological, Luleå
Gunnar Ramqvist, Sven-Erik Tegelmark
Stripa Mine Service, Storå
September 1984

IR 84-07
"Hydrogeological and Hydrogeochemical" Investigations in Boreholes — Fluid Inclusion Studies in the Stripa Granite
Sten Lindblom
Stockholm University, Sweden
October 1984

IR 84-08
"Crosshole investigations — Tomography and its Application to Crosshole Seismic Measurements"
Sven Ivansson
National Defence Research Institute, Sweden
November 1984

1985

IR 85-01
"Borehole and Shaft Sealing — Site documentation"
Roland Pusch
Jan Nilsson
Swedish Geological Co
Gunnar Ramqvist
Eltekno AB
Sweden
February 1985

IR 85-02
"Migration in a Single Fracture — Instrumentation and site description"
Harald Abelin
Jard Gidlund
Royal Institute of Technology
Stockholm, Sweden
February 1985

TR 85-03
"Final Report of the Migration in a Single Fracture — Experimental results and evaluation"
H. Abelin
I. Neretnieks
S. Tunbrant
L. Moreno
Royal Institute of Technology
Stockholm, Sweden
May 1985

IR 85-04
"Hydrogeological and Hydrogeochemical Investigations in Boreholes — Compilation of geological data"
Seje Carlsten
Swedish Geological Co
Uppsala, Sweden
June 1985

IR 85-05
"Crosshole Investigations — Description of the small scale site"
Seje Carlsten
Kurt-Åke Magnusson
Olle Olsson
Swedish Geological Co
Uppsala, Sweden
June 1985

TR 85-06
"Hydrogeological and Hydrogeochemical Investigations in Boreholes — Final report of the phase I geochemical investigations of the Stripa groundwaters"
D.K. Nordstrom, US Geological Survey, USA
J.N. Andrews, University of Bath, United Kingdom
L Carlsson, Swedish Geological Co, Sweden
J-C. Fontes, Universite Paris-Sud, France
P. Fritz, University of Waterloo, Canada
H. Moser. Gesellschaft für Strahlen- und Umweltforschung, West Germany
T. Olsson, Geosystem AB, Sweden
July 1985

TR 85-07
"Annual Report 1984"
Swedish Nuclear Fuel and Waste Management Co.
Stockholm, July 1985

IR 85-08
"Hydrogeological and Hydrogeochemical Investigations in Boreholes—Shut-in tests"
L. Carlsson
Swedish Geological Co
T. Olsson
Uppsala Geosystem AB
July 1985

IR 85-09
"Hydrogeological and Hydrogeochemical Investigations in Boreholes—Injection-recovery tests and interference tests"
L. Carlsson
Swedish Geological Co
T. Olsson
Uppsala Geosystem AB
July 1985

TR 85-10
"Hydrogeological and Hydrogeochemical Investigations in Boreholes—Final report"
L. Carlsson
Swedish Geological Co
T. Olsson
Uppsala Geosystem AB
July 1985

TR 85-11
"Final Report of the Buffer Mass Test— Volume I: scope, preparative field work, and test arrangement"
R. Pusch
Swedish Geological Co, Sweden
J. Nilsson
Swedish Geological Co, Sweden
G. Ramqvist
El-tekno Co, Sweden
July 1985

TR 85-12
"Final Report of the Buffer Mass Test— Volume II: test results"
R. Pusch
Swedish Geological Co, Sweden
L. Börgesson
Swedish Geological Co, Sweden
G. Ramqvist, El-tekno Co, Sweden
August 1985

IR 85-13
"Crosshole Investigations — Compilation of core log data from F1-F6"
S. Carlsten.
A. Stråhle.
Swedish Geological Co, Sweden
September 1985

TR 85-14
"Final Report of the Buffer Mass Test— Volume III: Chemical and physical stability of the buffer materials"
Roland Pusch
Swedish Geological Co.
Sweden
November 1985

1986
IR 86-01
"Crosshole Investigations — Description of the large scale site"
Göran Nilsson
Olle Olsson
Swedish Geological Co, Sweden
February 1986

IR 86-02
"Hydrogeological Characterization of the Ventilation Drift (Buffer Mass Test) Area, Strip Sweden"
J.E. Gale
Memorial University, Nfld., Canada
A. Rouleau
Environment Canada, Ottawa, Canada
February 1986

IR 86-03
"Crosshole Investigations — The method, theory and analysis of crosshole sinusoidal pressure tests in fissured rock"
John H Black
John A Barker*
David J. Noy
British Geological Survey, Keyworth, Nottingham, United Kingdom
*Wallingford, Oxon, United Kingdom
June 1986

TR 86-04
"Executive Summary of Phase 1"
Swedish Nuclear Fuel and Waste Management Co.
Stockholm, July 1986

TR 86-05
"Annual Report 1985"
Swedish Nuclear Fuel and Waste Management Co.
Stockholm, August 1986

1987

TR 87-01
"Final Report of the Borehole, Shaft, and Tunnel Sealing Test — Volume I: Borehole plugging"
R. Pusch
L. Börgesson
Swedish Geological Co, Sweden
G. Ramqvist
El-Tekno Co, Sweden
January 1987

TR 87-02
"Final Report of the Borehole, Shaft, and Tunnel Sealing Test — Volume II: Shaft plugging"
R. Pusch
L. Börgesson
Swedish Geological Co, Sweden
G. Ramqvist
El-Tekno Co, Sweden
January 1987

TR 87-03
"Final Report of the Borehole, Shaft, and Tunnel Sealing Test — Volume III: Tunnel plugging"
R. Pusch
L. Börgesson
Swedish Geological Co, Sweden
G. Ramqvist
El-Tekno Co, Sweden
February 1987

TR 87-04
"Crosshole Investigations — Details of the Construction and Operation of the Hydraulic Testing System"
D. Holmes
British Geological Survey, United Kingdom
M. Sehlstedt
Swedish Geological Co., Sweden
May 1986

IR 87-05
"Workshop on Sealing Techniques, tested in the Stripa Project and being of General Potential use for Rock Sealing"
R. Pusch
Swedish Geological Co., Sweden
February 1987

TR 87-06
"Crosshole Investigations — Results from Seismic Borehole Tomography"
J. Pihl
M. Hammarström
S. Ivansson
P. Morén
National Defence Research Institute, Sweden
December 1986

TR 87-07
"Reflection and Tubewave Analysis of the Seismic Data from the Stripa Crosshole Site"
C. Cosma
Vibrometric OY, Finland
S. Bähler
M. Hammarström
J. Pihl
National Defence Research Institute, Sweden
December 1986

TR 87-08
"Crosshole Investigations — Short and Medium Range Seismic Tomography"
C. Cosma
Vibrometric OY, Finland
February 1987

TR 87-09
"Program for the Stripa Project Phase 3, 1986—1991"
Swedish Nuclear Fuel and Waste Management Co. Stockholm, May 1987

TR 87-10
"Crosshole Investigations — Physical Properties of Core Samples from Boreholes F1 and F2"
K-Å. Magnusson
S. Carlsten
O. Olsson
Swedish Geological Co, Sweden
June 1987

TR 87-11
"Crosshole Investigations—Results from Borehole Radar Investigations"
O Olsson, L Falk, O Forslund, L Lundmark, E Sandberg
Swedish Geological Co, Sweden
May 1987

TR 87-12
"State-of-the-Art Report on Potentially Useful Materials for Sealing Nuclear Waste Repositories"
Swedish Nuclear Fuel and Waste Management Co, Stockholm
June 1987

IR 87-13
"Rock Stress Measurements in Borehole V3"
B. Bjarnason
G. Raillard
University of Luleå, Sweden
July 1987

TR 87-14
"Annual Report 1986"
August 1987

TR 87-15
"Hydrogeological Characterization of the Stripa Site"
J. Gale
R. Macleod
J. Welhan
Memorial University, Nfld., Canada
C. Cole
L. Vail
Battelle Pacific Northwest Lab.
Richland, Wash., USA
June 1987

TR 87-16
"Crosshole Investigations – Final Report"
O. Olsson
Swedish Geological Co, Sweden
J. Black
British Geological Survey, United Kingdom
C. Cosma
Vibrometric OY, Finland
J. Phil
National Defence Research Institute, Sweden
September 1987

TR 87-17
"Site Characterization and Validation – Geophysical Single Hole Logging
B. Fridh
Swedish Geological Co, Sweden
December 1987

TR 87-18
"Crosshole Investigations – Hydrogeological Results and Interpretations
J. Black
D. Holmes
M. Brightman
British Geological Survey, United Kingdom
December 1987

TR 87-19
"3-D Migration Experiment – Report 1 Site Preparation and Documentation"
H. Abelin
L. Birgersson
Royal Institute of Technology, Sweden
November 1987

TR 87-20
"3-D Migration Experiment – Report 2 Instrumentation and Tracers"
H. Albelin
L. Birgersson
J. Gidlund
Royal Institute of Technology, Sweden
November 1987

TR 87-21
Part I "3-D Migration Experiment – Report 3 Performed Experiments, Results and Evaluation"
H. Abelin
L. Birgersson
J. Gidlund
L. Moreno
I. Neretnieks
H. Widén
T. Ågren
Royal Institute of Technology, Sweden
November 1987

Part II "3-D Migration Experiment – Report 3 Performed Experiments, Results and Evaluations Appendices 15, 16 and 17"
H. Abelin
L. Birgersson
J. Gidlund
L. Moreno
I. Neretnieks
H. Widén
T. Ågren
Royal Institute of Technology, Sweden
November 1987

TR 87-22
"3-D Migration Experiment – Report 4 Fracture Network Modelling of the Stripa 3-D Site"
J. Andersson
B. Dverstorp
Royal Institute of Technology, Sweden
November 1987

1988

TR 88-01
"Crosshole Investigations – Implementation and Fractional Dimension Interpretation of Sinusoidal Tests"
D. Noy
J. Barker
J. Black
D. Holmes
British Geological Survey, United Kingdom
February 1988

IR 88-02
"Site Characterization and Validation – Monitoring of Head in the Stripa Mine During 1987"
S. Carlsten
O. Olsson
O. Persson
M. Sehlstedt
Swedish Geological Co., Sweden
April 1988

TR 88-03
"Site Characterization and Validation – Borehole Rodar Investigations, Stage I"
O. Olsson
J. Eriksson
L. Falk
E. Sandberg
Swedish Geological Co., Sweden
April 1988

TR 88-04
"Rock Sealing – Large Scale Field Test and Accessory Investigations"
R. Pusch
Clay Technology, Sweden
March 1988

TR 88-05
"Hydrogeochemical Assessment of Crystalline Rock for Radioactive Waste Disposa The Stripa Experience"
J. Andrews
University of Bath, United Kingdom
J-C. Fontes
Université Paris-Sud, France
P. Fritz
University of Waterloo, Canada
K. Nordstrom
US Geological Survey, USA
August 1988

TR 88-06
"Annual Report 1987"
June 1988

IR 88-07
"Site Characterization and Validation – Results From Seismic Crosshole and Reflection Measurements, Stage I"
C. Cosma
R. Korhonen
Vibrometric Oy, Finland
M. Hammarström
P. Morén
J. Pihl
National Defence Research Institute, Sweden
September 1988

IR 88-08
"Stage I Joint Characterization and Stage II Preliminary Prediction using Small Core Samples"
G. Vik
N. Barton
Norwegian Geotechnical Institute, Norway
August 1988

IR 88-09
"Site Characterization and Validation – Hydrochemical Investigations in Stage I"
P. Wikberg
M. Laaksoharju
J. Bruno
A. Sandino
Royal Institute of Technology, Sweden
September 1988

IR 88-10
"Site Characterization and Validation — Drift and Borehole Fracture Data Stage I"
J. Gale
Fracflow Consultants Inc., Nfld., Canada
A. Stråhle
Swedish Geological Co, Uppsala, Sweden
September 1988

TR 88-11
"Rock Sealing — Interim Report on the Rock Sealing Project (Stage I)"
R. Pusch
L. Börgesson
A. Fredrikson
Clay Technology, Sweden
I. Markström
M. Erlström
Swedish Geological Co, Sweden
G. Ramqvist
El-Tekno AB, Sweden
M. Gray
AECL, Canada
W. Coons
IT Corp., USA
September 1988

1989

TR 89-01
"Executive Summary of Phase 2"
Swedish Nuclear Fuel and Waste Management Co., Stockholm
February 1989

TR 89-02
"Fracture Flow Code Cross – Verification Plan"
W. Dershowitz
Golder Associates Inc., USA
A. Herbert
AERE Harwell Laboratory, U. K.
J. Long
Lawrence Berkeley Laboratory, USA
March 1989

TR 89-03
"Site Characterization and Validation Stage 2 – Prelimiary Predictions"
O. Olsson
ABEM AB, Sweden
J. Black
Golder Associates, U. K.
J. Gale
Fracflow Inc., Canada
D. Holmes
British Geological Survey, U. K.
May 1989

IR 89-04
"Site Characterization and Validation - Single Borehole Hydraulic Testing"
D. Holmes
British Geological Survey, U.K.
March 1989

TR 89-05
"Annual Report 1988"
Swedish Nuclear Fuel and waste Management Co
Stockholm
May 1989

IR 89-06
"Site Characterization and Validation — Monitoring of Head in the Stripa Mine During 1988"
O. Persson
Swedish Geological Co., Uppsala, Sweden
O. Olsson
ABEM AB, Uppsala, Sweden
M. Sehlstedt
Swedish Geological Co., Malå, Sweden
April 1989

IR 89-07
"Site Characterization and Validation — Geophysical Single Hole Logging Stage 3"
P. Andersson
Swedish Geological Co., Uppsala, Sweden
May 1989